PRACTICAL POWER AND COMBUSTION INVESTIGATIONS ON FIRST WAVE DISK ENGINE PROTOTYPES

By

Pablo F. Parraga-Ramirez

A DISSERTATION

Submitted to
Michigan State University
in partial fulfillment of the requirements
for the degree of

Mechanical Engineering- Doctor of Philosophy

2013

ABSTRACT

PRACTICAL POWER AND COMBUSTION INVESTIGATIONS ON FIRST WAVE DISK ENGINE PROTOTYPES

By

Pablo F. Parraga-Ramirez

The Wave Disk Engine (WDE) is a revolutionary engine that utilizes principles of unsteady flow and fast combustion, taking advantage of shock waves and constant-volume heat addition. The WDE references the Atkinson cycle (also called the Humphrey cycle), which combines both confined combustion, as in the Otto cycle, and complete gas expansion, as in the Brayton cycle. This new engine concept, with few moving parts, has the potential to significantly outperform existing heat engines. Four WDE prototypes have been developed and built and two test cells have been used for testing. A working, real-size WDE prototype has been used for testing and evaluation of the performance of new parts and settings and an Optical WDE prototype has been used to optically analyze the combustion inside the WDE. The objective of the work is to enhance the understanding of the practical WDE operation for the further development of new WDEs prototypes with increased performance.

The work details practical challenges and methods to successfully overcome these. This includes a description of the developed electromechanical testing facility with computer control system, diagnostic techniques, and power measuring equipment. Power analyses of the working WDE prototype are performed on the bases of acceleration of the WDE measured on the test stand. The results are related to the Air/Fuel Ratio (A/F) and the number of return channels in the design. Further operational conclusions are drawn from a flame speed analysis of the combustion inside the Optical WDE. High Speed Imaging of combustion was used to track flame fronts inside the

WDE providing data for the understanding of how Equivalence Ratio, Rotational Speed (RPM), Spark Plug Position, and Injection System relate to the flame front speed.

DEDICATION

I dedicate this work to my Mom, Gilma Cecilia Ramírez Guzman. She has been the strongest example of self improvement, and relentlessness I have. I profoundly admire her not only because she is my mom, but because of the extreme difficulties she has overcome, always with dignity, and a smile. Love you Mom!

Le dedico este trabajo a mi Mamá, Gilma Cecilia Ramírez Guzman. Ella ha sido el ejemplo más fuerte de superación personal y de aguante que yo haya tenido. La admiro profundamente no sólo por ser mi Mamá, también por las extremas dificultades que ha superado siempre con dignidad y una sonrisa. Te Quiero Mucho Mamá.

ACKNOWLEDGMENTS

Thanks to Dr Muller, for giving me freedom and guidance, best professor I ever had! Lucky me I had him as PhD advisor. He builds true engineers and gets the best out of us supporting our ingenuity, ethics, and hard work.

Thanks to Dr Janusz Piechna, true genius. Great person, great knowledge great wisdom, and great guidance.

Thanks to My Team: Every single one of them, TJ, Ying, Blake, Guangwei, Raul, Mohit, Rohit, Eric, Varney, Dewashish, Zack, Jeremy, Varun, and Steve Hammak. But overall to Eric Tarkleson, TJ, and Mike Varney.

Thanks to ARPA-E for sponsoring this beautiful project, which suddenly became my reason to live.

TABLE OF CONTENTS

LIST OF TABLES

LIST OF FIGURES

INTRODUCTION

World oil consumption has increased from approximately 75 million barrels per day in 1999 to 85 million barrels per day in 2010 [1], an increase of 13.3%. Coal consumption has increased from 2316 million tonnes oil equivalent in 1999 to 3555.8 million tonnes oil equivalent in 2010 [1] an increase of 53.53%. Despite the higher increase on the consumption of cheaper combustibles like coal, crude oil barrel prices have risen from US $23.52 in 1999 to a peak of US $98.50 in 2008 (in 2010 dollars) [1], an increase of 326.1%. High demand for fossil fuels seems inelastic with respect to the commodity price, and is increasing globally [2].

The use of organic combustibles as a primary energy source[3] has caused environmental problems like climate change and some respiratory problems linked to gases produced from combustion. On December 7 of 2009, carbon dioxide, the main product of combustion, together with other green house effect gases were declared dangerous to public health by the Environmental Protection Agency (EPA) [4]. The increase in fuel consumption proportionately increases the amount of carbon dioxide and other combustion products released to the atmosphere, thus increasing the consequences of air pollution as the global economy grows. The problem has also a social aspect; there is a change in the distribution of wealth for the common U.S. citizen. The price of gasoline increased from US $1.121 per gallon on march 29 of 1999, to US $3.884 in March 15, 2012 [5], an increase of 218%, causing a decrease in the money spent on other goods and services[6]. Oil and its derivatives are used widely in the production of goods and services in the U.S; its high prices have an effect of either increasing the retail price of such goods and services or force companies to reduce production costs. This affects household welfare by decreasing the access to this goods and services or by laying off workers and closing plants to keep prices low[6].

The way energy is used today is inefficient. Cullen and Allwood (2010), compared efficiency of different end use devices taking into account the upstream losses [7]. For example, the electric motor transforms the electricity it receives into motion with 95% efficiency, but that efficiency does not account for either how the electricity was produced or how it was transported. Tracing the energy flow throughout the different energy conversion processes from fuels to end-use devices yields an average efficiency of energy conversion of 11%[7]. Thus, from all the resources we burn, only 11%, on average, serves an intended purpose and the other 89% is lost. For example, an incandescent light bulb has an average efficiency of 4%, the electrical motor powering a washer machine, or a garage door or a sewer pump is 17% efficient and the Otto engines that drive most cars in the United States are in average 12% efficient[7].

Unlike the Otto engine the Wave Disk Engine (WDE) is a piston-less engine, with an efficiency potential of 60%. The WDE reduces the amount of heat loss in the energy release process due to pressure gain combustion, like in a piston engine; reduces the energy loss in the expansion process by complete expansion, like in a gas turbine; and is best described by the Humphrey cycle. In addition to these fundamental gains, the WDE virtually eliminates frictional losses between parts because there are no rubbing parts, other than 2 bearings (a 4-piston engine has 18) which can be eliminated if the WDE's shaft and electrical generator shaft are the same piece.

The WDE uses shockwaves to enhance the pre-compression of the air-fuel mixture. The use shockwaves is an efficient mechanism to compress and expand gases; it relies on the fluid properties to transmit energy avoiding the use of mechanical parts that add inertia to the engine.

Despite the advantages of the use of shockwaves, only a few projects have attempted to use them for energy conversion devices and even fewer have attempted to design a self-driven or power-generating shockwave device [8]. The WDE project is one of the first attempts if not the first one to design and develop a complete engine based on shockwave compression.

The WDE is a disk-shaped machine, similar to a brake-rotor, consisting of a disk with protruded channels rotating on a shaft. The housing consists of partial-annular inlet and exhaust ports located at the center and at the periphery respectively, as shown in Figure 1. Each channel acts as an individual combustion chamber, which periodically charges and discharges as it rotates past the ports, with the end walls functioning as the inlet and exit valves. The premixed air-fuel mixture enters through the central inlets as the rotor spins filling the channels with mixture. During the filling process, the sudden closing of the outer wall, produces an instantaneous buildup of pressure triggering a shock wave (hammer shock), that travels from the outer wall towards the inlet of the channel compressing the mixture. At the moment the shock wave reaches to the inlet port, this port closes. By closing the inlet port, both ends of the channel are now closed, keeping the pressure generated by the shockwave inside the channel. While the pressure still high the combustion process is initiated and can occur at a nearly constant-volume condition that generates a second pressure rise within the channel. Once the rotating-channel does reach the exit port, the burned gases discharge to the surroundings in tangentially exiting jets. The tangentially exiting jets have moved over curved blades extracting power from the fluid by the principles of turbo-machinery hence producing torque on the disk. During a complete cycle of operation, the exhaust process is followed by a scavenging process which fills the channels and the next cycle starts.

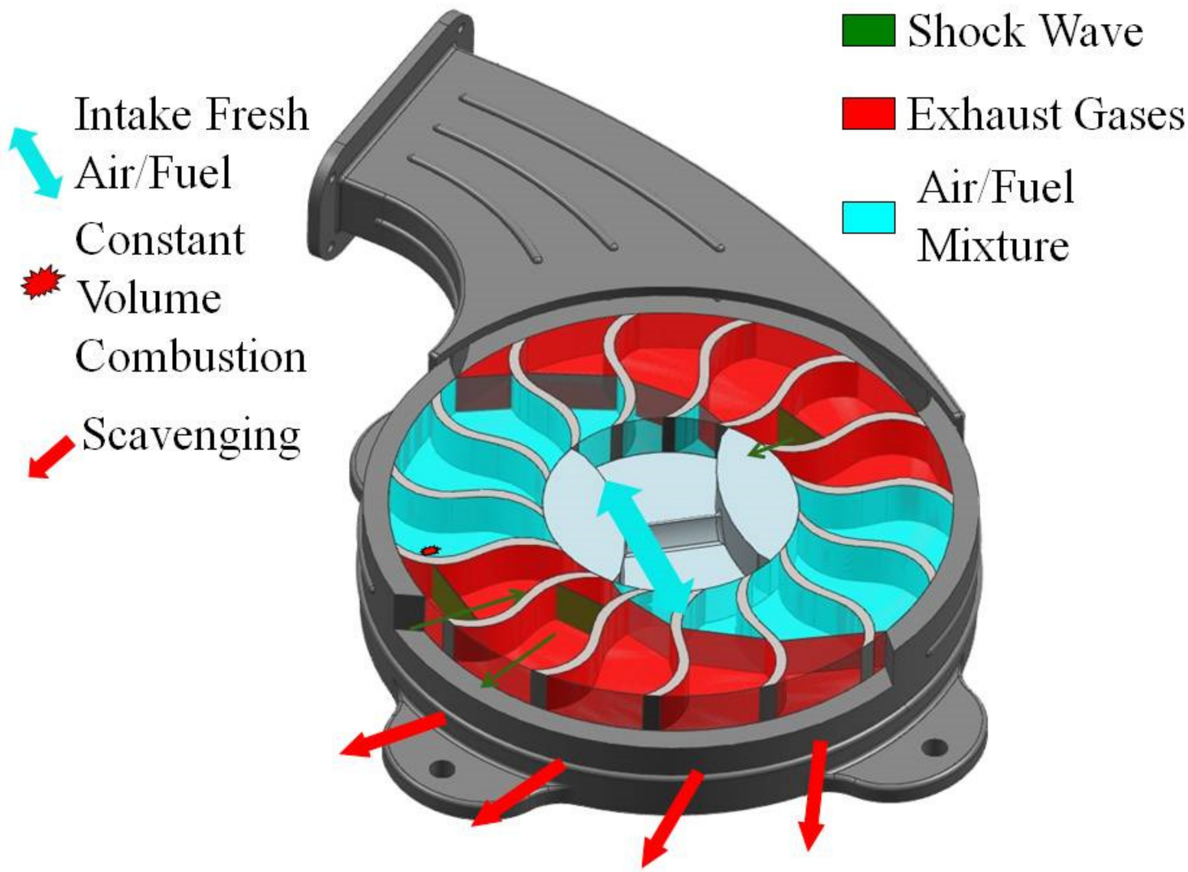

Figure 1: Schematic illustration of the Wave Disk Engine (WDE).

(For interpretation of the references to color in this and all other figures, the reader is referred to the electronic version of this thesis (or dissertation)

This dissertation intends to explain experiments, development, and some test results of the WDE. The first chapter will be about facility development of the WDE project. This chapter will discuss the equipment purchased and installed, some manufacturing details of custom equipment as well as WDE prototypes. The second chapter will analyze the power output of the WDE. The third chapter will be about deflagration speed on rotating channels; and the effect different fuel injection methods have on the speed of deflagration. This chapter will be based on high speed imaging of combustion inside an optical WDE. The last chapter will compile the conclusions of the studies in chapter two and three.

DEVELOPMENT OF A WAVE DISK ENGINE EXPERIMENTAL FACILITY

Introduction

Comparing internal combustion (IC) engines and gas turbine engines, one can observe their advantages and limitations. In the gas turbine engine, the combustor remains open to both intake and exhaust, allowing continuous flow at ideally constant pressure (in reality there is a loss in total pressure across the combustor) and the energy of the exiting gas is used through the dynamic action of the turbine blades to produce work. In an IC engine, combustion takes place in a closed volume causing a pressure rise that moves the piston. However, the work extraction process (expansion) is limited by the piston stroke; the gases are not completely expanded and the maximum possible work from the burned gases is not fully utilized. In contrast, the gas turbine allows for complete expansion of burned gases. Combining confined combustion and complete expansion in a new engine, the WDE [9] thermodynamically modeled with the Atkinson/Humphrey cycle, could lead to higher efficiencies. The WDE is a new engine concept, utilizing the best of piston and the turbine engines with reduced hardware, well suited for relatively small power generation. Compared to a gasoline engine, the WDE eliminates components like pistons, crankshafts, valves, and many bearings and parasitic systems because it has only one moving part: a rotating disk. Compared to a turbine engine, the WDE eliminates several stages of compression, reducing weight and frictional losses that reduce efficiency. Additionally, the WDE aims to use shock waves to pre-compress gas mixtures before heat addition, increasing the efficiency further. For moderate pressure ratios (e.g. up to 2.5) shock waves are a more efficient way to realize pre-compression than mechanical compression devices

[8] like pistons or rotating blades. The WDE is new and still in its infancy; no commercialized application has been reported yet.

How Does the WDE Work?

The WDE concept results from collaborative research began in 2001 between MSU and Warsaw University of Technology in Poland [9] ,[10]. The WDE shares features of the wave engine [11] and the IC engine. The WDE is disk-shaped, similar to a brake-rotor, and consists of a disk with protruded channels rotating on a shaft, as shown in Figure 1.

The partial-annular housing contains inlet and exhaust ports located at the center and at the periphery, respectively. Each channel acts as an individual combustion chamber, which periodically charges and discharges as it rotates past the ports, with the end walls functioning as contactless inlet and exit valves. The premixed air-fuel mixture enters the channels through central inlets as the rotor spins, and the hot gases exit the channels at the periphery through the exhaust port. During the filling process, the sudden closing of the outer wall triggers a shock wave (hammer shock) that travels from the outer wall towards the inlet of the channel, compressing the mixture. The compression of the mixture prior to burning beneficially causes a decrease in entropy production. At the moment the shock wave reaches to the inlet port, this port closes. By closing the inlet port, both ends of the channel are now closed and the mixture is kept with a higher pressure within the channel. The combustion process is initiated at a quasi-constant-volume condition that generates a further pressure rise in the channel. Once the rotating channel reaches the exit port, the burned gases tangentially discharge to the surroundings. These hot jet gases move over curved blades extracting power from the fluid by the principles of turbomachinery, producing torque on the disk. During a complete cycle, the exhaust process is followed by the filling process and the next cycle starts. Previous numerical simulations have confirmed the validity of the theory of operation [12].

Physical Phenomena Expected During Tests and Influencing Test Rig Construction

The WDE features characteristics from both piston and turbine engines together with unsteady flow phenomena for mechanical power generation. Consequently, the test rigs are designed to resist static and cyclic vertical loads, cyclic horizontal loads, and high temperatures from the engines.

Characteristic phases of combustion like chamber scavenging, air-fuel mixture refilling, compression, ignition, combustion, and expansion are realized in atypical ways. Flow inertial effects (steady and unsteady), unsteady combustion effects, mixing effects, and diffusion effects inherently occur in the WDE. Some unsteady effects are used for the air-fuel mixture compression and centrifugal forces are to improve scavenging.

Air-fuel mixture at different air-fuel ratios with controlled lean and locally rich mixture and other enhancements have been investigated for shorter combustion time. The WDE's flame propagation process can be rather complicated. A WDE with optical ports at the top side of the rotor has been designed to optically analyze the flame propagation process, monitoring flame structure and flame speed.

Tracking unsteady compression waves requires pressure transducers with fast response times. Pressure transducers must also be temperature resistant or have additional measures to protect them from the heat of the engine. Ducts separating transducers enable transducer cooling but strongly reduce the dynamic characteristics of pressure registration line. Signal conditioning electronics are typically the most heat-sensitive components in pressure transducers, and temperature resistant probes typically require external electronics for signal conditioning. Ion probes track flame propagation. Installation of dynamic pressure transducers and ion probes within the channel walls requires a telemetry system to transfer data from the moving rotor to stationary receiver.

Experimental Facilities

A new space was provided by the university to house the test facility. Figure 2 schematically shows the WDE facility layout. It consists of four sections: the test cell, the gas storage room, the courtyard, and the control room. The courtyard is an open space where the electromechanical parts of the room exhaust, ventilation, and cooling systems are placed. The control room has the electric controls for the above systems, a virtual window (TV connected to cameras in the test room) to the test facility, and the computers that control the data acquisition (DAQ) and control system. The gas room has two gas supply lines. Inert gas and fuel, equipped with safety solenoids, ball valves, and standard regulators that are attached to the gas tanks. The regulators and safety solenoids are controlled and monitored electronically via Labview. Methane, Ethane, Propane, Hydrogen, and Air are used as the fuels and oxidizer respectively. Methane and Ethane are the most used gases in WDE experiments. The cases studied in this dissertation are based in tests using Ethane as a fuel. Methane is a common fuel in combustion studies and has a slow burning rate. One objective for commercial applications is to use natural gas as the fuel, which on average contains around 70% Methane.

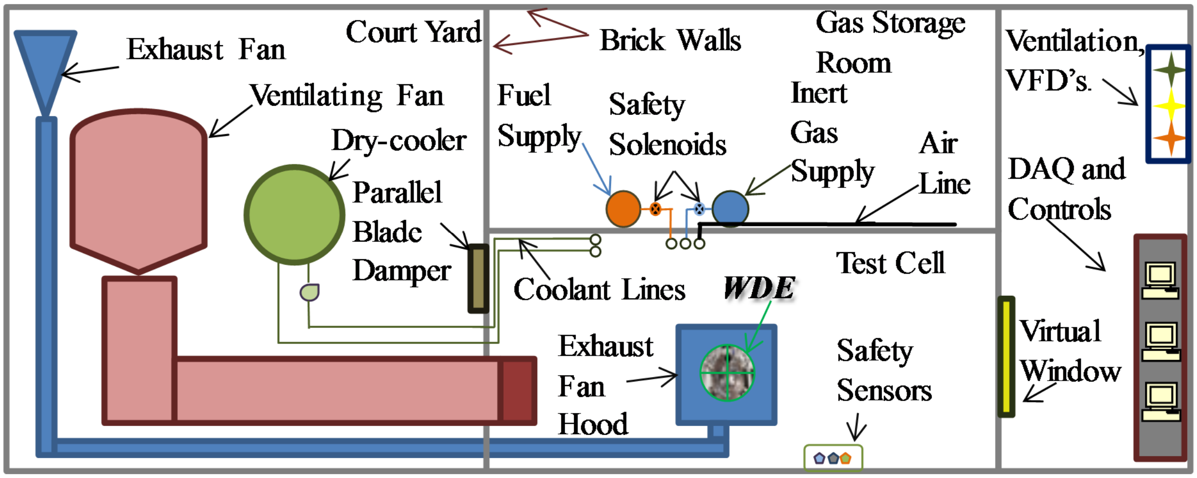

Figure 2: WDE test facility layout at MSU.

The test facility features state-of-the-art data acquisition and control equipment. It has over 500 channels available for monitoring and control. The test room is explosion proof, with hazardous emission gases controlling a standard three level emergency-stop (E-stop) system. It has complete video and audio feedback with recording; and the remote control room allows engine parameters to be monitored, recorded, and controlled.

Figure 3 is a picture of the test rig including the base, drive assembly, and supply lines. The WDE is installed on a 23-inch square aluminum base at a height of 38 inches. A variable speed electric starter motor-generator is located under the rotating disk connected to the rotor by a shaft. Rotors are assembled and aligned with the starter before test.

Figure 3: WDE test facility at MSU.

For optical combustion diagnostics, a smaller test rig with optical access, was built and is located in the Laser Diagnostics Laboratory at MSU, as shown in Figure 4. This laboratory also has ventilation and safety equipment necessary for testing engines, but all the systems are confined by 3/4-inch-thick, clear Lexan panels that isolate the test rig and allow visibility of the experiments. This smaller test rig also includes complete monitoring and control via a reduced data acquisition system.

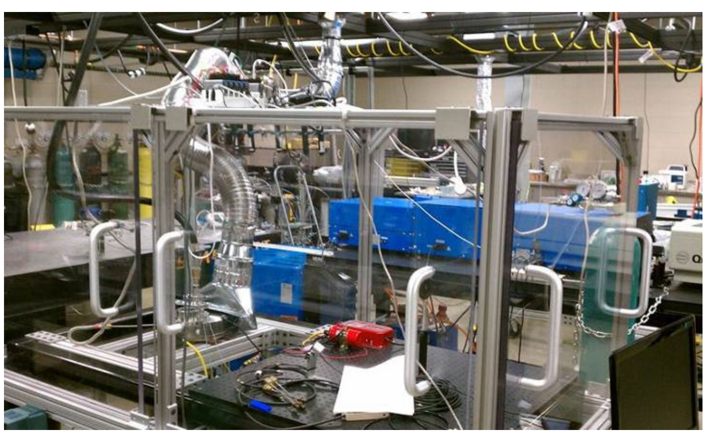

Figure 4: Second WDE test facility with optical access.

Safety and Ventilation

The test cell has been designed and tested to insure safe operation. It has adequate exhaust ventilation, engine cooling, and hazardous gas detection. Room environmental controls monitor gas levels and temperature and several high speed fans allow the air in the room to be evacuated quickly.

The exhaust collection system capacity is 600 cubic feet per minute (CFM) equipped with a fan located at the courtyard that is connected through a 12-inch diameter duct to a hood above the engine. The room ventilation system capacity is 4500 CFM using second fan connected through a 24-inch diameter duct to the test room. It circulates air from the outside through a parallel blade damper, which is controlled with a thermostat. The test cell also has a cooling system for the engine with 30 gallons per minute glycol capacity. The system consists of a drycooler that can reject 92380 Btu/hr of heat and a glycol pump with a total discharge head of 47 ft. The drycooler and the pump are also in the courtyard connected to the test room through a 2-inch closed circuit pipeline. There are two Polytron hazardous and toxic gas detection systems to protect against dangerous concentrations of H_2, CO, and natural gas in the test room.

The engine controls include a keyed start box as well as several layers of E-stop. An on screen E-stop stops the motor but leaves all peripherals running. A manual E-stop, forces all controls to zero to insure gas controls stop and ignition is disabled. A room E-stop shuts off all power to the test cell in the event of a major malfunction. The environmental controls are built into the "major" E-stop so the system will trip without human interaction. All personnel running the test are required to receive proper safety training and procedures prior to start of the test program.

Ignition System

The WDE ignition system is designed to utilize up to four spark plugs simultaneously, with a power of ~330 mJ per spark. They can be either mounted on the outer ring or on the top plate. The system is comprised of two, off-the-shelf MSD 8-plus ignition control modules, one hall sensor magnetic pickup, and a custom-made magnetic timing-disk. The timing disk can insure that there is exactly one spark in the middle of each channel as it passes by the spark plug. This is essentially a motor angle/position sensor and can be used to track many system variables, including rotor position and speed when interfaced with the main DAQ system. Figure 5 shows the sensor disk mounted on the rotating shaft. Each sensor disk has a magnet aligned with each channel in the WDE, which is designed to be hooked directly up to the MSD ignition modules magnetic sensor input. Sensor disks can be changed with the WDE rotor to accommodate rotors with different numbers of channels.

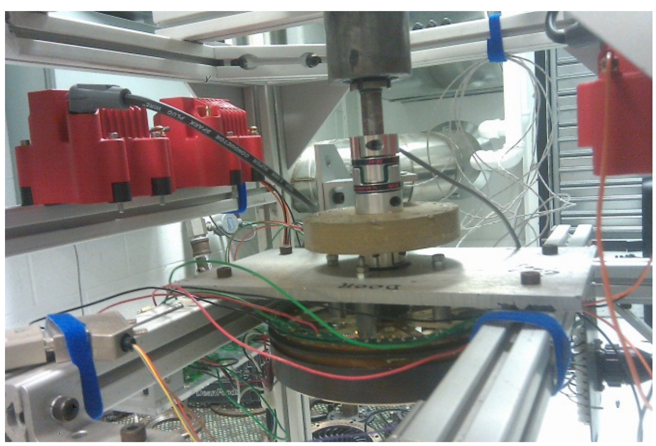

Figure 5: Magnetic sensor disk connected to the shaft.

A WDE ignition system based on spark plugs requires special treatment due to very high spark rates. While an IC engine spark plug fires on a four cylinder engine once per 2 revolutions, a

WDE spark plug may fire 30 times per revolution. Taking a cue from a previous experimental wave engine rig [13] torch ignition has been explored as an alternative to IC type spark ignition for normal-speed operation of the engine. A torch can be fitted to the engine and combusted gases can be recirculated. Both were tested with self-sustained combustion achieved.

A simple schematic of the spark ignition system is illustrated in Figure 6. The outputs from the hall sensors feed directly into the ignition control, which sparks the plugs whenever it gets a low (0 volt) signal from the sensor. In the way the magnets are aligned with the center (or beginning) of the WDE channels, a spark will occur every time the magnetic sensor detects a channel.

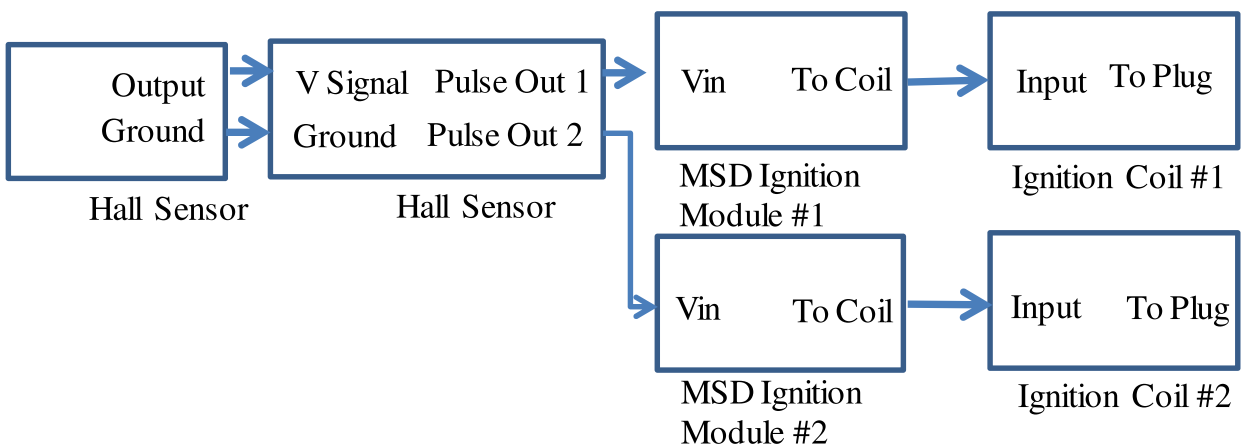

Figure 6: Schematic of the ignition system operation.

The timing and ignition system is a mix between traditional ignition technology and variations on other types of control systems to realize. In a traditional IC engine or generator a timing belt or disk tells each cylinders spark plug when to fire. At high rpm this occurs about 233 times a sec (233 Hz). A WDE operates much faster, a relationship between its rotational speed, channels, and firing rate follows $r = x \cdot c/60$ where r, x, c represent ignition firing rate (Hz), rotational speed (rpm), and number of channels, respectively. For instance, for a WDE with 32 channels rotating at a speed of 10,000 rpm a spark plug must fire at a rate of 5.33 kHz to fire once per channel. This represents an enhancement from current technology where a typical 4-cylinder 4-stroke IC engine running at 4000 rpm, sparks with a rate of only 8000 sparks/minute or 133 Hz. As the speed of an ignition continues past its maximum specifications, the energy in the spark decreases because the capacitor (and/or inductor) cannot fully charge before the next spark. High-speed, high-voltage ignitions are well within current design possibilities, but cannot be easily found because there is currently not a large market for this type of ignition.

Test Rig Flexibility.

Prototype engines should have several configurations available to accommodate planned and provisional modifications. The WDE test cell has complete flexibility with respect to many of its operating variables. The test rig permits adjustment of the starter-generator drive position, the rotor position with respect to inlets and outlets, fuel and air injection locations, ignition position and firing angle, and the amount and position of pressure transducers and thermocouples, to control and measure configuration changes of the WDE. The test rig also allows controlled fuel flow for multi-port injection, controlled scavenging, and flashback prevention. In addition, the test rig is as flexible that the system can be quickly modified for unforeseen circumstances. The data acquisition (DAQ) system has the capacity for additional input or output channels and the motor controllers can use many different control algorithms. For example, a speed controlled WDE allows to measure pure power extracted at a single speed, while a quick switch to torque control allows to examine the torque that the engine is producing as well as implement other controls via Labview interfaces.

Data Acquisition and Control System

The data acquisition and control system for the WDE test facility was designed to control engine tests and measure relevant data. The controls include starter motor-generator speed control and feedback, fuel and air flow control and feedback, and ignition system control and feedback. The data acquisition includes real time power measurements, rotational speed measurements, pressure and temperature measurements, and gas flow measurements. The computer interface was implemented in National Instruments' (NI) Labview software. The electrical I/O hardware is state-of-the-art NI Compact DAQ equipment. One of the advantages of using a modular acquisition system is that it can be reconfigured as the tests need to change. However, the system is typically setup to accommodate 8 pressure measurements, 16 temperature measurements, 4 mass flow controller interfaces, 1 motor controller interface, 1 ignition control relay, 1 tachometer input as well as all safety monitoring and feedback instruments. In addition to the Compact DAQ system, one of the motor drives is directly controlled by Labview via Ethernet Industrial Protocol. A block diagram of the DAQ is illustrated Figure 7.

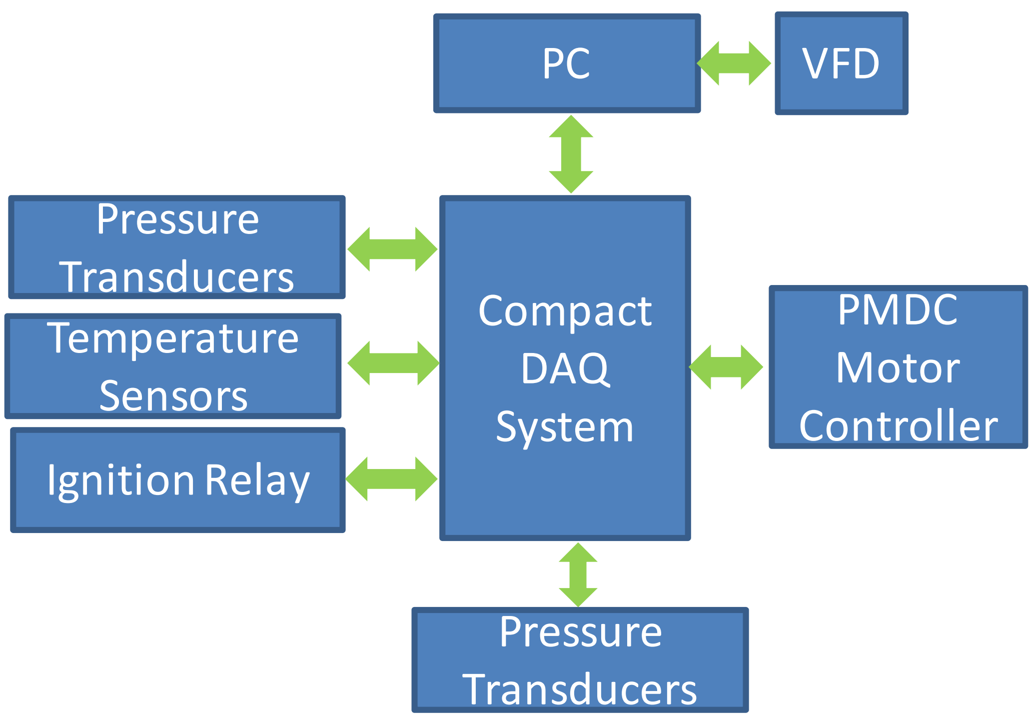

Figure 7: DAQ and control system S block diagram.

Engine Start and Power Production

The WDE uses a starter motor-generator to spin the engine up to the testing intended operational speed, and to monitor and dissipate power while the engine is producing torque. The WDE test facility utilizes mainly two different motors for this purpose, one suited for low-speed tests, and one suited for high-speed tests (Figure 8, and Figure 9, respectively). The low-speed Thingap motor is rated for 1.5 kW at 6,800 rpm. It is controlled by an Advanced-Motion-Controls B100A40AC DC motor drive. The high-speed motor is a custom-designed, PMDC motor capable of 30 kW at 30,000 rpm. This motor was designed specifically for the WDE by the Power Electronics and Drives Laboratory. It is controlled by a Yaskawa A1000 series CIMR-AU2A0040FAA variable frequency drive. This high speed motor is designed for constant-torque operation for up to 30,000 rpm.

Figure 8: Low-speed Thingap PMDC motor on custom mount.

Figure 9: High-speed motor designed and bulit by Electrical Machines and Drives Lab

Speed, power, and torque can be obtained from the motor controller feedback outputs. Engine speed is also measured by the motor controller, and is verified and calibrated using a tachometer. Starter motor-generator power can be calculated from the torque output and the shaft speed. Pressure sensors used are Dwyer Instruments's IS626 series pressure transducers. Both RTDs and thermocouples are implemented for temperature monitoring. Fuel and air flow control and monitoring is performed by two Omega FMA-2600 series mass flow controllers, capable of 1500 standard liter per minute (slm) of air and 50 slm of fuel, respectively. Ignition is controlled simply by a relay output wired in series with the ignition enable on the ignition modules.

Pre Test Debugging

An iPad is used for system maintenance, setup and testing, as shown in Figure 12. A remote log-on program allows the operation of the Labview interface, consequently, the whole test cell to be run from the iPad. This helps debugging before testing, because each aspect of the system can be controlled safely from within the test cell, and every system operation can be manually verified before the room is sealed and the test begins. The iPad can also control the entire test from the operator hands from directly outside the door and. This technique is also used to verify the engine operability before running a test matrix.

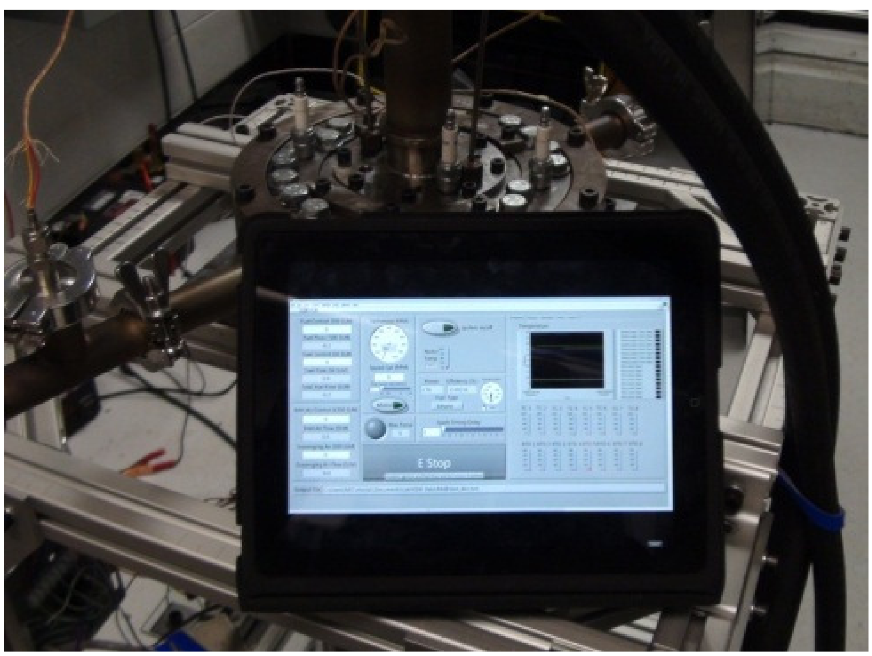

Figure 10: Labview interface on Ipad.

Pressure and Temperature Measurments

Monitoring pressure and temperatures inside the engine during combustion, specifically pressure variations both between channels, and before and after combustion, allows studying combustion phenomena, how sealing and pressure are related, and track changes for different operation modes. In addition, isolated, high-temperature, high -speed thermocouple elements can be used to monitor the temperature of the fluid inside the channel(s) and Ion probes can be used to track flame propagation.

Several custom high sensitivity differential pressure transducers, and high-temperature high-speed thermocouples assemblies were built. Figure 13 (left) shows a custom pressure transducer assembly. It consists of a small Honeywell transducer, which can be easily configured to give absolute or differential pressure. First sensors with a maximum range of +5 and +1 psi were built. These sensors are carefully shielded from the high harmonics created by the ignition system and the starter/generator drive. A temperature sensor is shown in Figure 13 (right).

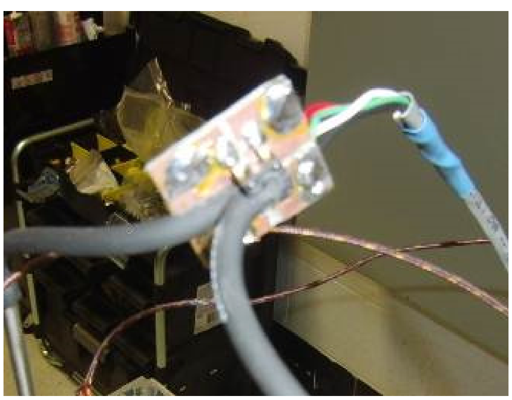

Figure 11: Pressure (left) and temperature (right) sensors.

Conclusion/Future Plans

The test facilities include several rotating engines, two test cells, measurement equipment, and associated control systems. The goal of the WDE test has been to verify the new engine concept by measuring the power output of a prototype WDE. Quasi- constant-volume combustion has been successfully achieved within the rotating channels and the engine has produced power. Continuous efforts are being conducted to optimize and enhance the engine efficiency. A second generation versatile test engine for higher power output and efficiencies is in preparation.

TESTING

The WDE prototype testing, attempts to find the variables that have the strongest influence in the WDE's power, and efficiency output. Preliminary tests for different RPM, inlet-exhaust overlaps, spark-plug position, and injection type were done with a Monte Carlo approach to find what configurations would make the WDE self sustained and optimize them. Once the first prototype produced power the WDE has been thoroughly tested to correlate power to input variables. The input variables are: air mass-flow, fuel mass-flow, spark plug position, fuel injection position, inlet position and rpm. There are two types of tests, free spin to measure the RPM gain by combusting fuel and the second where the starter/generator drive is used to restrain the WDE and measure the power generated.

Preliminary tests were performed 'blindly', meaning there was no knowledge about the engine. There were many hypotheses but nothing for sure. These early tests were performed using the S/G drive as a restrain to check what power difference fuel burning made on WDE performance. Optimization of these preliminary tests showed the route to a self sustained power producing WDE. The main changes were done in fuel injection, ignition power and engine gaps. These results are not discussed since they led to modifications that worked but that have not been thoroughly studied. However, a first study on a power producing WDE prototype which relates performance to air fuel ratio, air mass-flow and fuel-mass-flow is discussed in this chapter.

Synchronization

The WDE design is modular and can have free positions for the inlet and the top plate to study performance vs. synchronization at different speeds. The objective is to find which configurations make the WDE have power output.

The wave disk engine uses shock wave compression before combustion to enhance its efficiency. The shockwave is produced when the air flowing from the inlet port through the channel at high speed, is suddenly blocked with the outer wall. This sudden closing of the exhaust port creates a moving shockwave that travels inside the channel towards the center of the rotor. The shockwave travels at the local speed of sound which depends on the gas temperature and specific heats. The pressure gain behind the shockwave is held inside the channel by closing the inlet port. Despite the shockwave speed is the same for every case, since the gas properties do not change, the timing of the WDE depends on the rotational speed. At different speeds the overlap between inlet and outlet can make a difference between getting a shockwave and losing the compression.

To further explain how the WDE works a single channel model is going to be explained in Figure 12:

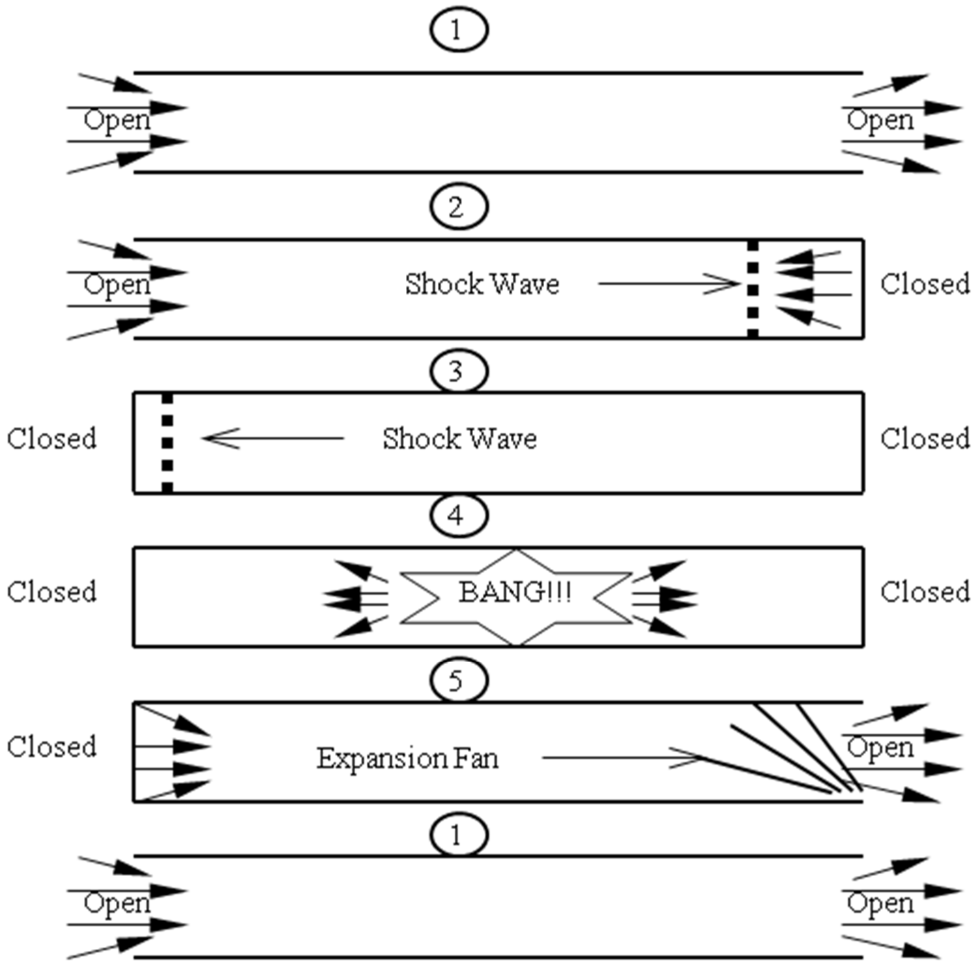

Figure 12: Single Channel Synchronization.

1. The inlet port and the outlet port are open and the air-fuel mixture moves freely in and out of the channel.
2. The moving shockwave is generated by the rapid closing of the exhaust port.
3. The shockwave pressure rise is kept inside the channel by closing the inlet port before the shockwave reaches the inlet port.
4. The air-fuel mixture is ignited at approximately constant volume, like in a piston engine.
5. After combustion has been completed the exhaust port opens and releases the high pressure combustion gas.

6. The inlet port opens again letting air-fuel mixture into the channel again, scavenging the low pressure combustion products towards the exhaust port starting again the process.

Figure 13 shows a WDE rotor. The shock wave travels from the outer edge towards the center. The channel length is ~7.00 cm. A moving shockwave travels (respect to the observer) at the local speed of sound towards the inlet port. The time it takes to travel the length of the channel depends on the gas temperature. However for the preliminary examination of the WDE, ambient air properties are assumed to calculate the shock wave speed, because we do not know yet the temperature the air fuel mixture reaches when it fills the channel. Another assumption is that a combustible mixture of methane and air has air properties; this assumption is safe because the air-fuel ratio is 17:1.

Figure 13: WDE-II Rotor

From gas dynamics, the angular distance traveled by the rotor, during the time the shockwave travels from the channel exit to the channel inlet, can be calculated with equation (1). Where '*a*' is the speed of sound, γ is the ratio of specific heats, R is the gas constant, air in this case, and T is the temperature of the mixture.

$$a = \sqrt{\gamma R T} \tag{1}$$

The time a shockwave takes to travel the channel is ~2.02*10E-4 s, the angle traveled by the rotor during this time at different RPM is calculated in Table 1. This is the angular overlap that should be used between inlet port and exhaust port when testing at a determined RPM.

RPM	Rad/s	Rotation During Shock Travel (rad)	degrees
1000	104.72	0.021	1.21
2000	209.44	0.042	2.43
3000	314.16	0.064	3.64
4000	418.88	0.085	4.85
5000	523.60	0.106	6.07
6000	628.32	0.127	7.28
7000	733.04	0.148	8.49
8000	837.76	0.169	9.71
9000	942.48	0.191	10.92
10000	1047.20	0.212	12.14
11000	1151.92	0.233	13.35
12000	1256.64	0.254	14.56
13000	1361.36	0.275	15.78
14000	1466.08	0.297	16.99
15000	1570.80	0.318	18.20
16000	1675.52	0.339	19.42
17000	1780.24	0.360	20.63
18000	1884.96	0.381	21.84
19000	1989.68	0.402	23.06
20000	2094.40	0.424	24.27

Table 1: Angular overlap between inlet and outlet for different RPM

After the overlap between inlet and exhaust port is calculated a position for the spark plug and the injector is chosen. Theoretically premixed air-fuel mixture would have a better performance than direct injection, however both are tested to see differences and make a performance analysis. WDE-II has written numbers (Figure 14) to locate the top plate and the inlet. This numbers help to have repeatability for the experiments, random positions are impossible to repeat and consequently finding consistency between different tests is not possible.

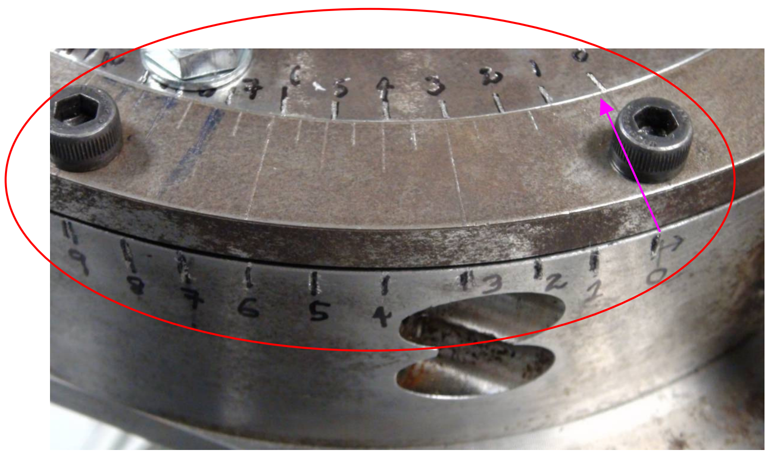

Figure 14: Numbering of the WDE at the timing ring and the top plate.

Power Calculation

For all the tests power is the output variable that best describes the WDE performance. Power is measured in two different ways using the S/G drive or making a calculation of acceleration over a free spin test from RPM data. In preliminary tests the first method was used since it provided a good enough power data. **Error! Reference source not found.** shows the control system interface in which RPM, air, and fuel mass-flows were the input, and depending on the type of test power or RPM were the outputs. Once the WDE was self sustained, power measurements from the S/G drive were not accurate enough since they were affected by the performance curves of the S/G drive and the control system, which could not be implemented in a constant. Then the rise in RPM by free spinning is a good indicator of the accelerating power and can be better used to do forecasting of the WDE performance.

The power from a free spinning is calculated with equations (2),(4), and (4). M_{Gas} and $M_{Bearings}$ are the momentums contributed by the gas expansion propelling the rotor and dissipated by the bearings, which are the main sources of power and dissipation respectively. These two momentums change with respect to the RPM and the temperature of the engine and are not calculated separately at this point. The system final momentum multiplied by the rotational speed yields the power produced during the acceleration of the WDE.

$$\sum M_{gas} - M_{bearings} = M_{System} = I_{system} * \alpha \qquad (2)$$

$$Power_{System} = M_{system} * \omega \qquad (3)$$

$$I_{system} \approx I_{Rotor} + I_{Spindle} + I_{sgdrive} \qquad (4)$$

The inertia of the system is calculated from the rotating parts: Rotor (Figure 13), Spindle, and Starter-Generator Drive (Figure 15). The inertia of the rotor and the spindle were calculated using the CAD program in which they were designed. The S/G drive inertia was part of the user information provided by the manufacturer.

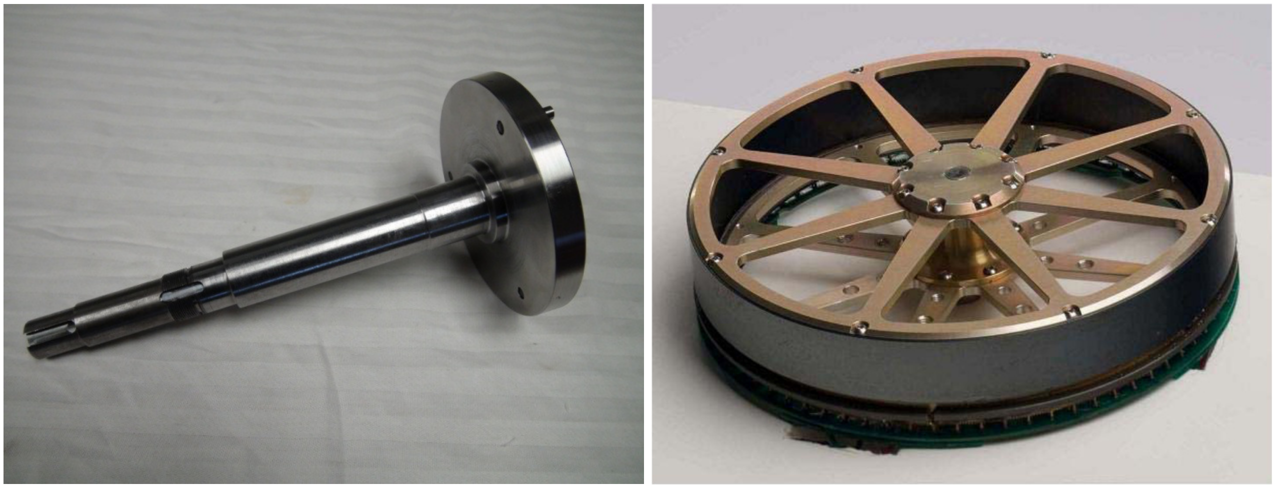

Figure 15: Spindle and Starter Generator Drive

Table 2 shows the inertia of the system used to calculate the free spin power of the WDE.

Part	Inertia (mm^2*kg)
Rotor	18917.39
Spndle	849.64
S/G Drive	7000.00
Total	26767.03

Table 2: Inertia of the System

Rotational acceleration is calculated from the data sheet Lab View records from each test. During the test Lab View records airflow, fuel-flow, rpm, time step and temperature. A numerical derivative taking the RPM in time steps *(i+1) –(i),* converted into rotational speed (rad/s) and divided into the size of the time step gives the rotational acceleration α (rad/s^2) of the WDE.

Power Tests

A power producing WDE has been tested to understand the influence of equivalence ratio, air mass-flow, and fuel mass flow on performance. This understanding can help to devise the next design steps. In this study 10 tests were analyzed; in half the tests the WDE produced power and the other half did not. These tests have thousands of data points and are analyzed graphically to better observe the difference between them

The WDE start speed is reached by using a reaction turbine principle. A compressed air line feeds the engine and spins the rotor. This line also works to simulate a supercharging effect of the engine. The maximum capacity of the air line is 1500slm which in a standard configuration can spin the WDE up to ~1550 RPM. Every test starts by spinning the rotor to 1200RPM then setting the air-flow to the test objective (500slm, 900slm, 600slm…etc) and starting the fuel and ignition once the rotor speed goes down to about 1000RPM. Once fuel and ignition are activated there are cases where there is flame outside the exhaust and no power produced (Figure 17) and cases where the flame is contained inside the rotor and power is produced (Figure 16).

Figure 16: Sequence of a Power Producing Test

The visual difference between a power and a no-power producing test are shown in Figure 16 and Figure 17. Figure 16 has six consecutive frames from Test 539 video. At this point fuel and ignition are activated. Frame A shows the WDE with no combustion happening. Frames B and C shows an explosion produced right before the spin up of the WDE, and then frame s D,E and F show a blue flame tail attached to the exhaust. Figure 17 has 8 frames from Test 546 video, at different points during the first 2 seconds of ignition. Frame A shows the WDE with no combustion. Frame B shows mild combustion happening. Frames C, D and E show an increase in the luminosity of the flame at the exhaust. And frames F,G, and H show a very brilliant red flame outside the exhaust.

- Power producing tests have an explosion before starting power production (Figure 17)Figure , frames B &C); the other tests have no explosion.

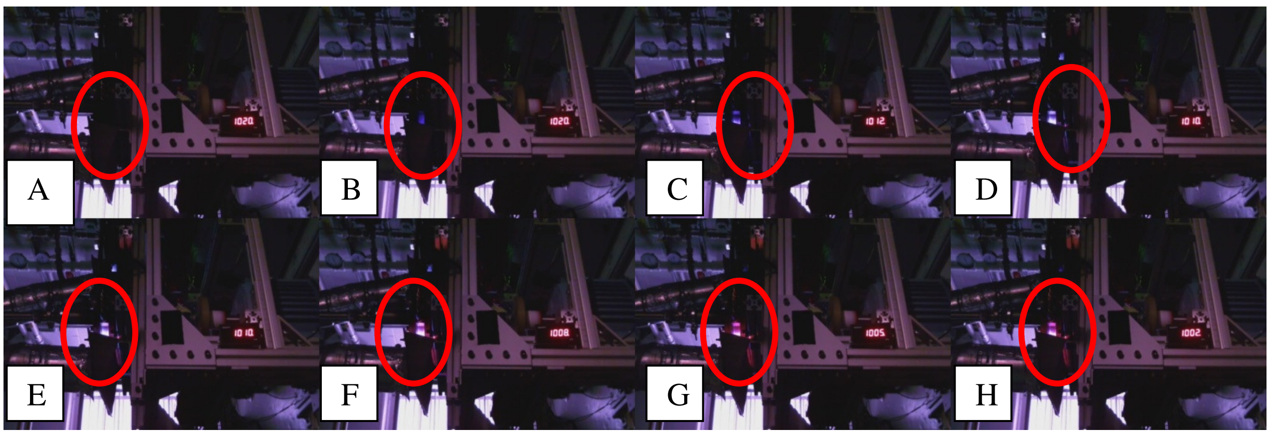

Figure 17: Sequence of a Non-Power Producing Test

A typical graph of RPM vs. Time has four sections. The first one shows the increment of RPM from 0 to ~1200 (Figure 18, Orange Line). Section 2 typically has negative slope (Figure 18, Yellow Line), called initial because is where the inputs are set to the test objective; ‘initial’ is more or less pronounced according to the airflow of the test. When power is produced a third section with positive slope appears (Figure 18, Green Line), it is called ramp up because starts when fuel is injected and ignited, and typically shows acceleration of the rotor. ‘Ramp Up’ comes after ‘Initial’ in the graph; it shows the rise of RPM due to fuel burning. Finally, in the cases where power is produced, there is a last section with a highly negative slope which reflects seizing (Figure 18 Red Line), called Ramp Down.

The main objective of this study is to understand the 'Ramp Up' section (Figure 18, Green Line) to find correlations between power produced and input variables. The 'Ramp Up' section occurs only when the WDE has acceleration due to combustion. There are cases where there is no change of slope in which no seizing is observed either.

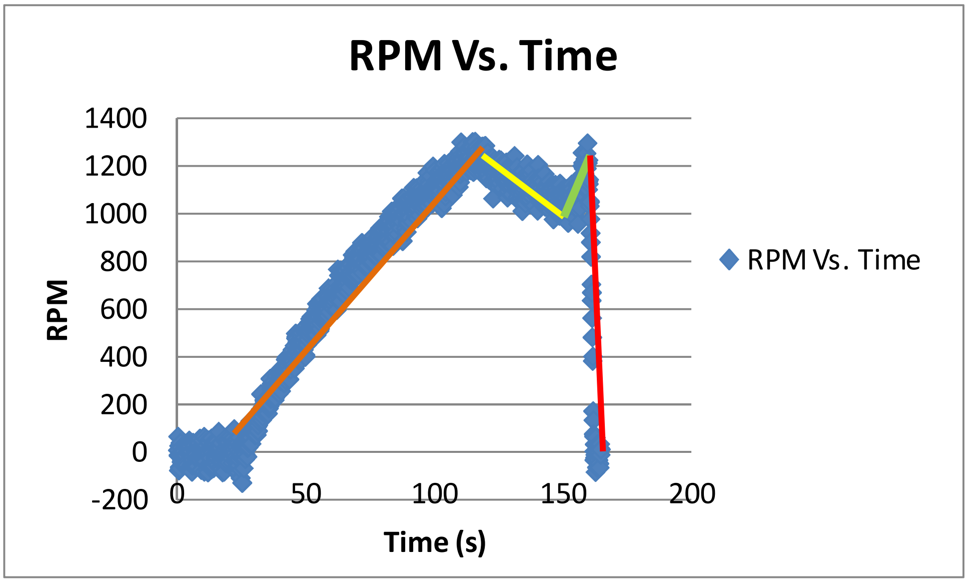

Figure 18: RPM Vs Time Graph with Analysis Explanation.

Test analysis is made for the data after the initial spin section (Figure 18, Orange Line). The first section analyzed is called "initial", and refers to the section of the graph where air has been set to the test objective and the rotor slows down, the graph looks like a mild negative-slope section of the graph. Then there are two cases, power produced or not. When there is no power the negative slope section continues, but when there is power there is an inflexion

The stage of development of the WDE limits our observations to a few seconds, when power is produced. After a short time the rotor thermal expansion is higher than the outer ring thermal expansion and the rotor seizes.

The tests are numbered 539 to 549 excluding test 542. Table 3 shows the inputs for each one of the tests, where φ [14] is the equivalence ratio and Φ [15] is the normalized equivalence ratio. Table 3 has a color code to observe that Φ was kept constant for several tests to set apart the influence of air-flow and fuel-flow from equivalence ratio.

Inputs						
	Air Flow (SLM)	**Fuel Flow (SLM)**	**$(A/F)_{stoich}$**	**$(A/F)_{test}$**	**φ**	**Φ**
Test 539	900	32	15.98	28.13	0.568	0.362
Test 540	500	20	15.98	25.00	0.639	0.390
Test 541	500	17	15.98	29.41	0.543	0.352
Test 543	600	24	15.98	25.00	0.639	0.390
Test 544	600	18	15.98	33.33	0.479	0.324
Test 545	700	21	15.98	33.33	0.479	0.324
Test 546	600	18	15.98	33.33	0.479	0.324
Test 547	500	17	15.98	29.41	0.543	0.352
Test 548	1200	36	15.98	33.33	0.479	0.324
Test 549	550	17	15.98	32.35	0.494	0.331

Table 3: Test Inputs.

For each one of the tests four graphs are presented: RPM vs. Time for the whole test, then a zoom in the ‘intial’ section, then a zoom in the ‘ramp up’ and lastly a zoom in the ‘ramp down section. After individual test results an analysis of the 10 tests ‘ramp up’ section is done where an average power during ‘ramp up’ is calculated to approximate the power produced by the WDE. This calculation only approaches the ‘Gas On’ accelerating power.

Test 539

Test 539 is a reproduction of a test where preliminary experiments found consistent power production. At lower airflows, power production can depend also on equivalent ratio and engine temperature. This test shows a clear 'ramp up' section and its graph shows a good correlation coefficient to the fitting curve.

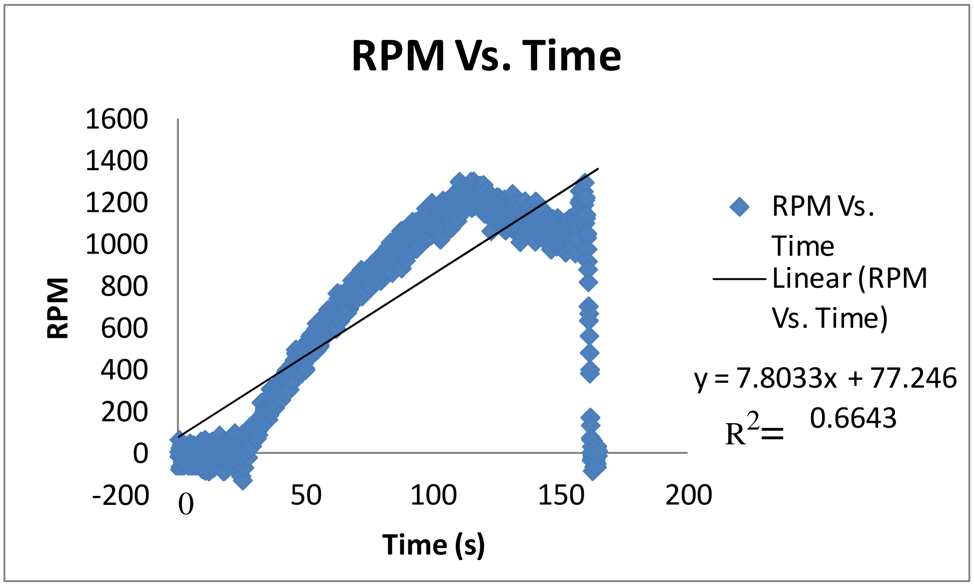

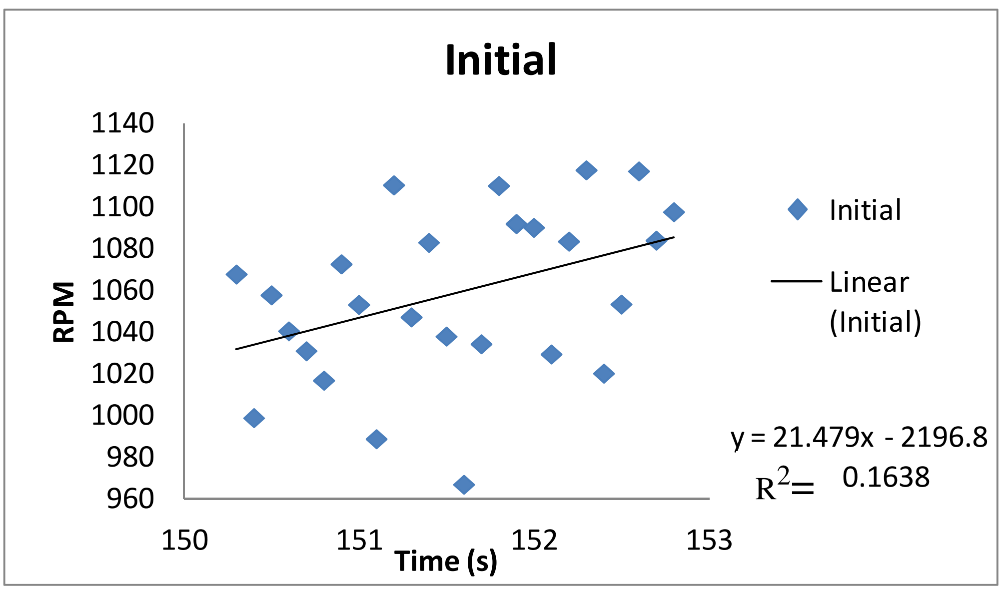

Figure 19: Test 539 Performance Graphs.

Figure 19 (Cont'd)

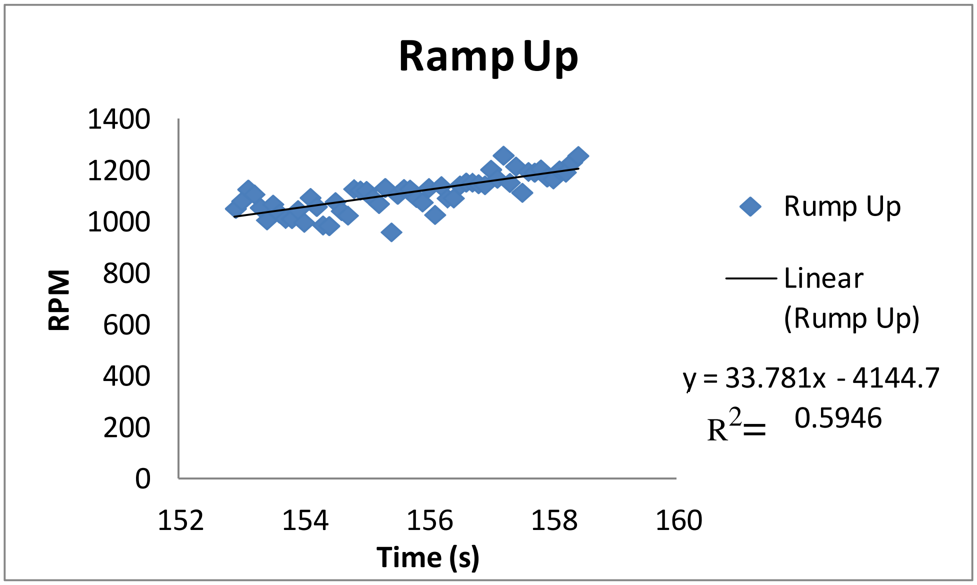

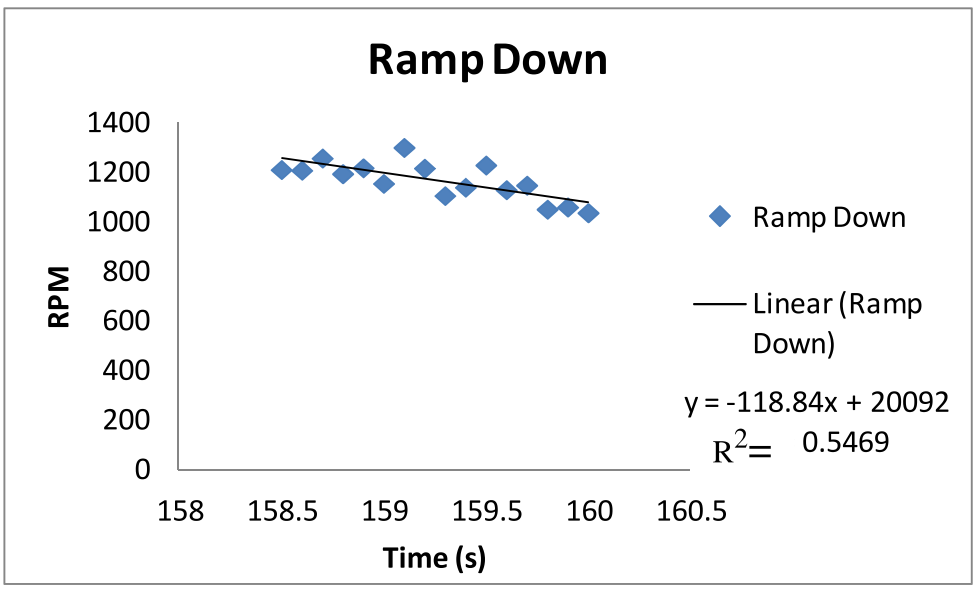

Test 540

This test has a very small 'ramp up' section. Low power is produced, followed by fast seizing. However power is positive, seizing is the best indicator of strong combustion happening inside the rotor. When combustion happens outside the rotor, or is mild the rotor does not seize until after a long time, preliminary tests have had up to 30 minutes running with mild combustion.

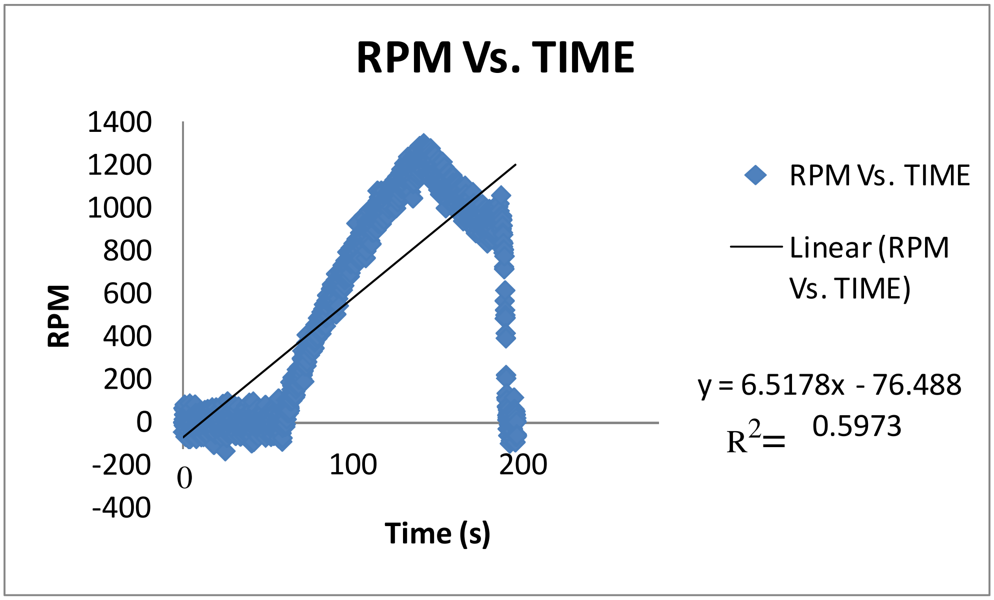

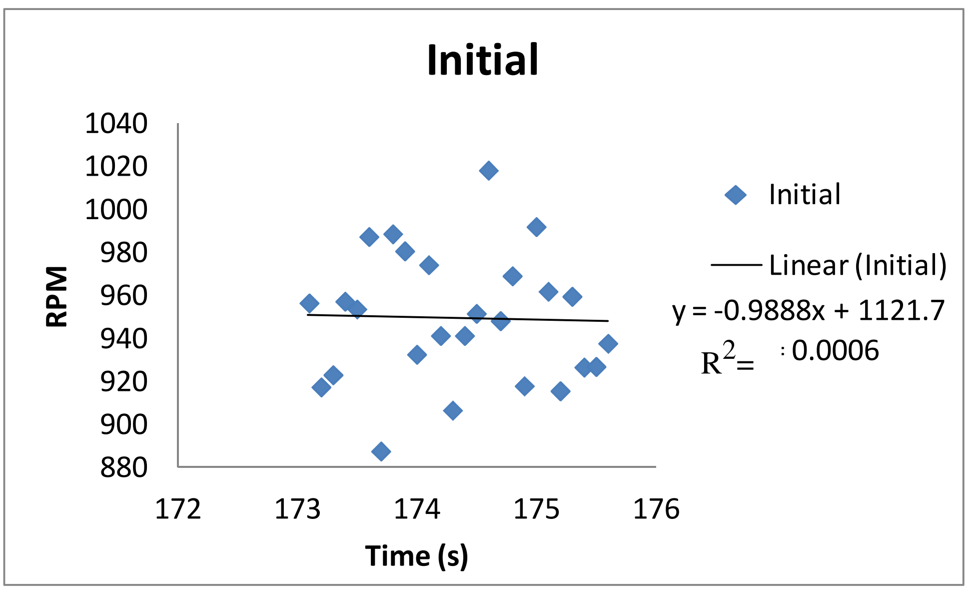

Figure 20: Test 540 Performance Graphs

Figure 20 (Cont'd)

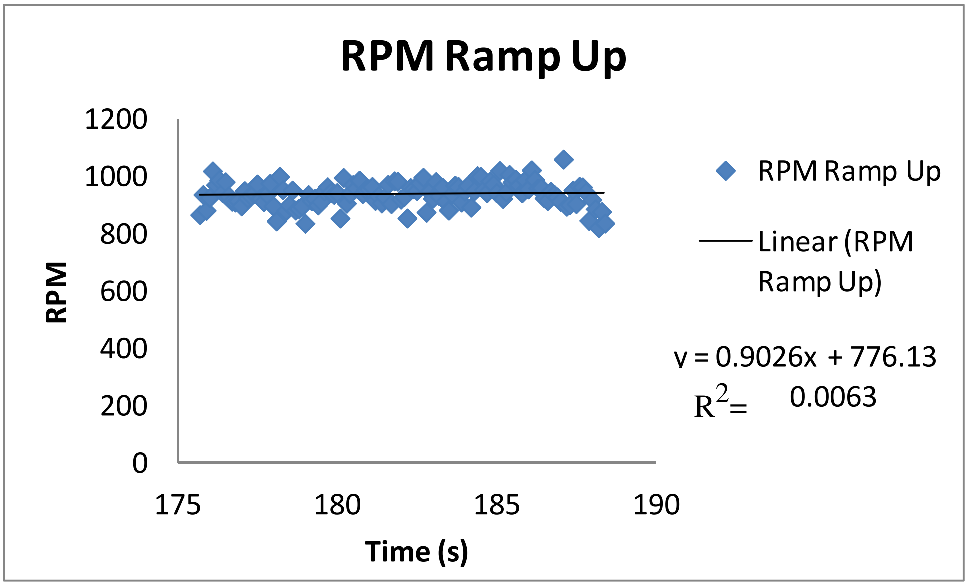

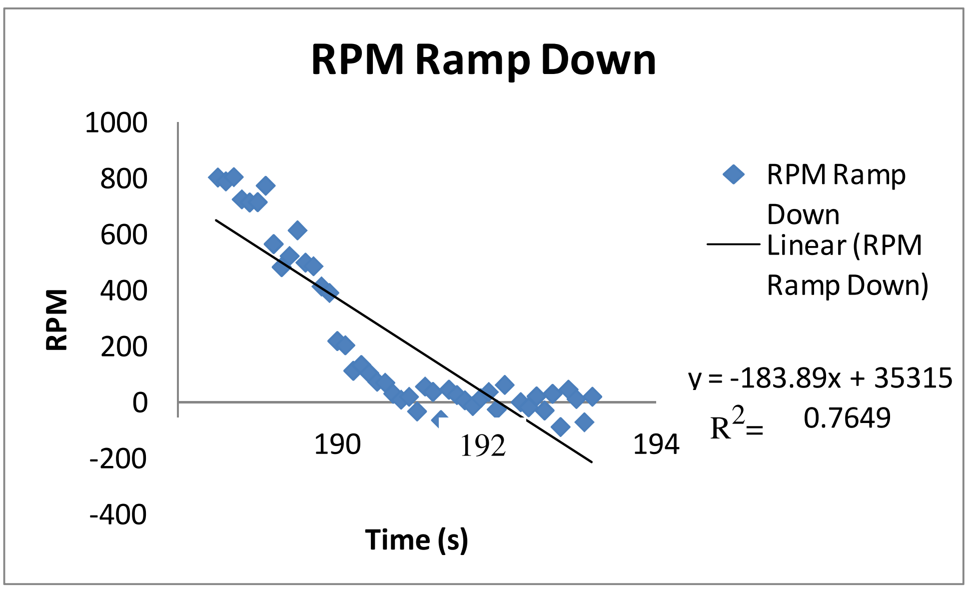

Test 541

In this test the WDE has two power producing stages which are very mild. The first one occurs right after injecting fuel and igniting, and the second one occurs after running for awhile with outside flame. The first power production part occurs with some strong explosions that alternate from one exhaust to the other; this situation happens randomly and cannot be related to a specific input variable yet. After that the WDE settles for combustion outside the exhaust and suddenly it jumps to power producing. The strength of this two power producing stages can be notice in the video because the WDE rises its speed by about 100RPM however is hard to notice in the test graphs because the data cable from the tachometer captures enough noise to cloud changes of less than 50 RPM.

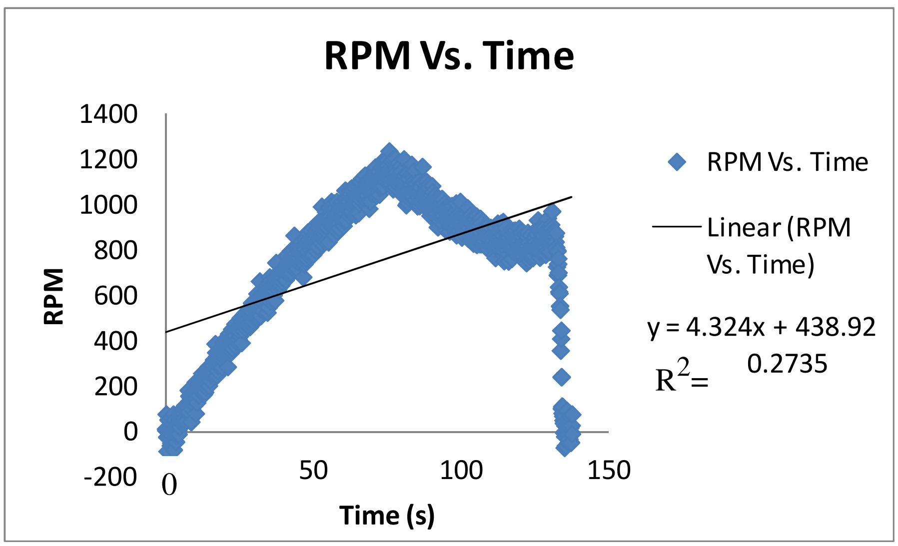

Figure 21: Test 541 Performance Graphs

Figure 25 (Cont'd)

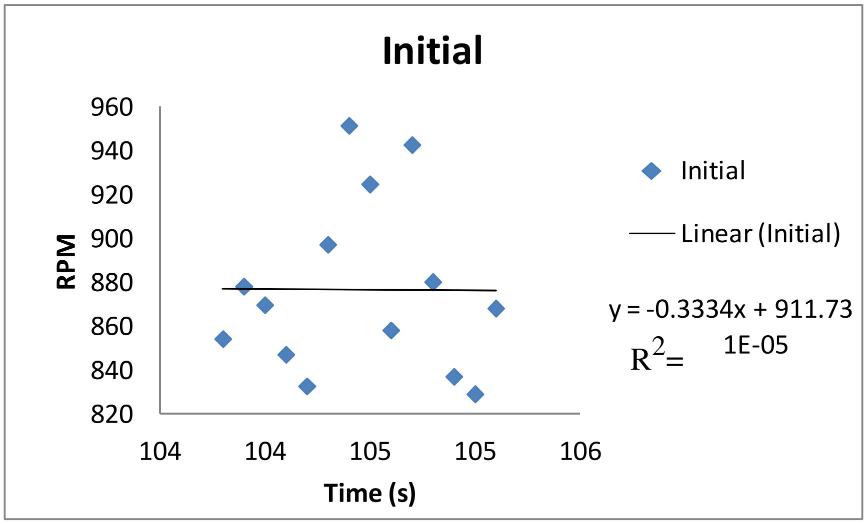

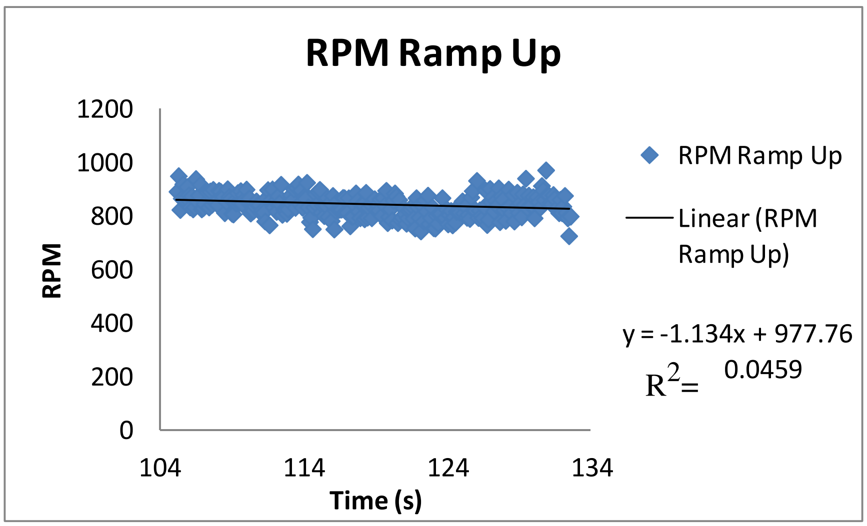

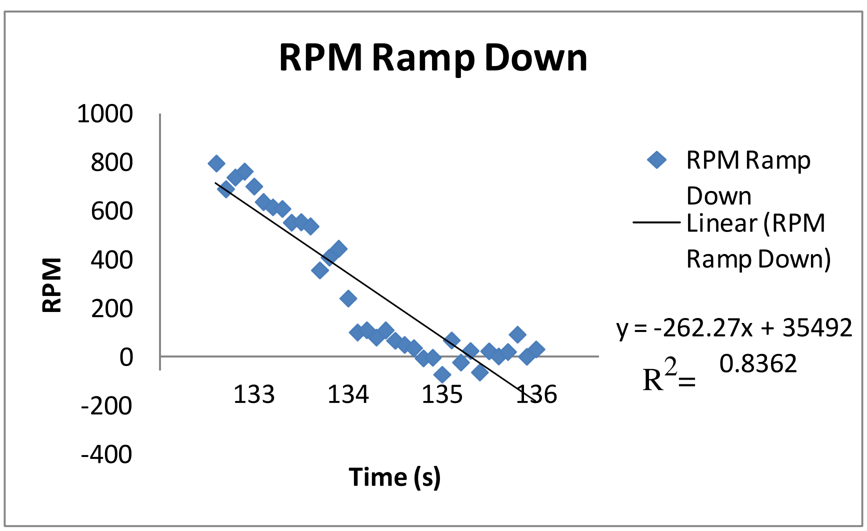

Test 543

Test 543 produces power almost instantly at the time of fuel injection and ignition. When watching its video is clear that the engine is producing power, the time and intensity are not long or strong enough and blend with the noise of the control system and the correlation coefficient is low because of this reason.

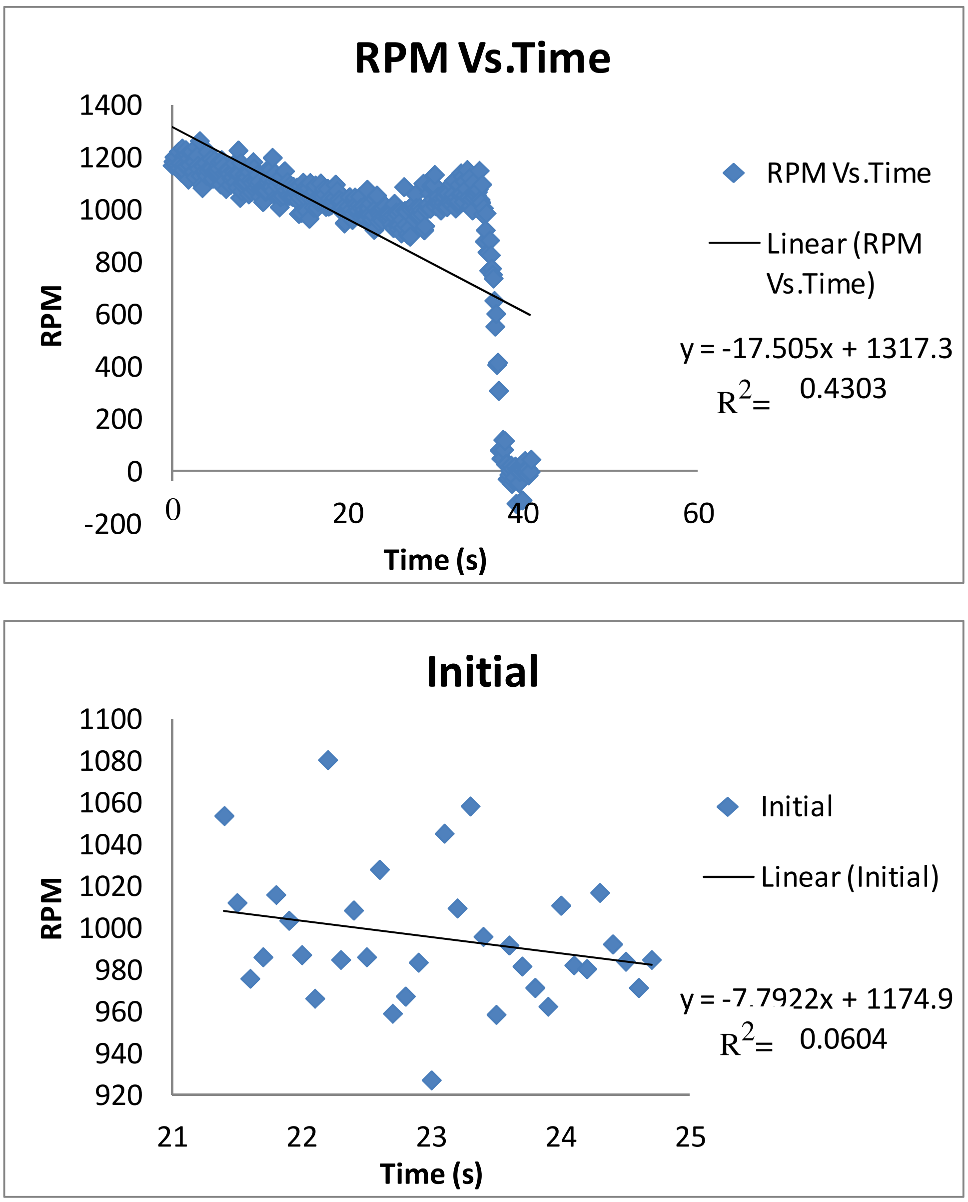

Figure 22: Test 543 Performance Graphs

Figure 22 (Cont'd)

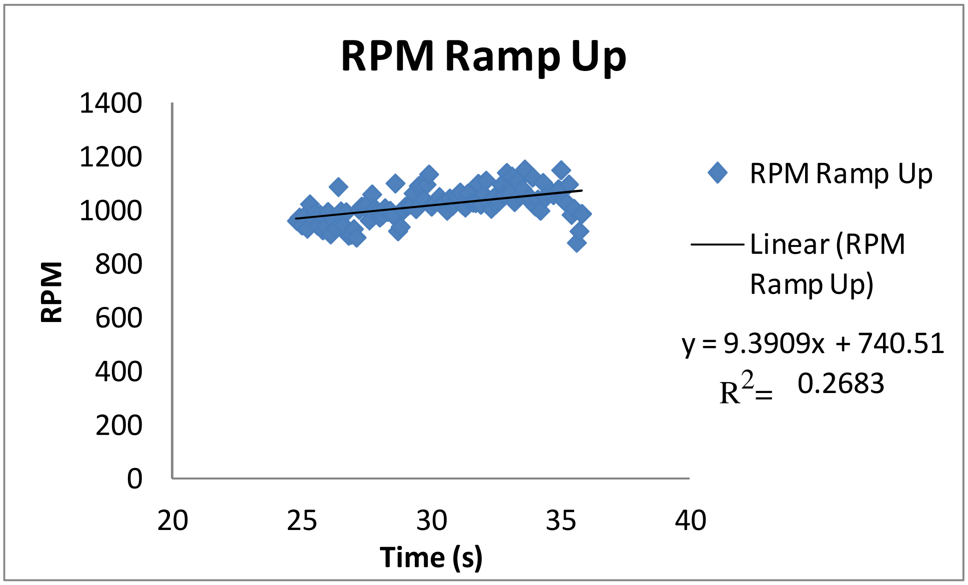

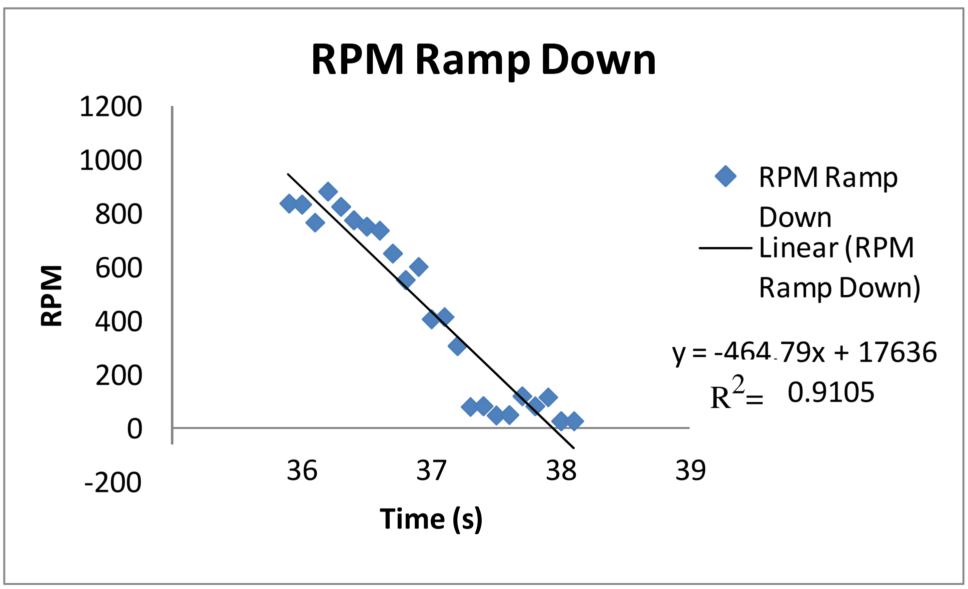

Test 544

Test 544 shows a ramp up part and then a fade out with no seizing. The video shows, right after ignition, consecutive explosions jumping from one exhaust to another accelerate the WDE for about 7s, and then combustions position itself outside the exhaust with a red flame and the WDE does not get to seize. Despite there is power production it does not happen in a controlled way nor can we repeat this situation by setting the inputs.

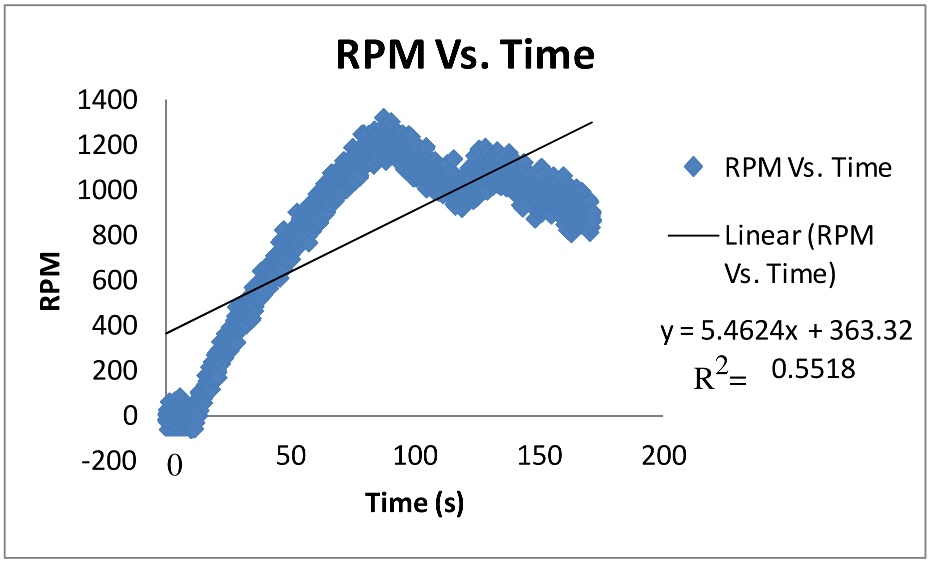

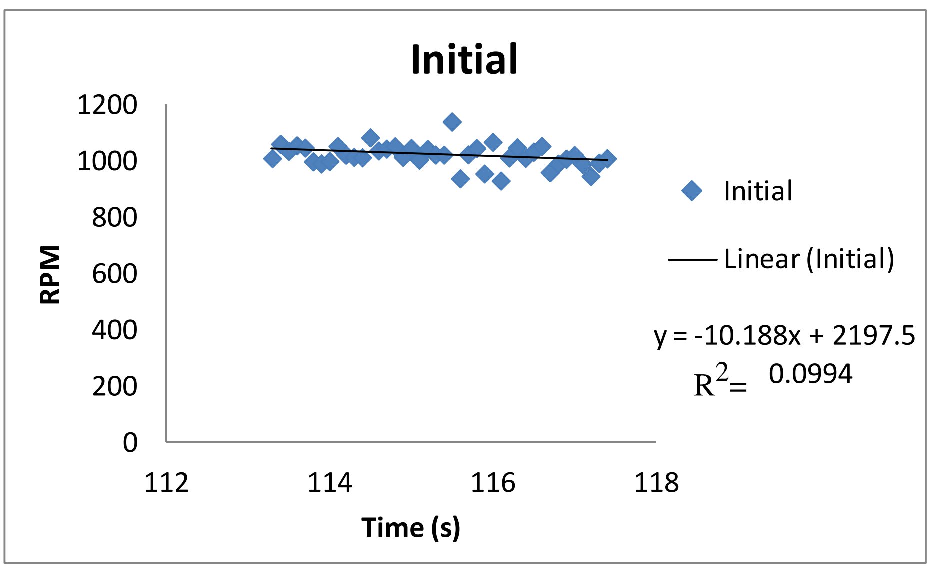

Figure 23: Test 544 Performance Graphs

Figure 23 (Cont'd)

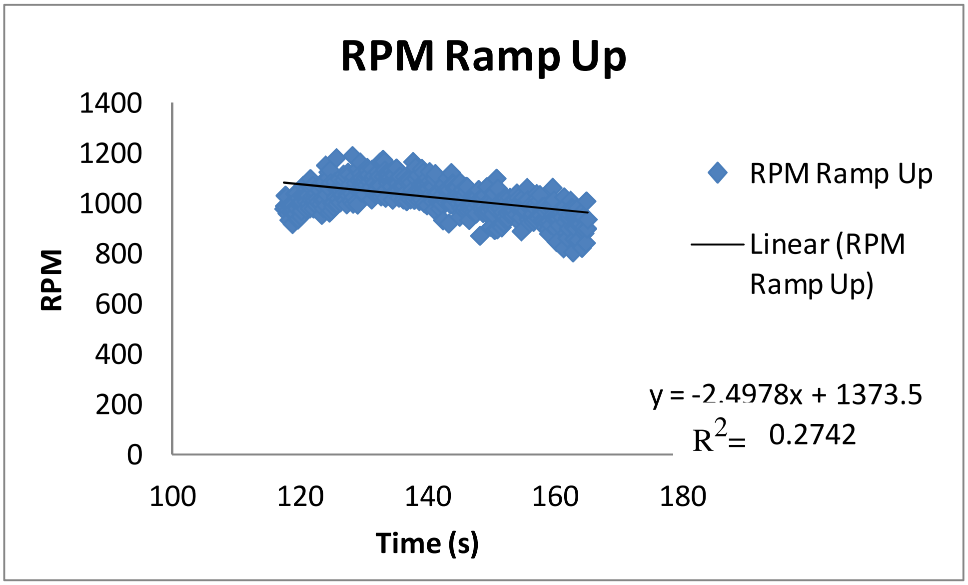

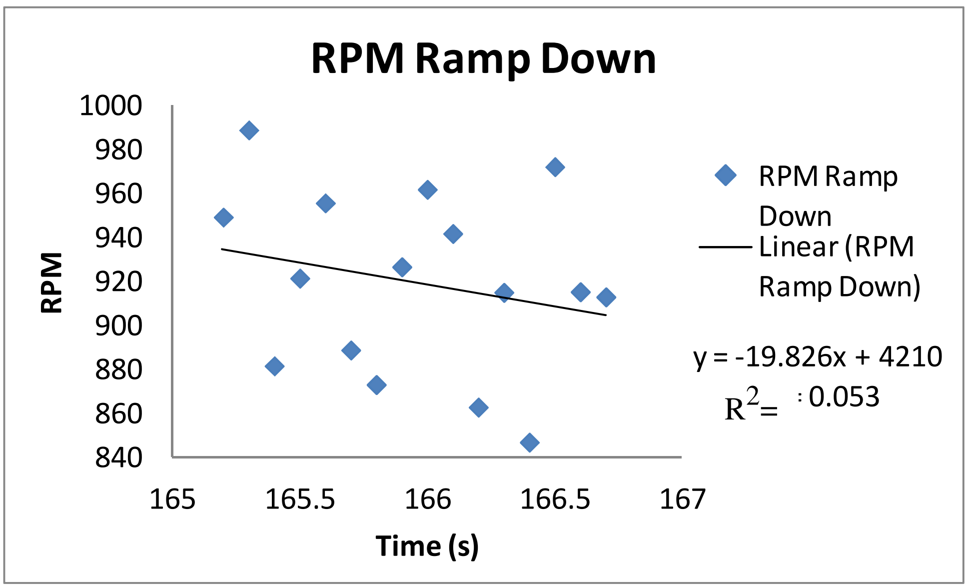

Test 545

Test 545 video shows few explosions jumping from one exhaust to another and then power production clearly happening followed by seizing. The correlation coefficient for the ramp up section is high and shows that the increase in RPM is stronger than the noise of the system, as opposed to test 543.

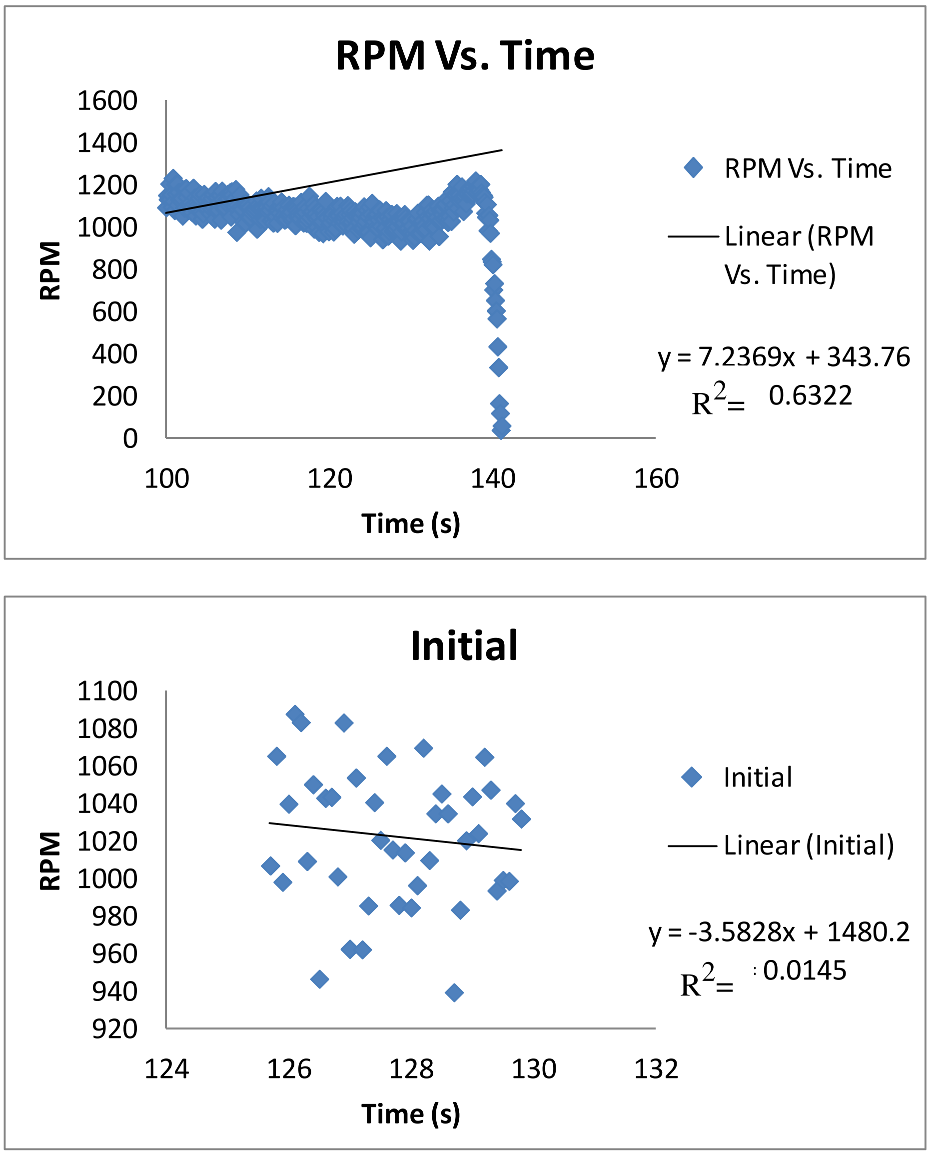

Figure 24: Test 545 Performance Graphs

Figure 24 (Cont'd)

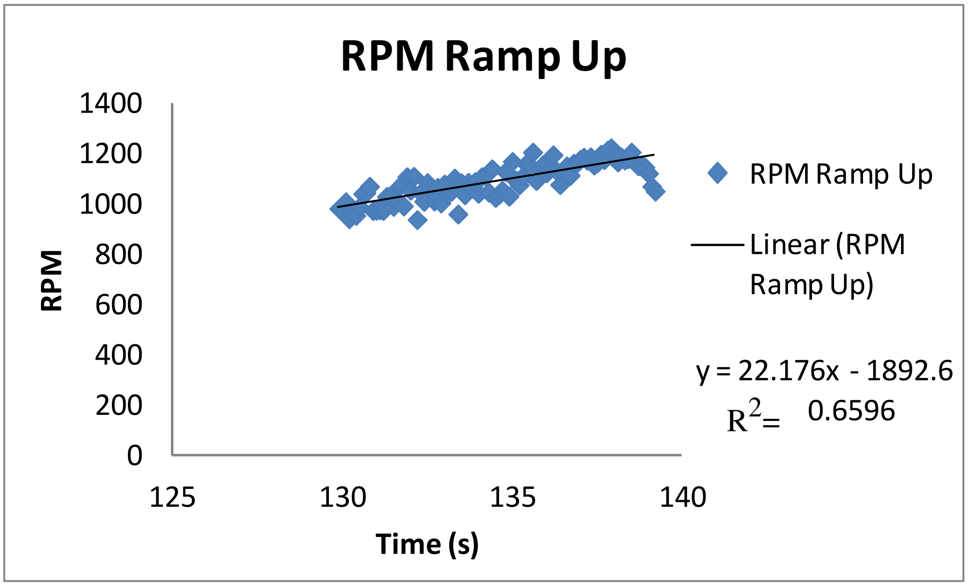

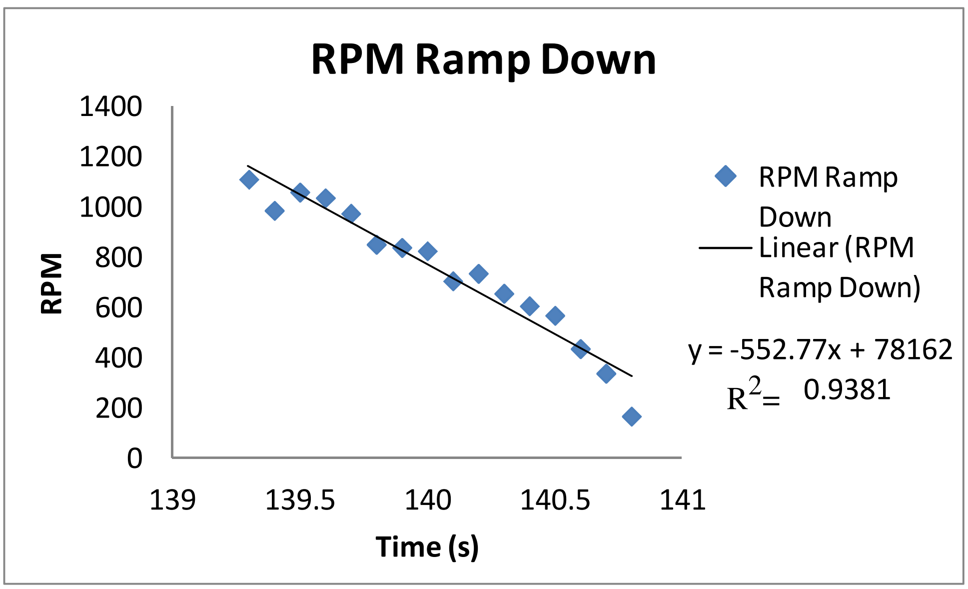

Test 546

Test 546 does not produce power. As can be observed in the graph of the complete test, there is no rise of RPM after air-mass flow was set to the test objective. The video shows ignition, a red flame outside the exhaust and then the RPM keeps fading out with approximately the same slope as in initial.

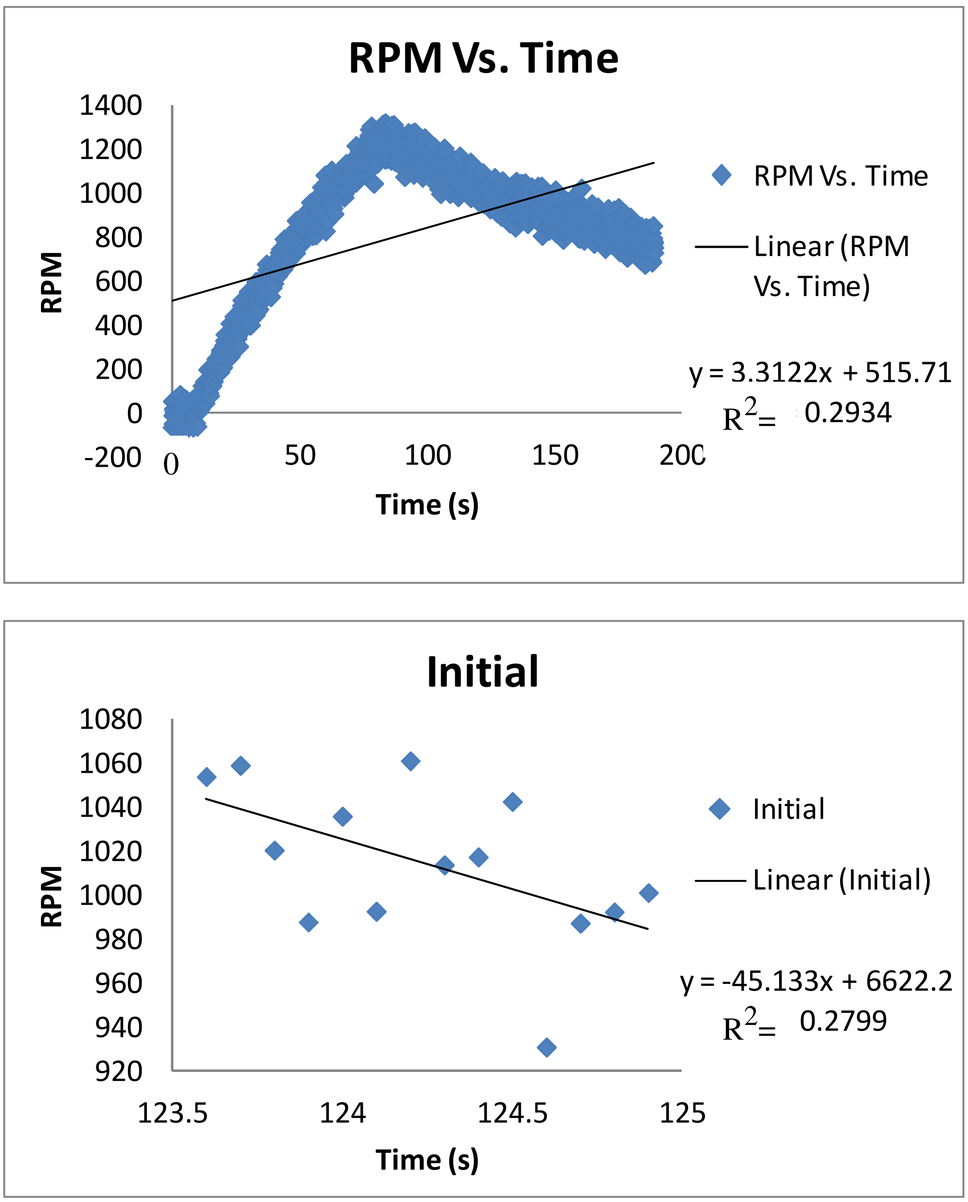

Figure 25: Test 546 Performance Graphs

Figure 25 (Cont'd)

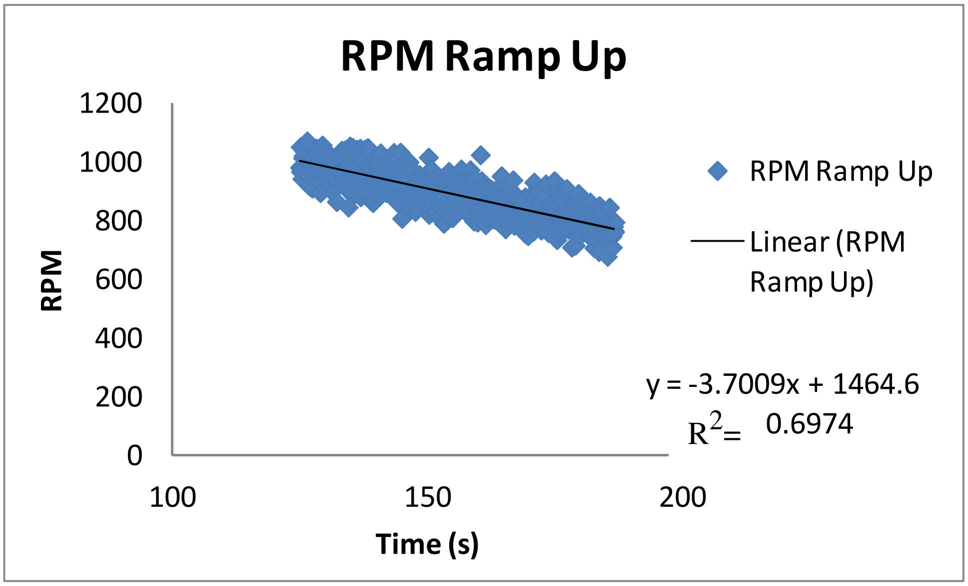

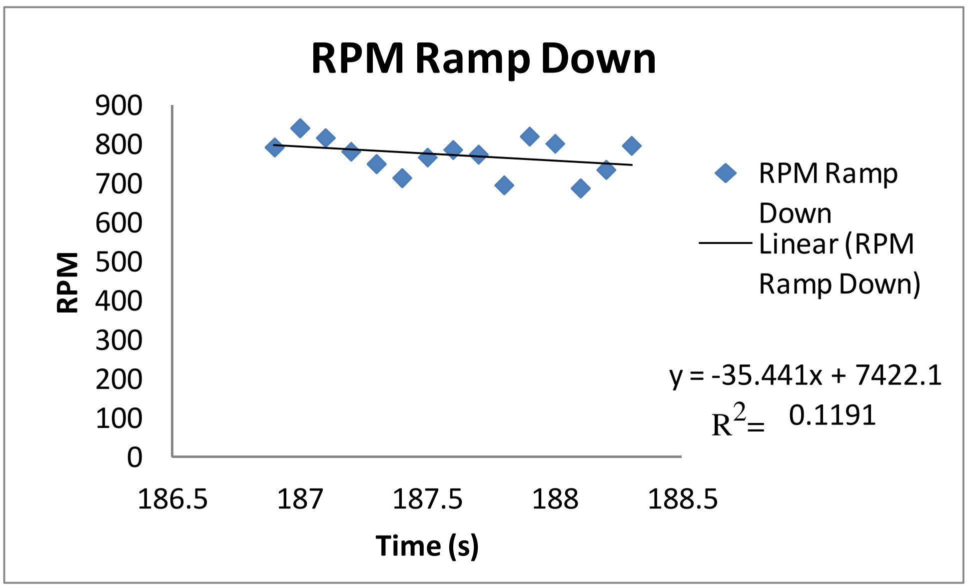

Test 547

Test 547 video shows right after ignition consecutive explosions that jump from one exhaust to another. Then combustion positions itself outside the exhaust with a red flame and the WDE does not get to seize for a while. At some point the flame outside the exhaust port heats up the pipeline of the ventilation system. Hypothetically the heat accumulated on the pipeline increases the ignition energy. Having stronger ignition makes the WDE change to power production for a short time. The power is produced with low intensity and lasts for a very short period of time. In the ramp up portion of the graph RPM blends with the noise of the system. However seizing is evident in the RPM Vs. Time graph, giving certainty about power production.

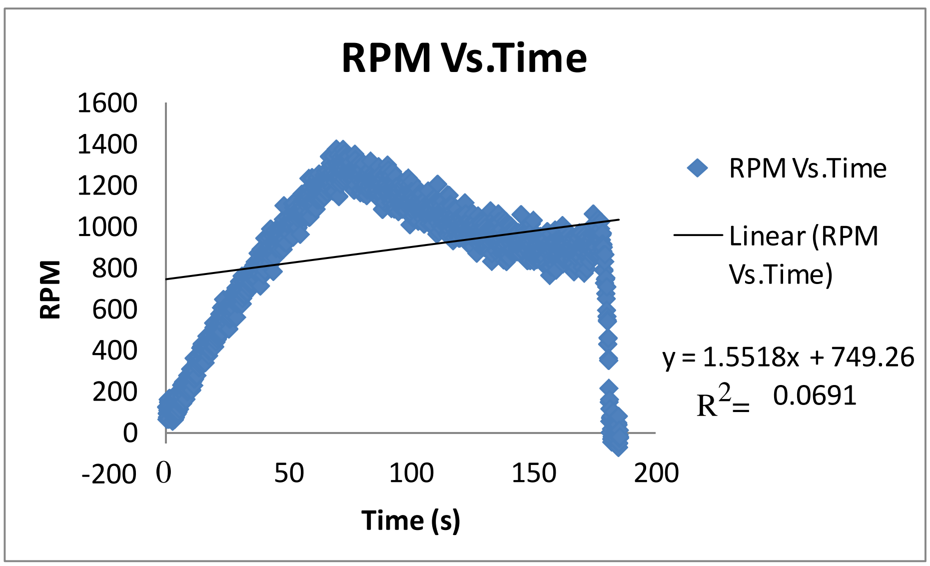

Figure 26: Test 547 Performance Graphs

Figure 26 (Cont'd)

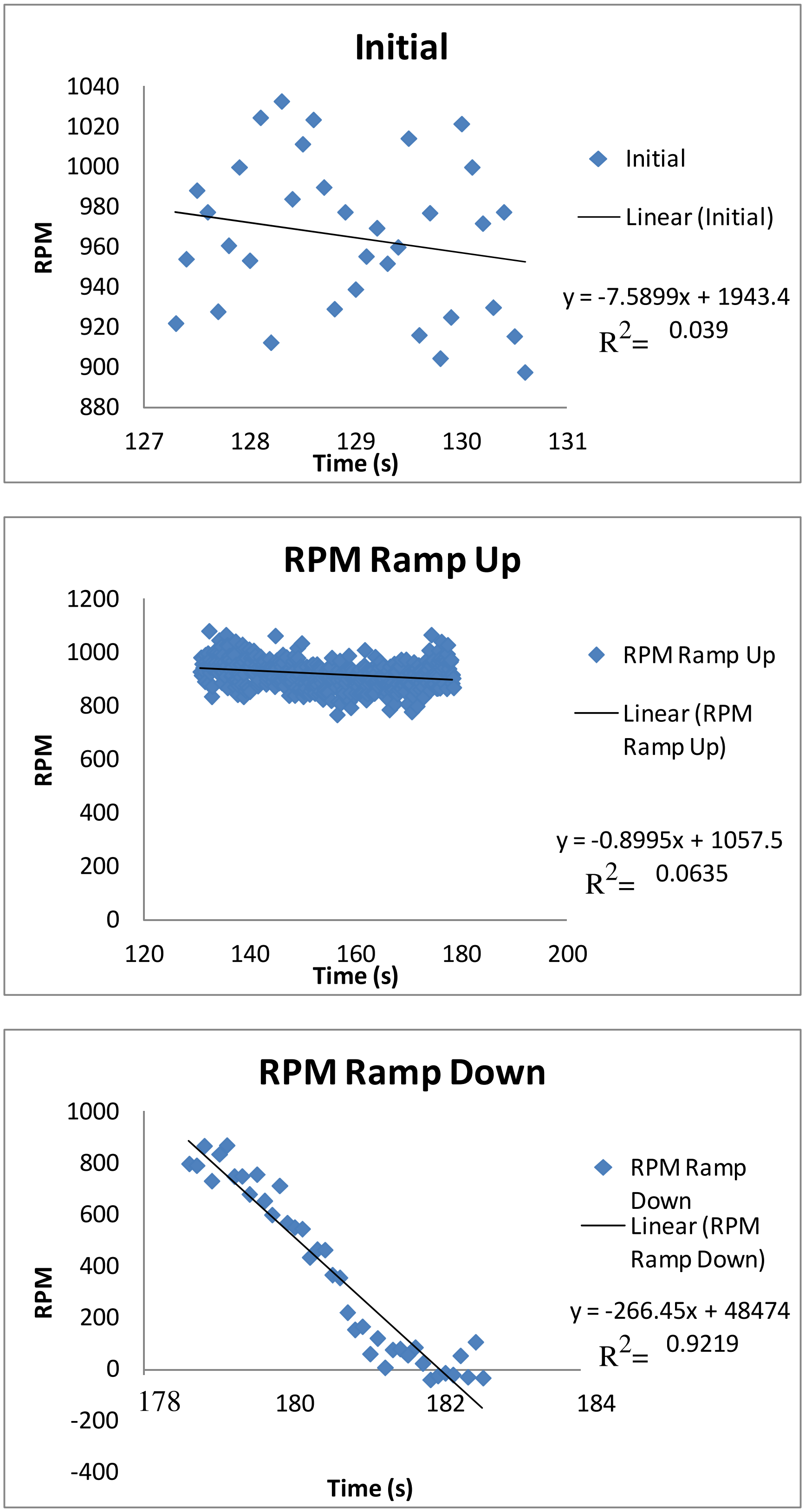

Test 548

Test 548 RPM Vs Time graph does not have the usual 'M' shape behavior as the other tests. In this case the airflow of 1200slm kept the rotor spinning up to ~1450. Fuel and ignition were activated once the WDE reached a plateau in RPM (around 1450 RPM). Then a clear ramp up section can be observed, and seizing after it. In the video after the initial explosion no flames could be observed at the exhaust, meaning all combustion happened inside the channel and seizing happened faster few seconds of running. This ramp up section has the clearest correlation coefficient to the fit line, meaning the noise of the system becomes irrelevant with this test conditions.

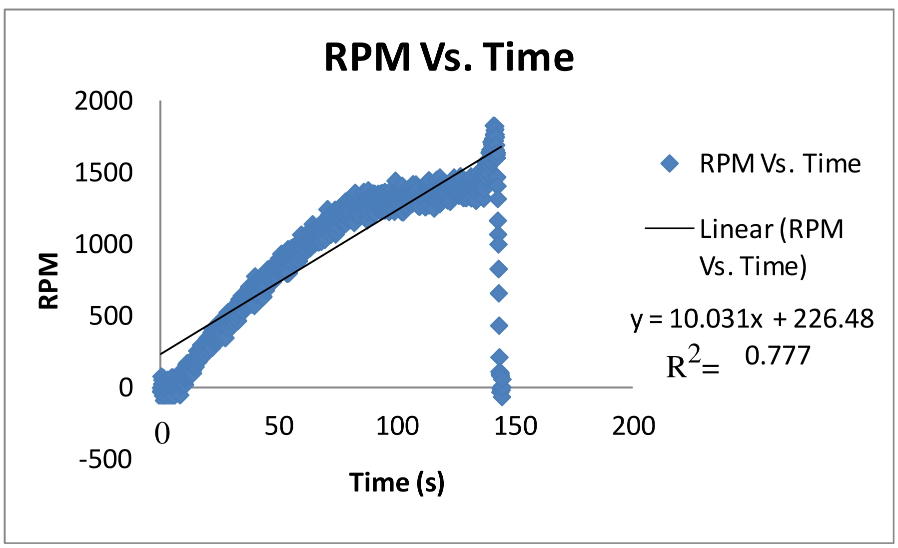

Figure 27: Test 548 Performance Graphs

Figure 27 (Cont'd)

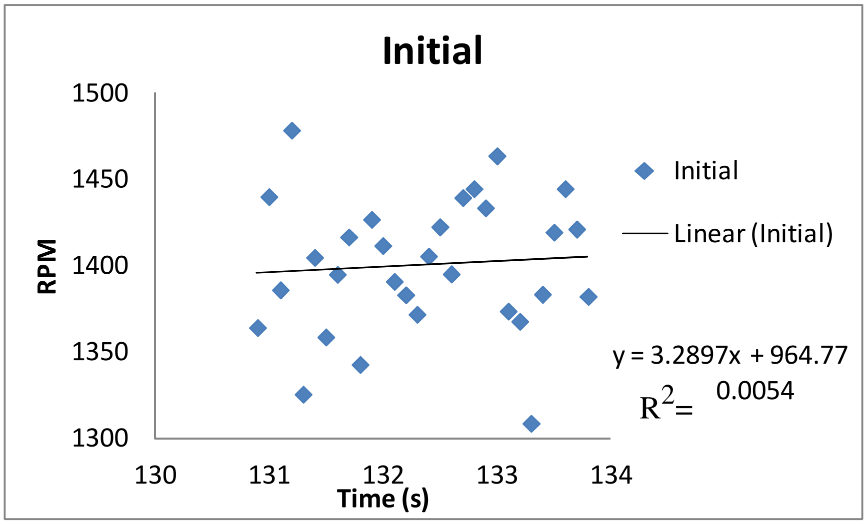

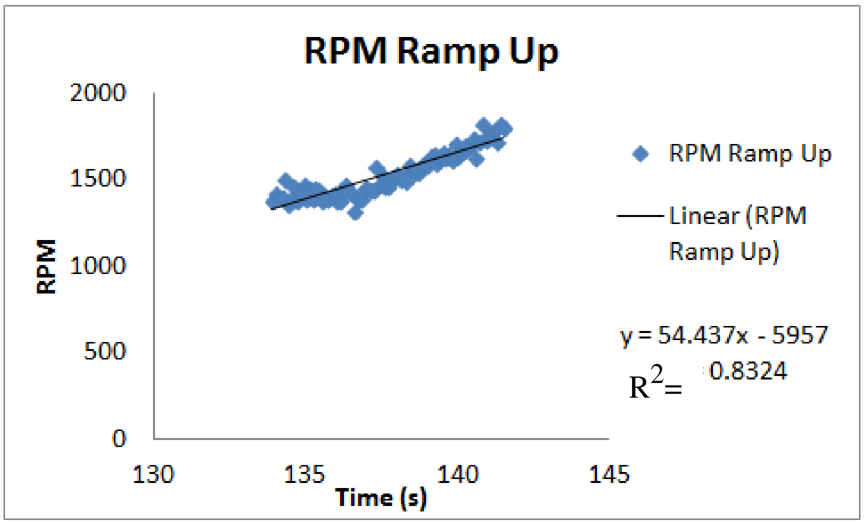

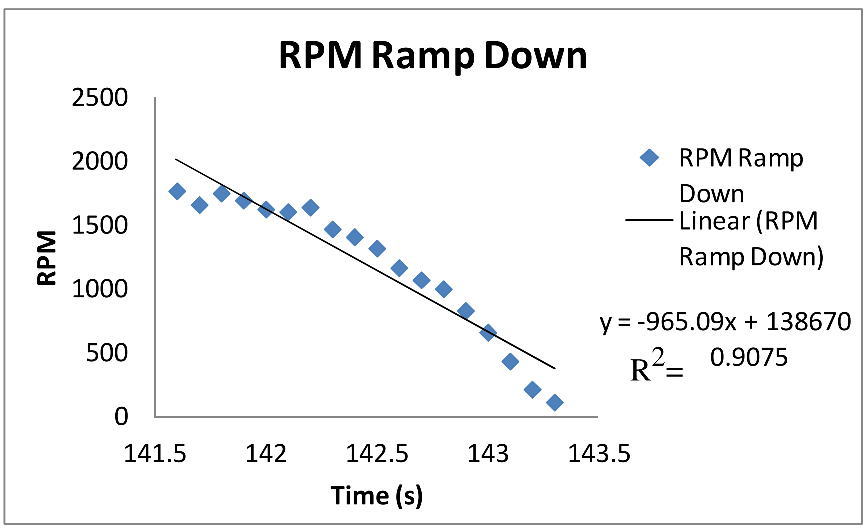

Test 549

Test 549 does not produce power. As can be observed in the graph of the complete test, there is no rise of RPM after air-mass flow was set to the test objective. The video shows ignition, a red flame outside the exhaust and then the RPM keeps fading out with approximately the same slope as in initial.

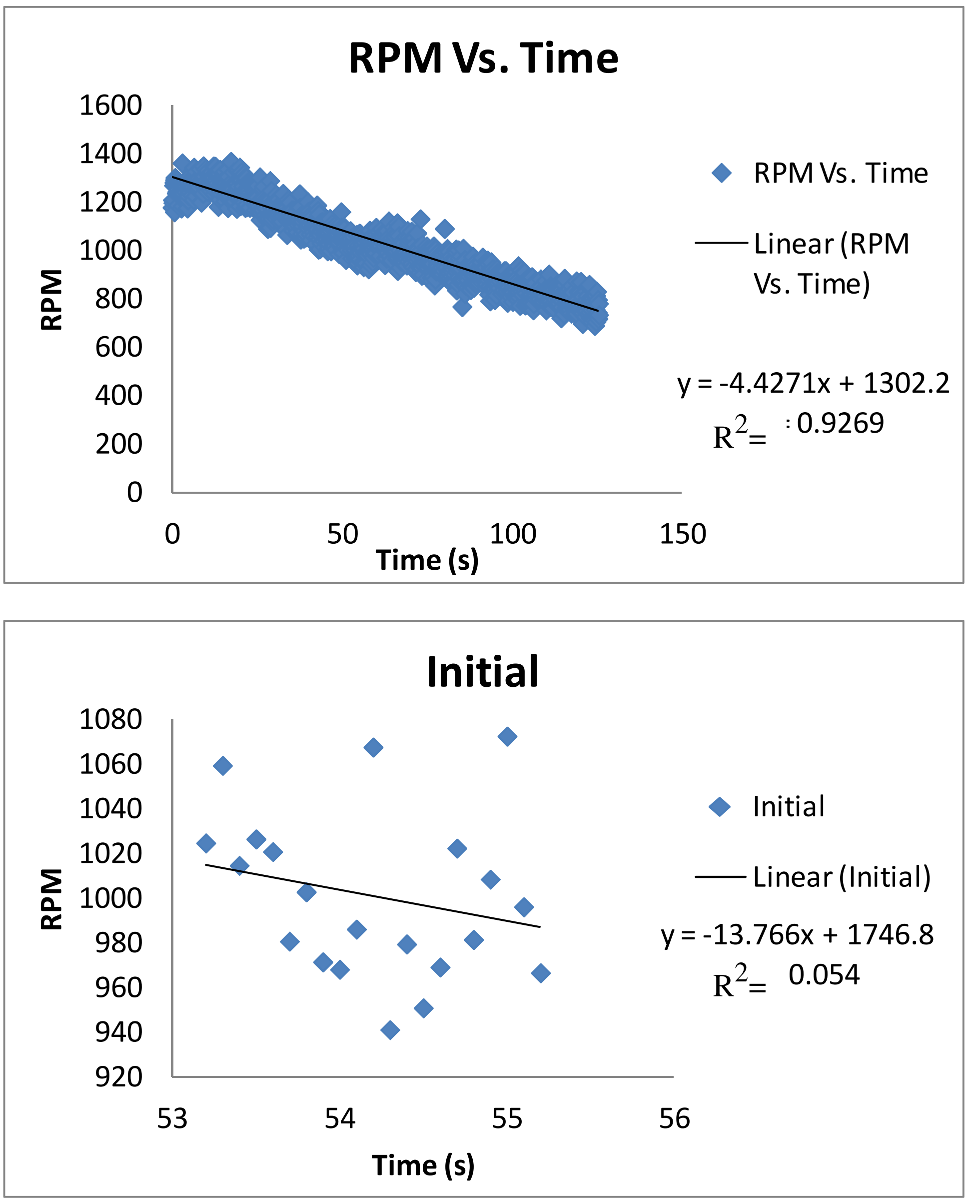

Figure 28: Test 549 Performance Graphs

Figure 28 (Cont'd)

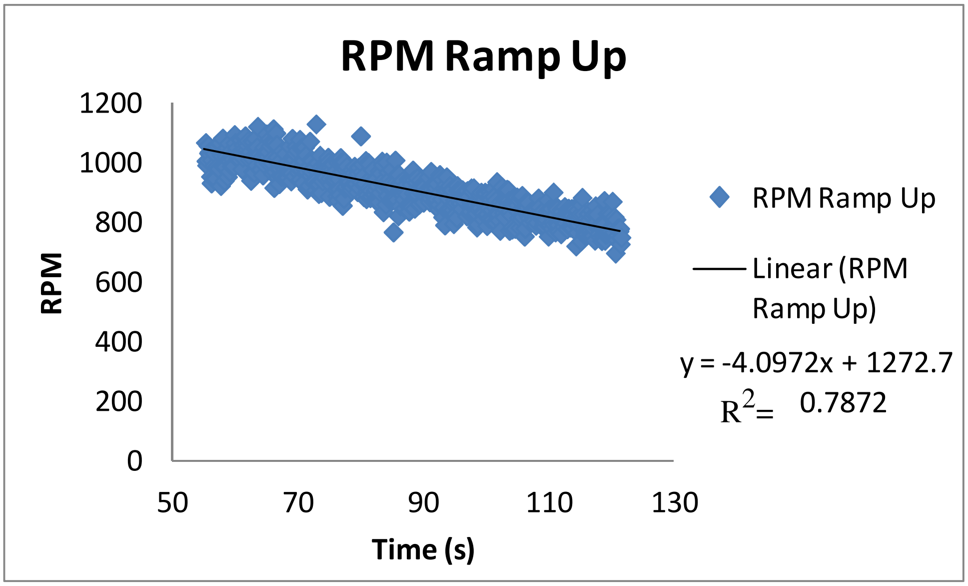

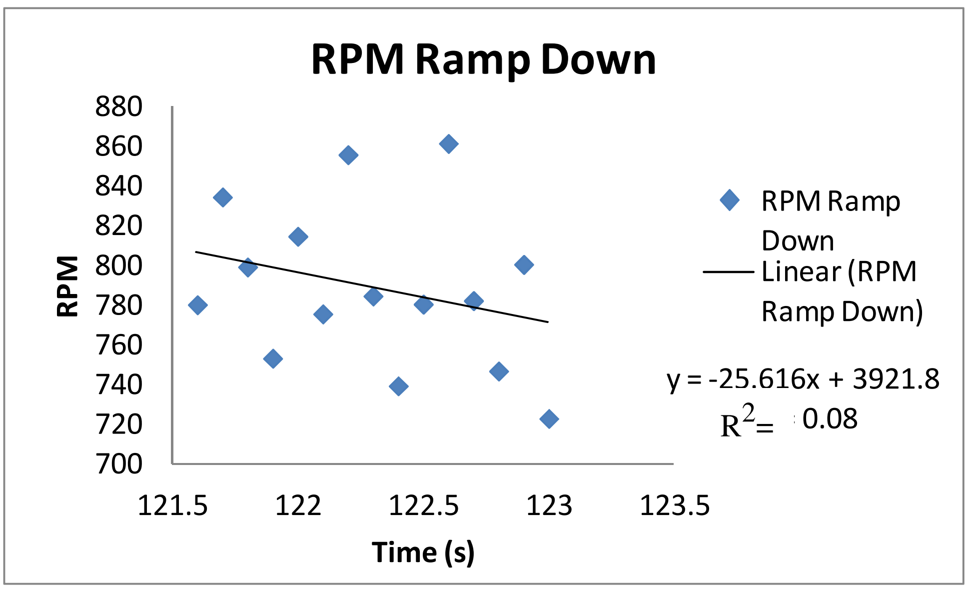

Analysis of the Tests

Table 4 shows calculations done from the data of the tests. This analysis is done over the 'gas on' acceleration portion of all the tests. The slope of the fitting line is a good approximation the rotational acceleration of the system at the 'ramp up' stage. An average of the RPM during ramp is calculated by taking the first and last time steps during ramp up. The average of the two is converted to angular speed ω (rad/s). With this values an average power during acceleration can be calculated using equation (2).

	Gas On Acceleration Portion				
	m=α (rad/s^2)	b	RPM avg	ω (rad/s)	Power(avg) (watt)
Test 539	33.781	-4144.7	1113.31	116.5858	105.42
Test 540	0.9026	776.13	940.45	98.48352	2.38
Test 541	-1.134	977.76	842.98	88.27709	-2.68
Test 543	9.3909	740.51	1025.054	107.3434	26.98
Test 544	-2.4978	1373.5	1020.561	106.8729	-7.15
Test 545	22.176	-1892.6	1091.181	114.2682	67.83
Test 546	-3.7009	1464.6	883.9288	92.56481	-9.17
Test 547	-0.8995	1057.5	918.4373	96.17853	-2.32
Test 548	54.437	-5957	1538.975	161.1611	234.83
Test 549	-4.0972	1272.7	910.5075	95.34812	-10.46

Table 4: Analysis of Tests as a Group 'Gas On' Acccelartion Portion

Figure 29 shows the relationships between power during acceleration and air mass flow (Figure 29, Top), fuel-flow (Figure 29, Center) and normalized equivalence ratio Φ(Figure 29, Bottom).

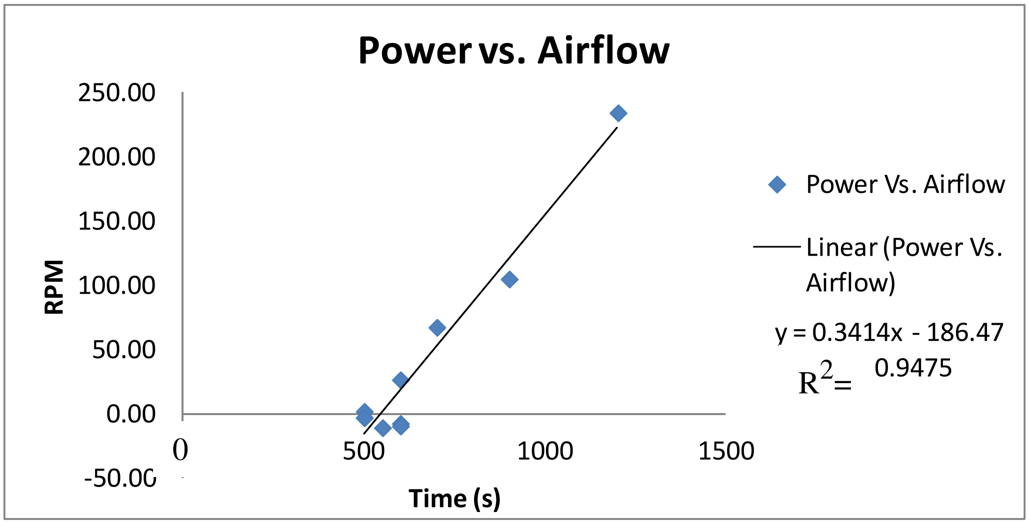

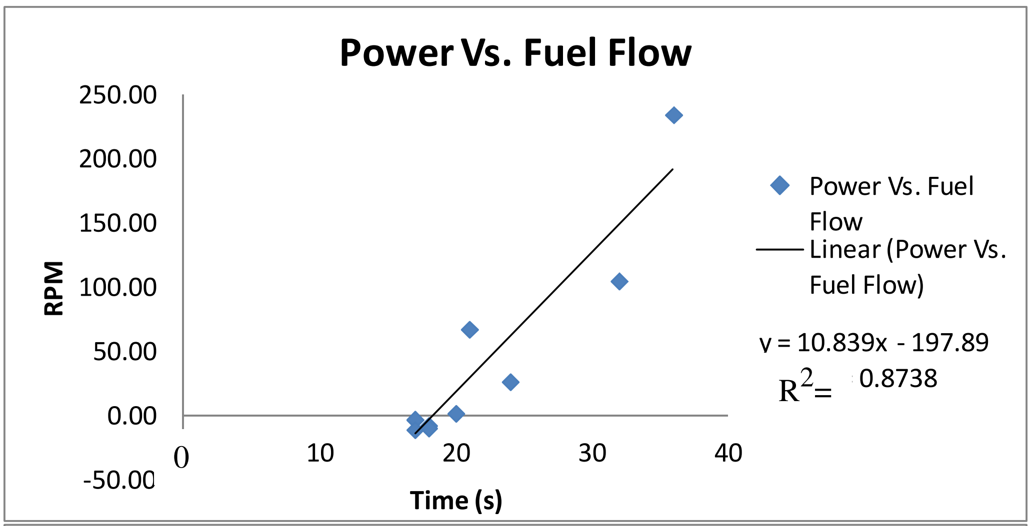

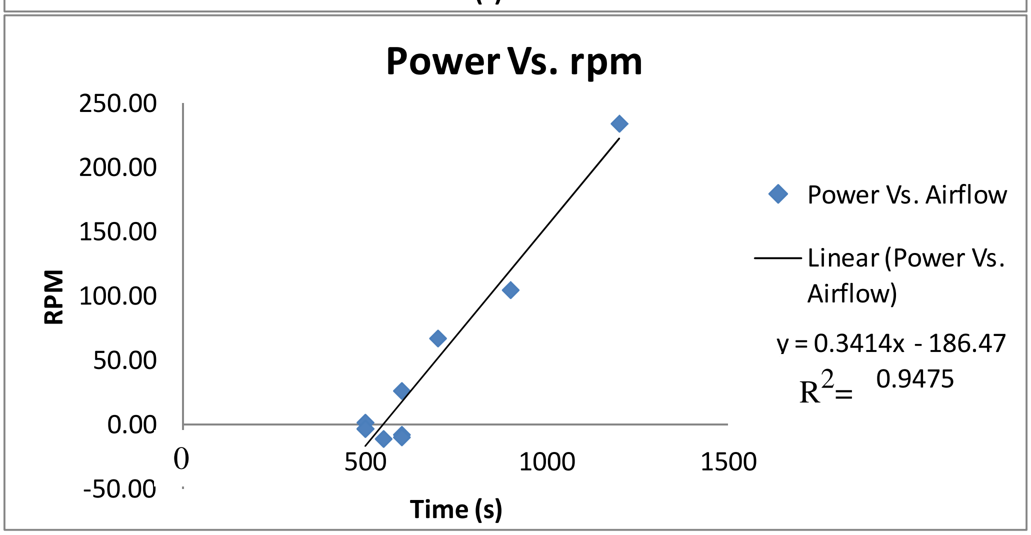

Figure 29: Power vs. Inputs Graphs

Discussion

The results from the bulk analysis of the tests showed in Figure 29 show a very good fit between air mass-flow and fuel mass-flow in relation to the power produced from the tests. Not such a good fit can be found when graphing power vs. equivalence ratio.

- Power output of the WDE depends more upon the mass flow to the engine than the equivalence ratio.
- The higher speed and higher air/fuel mass-flow the better combustion there is inside the engine. No visible flame outside the exhaust was observed in the test where more power was developed by the WDE.
- Higher rotational speed and higher mass-flow can create more turbulence which accelerates combustion.
- Seizing always happens within few seconds when there is power production. When no power is produced the WDE can remain rotating for several minutes without seizing despite having combustion.

Future Work

Since the data provided shows that the WDE is strongly dependent on the inlet airflow and mass flow, is suggested to install a supercharger that can provide between 900slm and 1200 of air to make the WDE independent of the outside compressor.

Some extra analysis not presented in this study, (because they do not have the statistical significance, show that the 'ramp up' section of the tests tends to be exponential. As a preliminary observation if there was no seizing the WDE would probably increase its speed exponentially only having the counter action of the bearings which also increases with speed and temperature. But it is expected to produce >= 1kW if the WDE reaches 7000 RPM. Future work should be focused on bearing systems and seizing.

OPTICAL ANALYSIS OF COMBUSTION INSIDE AN OPTICAL WAVE DISK ENGINE

Intro

In this chapter a study of speed of deflagration inside the Optical-WDE-channels is conducted. The Optical WDE was design to do combustion studies inside the WDE to better understand direction of deflagration, speed of deflagration and the variables influencing combustion processes.

In this study, four main variables are accounted for in order to get the first grasp of their effect on flame deflagration speed. These are: WDE rotational speed, equivalence ratio of the fuel injected, injection procedure (direct or premixed), and spark plug position and amount.

An Optical Window WDE was designed and manufactured to modify WDE-III. WDE-III and the optical designs are documented on the manufacturing chapter. The Optical WDE has two iterations the first one (Figure 30) has one optical port and the second (Figure 31) has 6 optical ports for diagnostics and monitoring of combustion.

An analysis showing the approximate flame speed inside the channel, vs. equivalence ratio of the air/fuel mix at different RPMs is showed and conclusions are derived from these observations.

Figure 30: Top Plate with 1 optical access

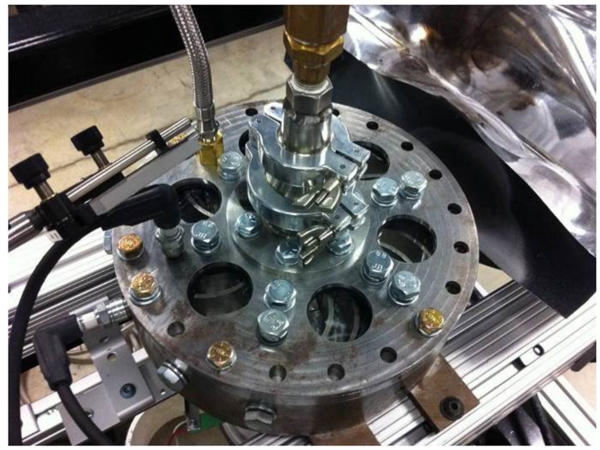

Figure 31: Top place with 6 optical access windows

The preliminary tests made with the single window WDE showed combustion happening at different parts of the engine depending on RPM, fuel mass-flow and sparkplug positions. The second multi-window optical WDE was design to further examine the observations made on the single window WDE.

Preliminary Tests

The night of Tuesday 18 of January 2011 a test was run at 500 RPM with the first consistent flame inside the channel results. The first videos of flame propagation inside the channel were recorded from the single optical window WDE that night. In Figure 32 and Figure 33 a flame apparently moves from the outside of the engine towards the center. These two pictures were taken from a video recorded with a normal webcam.

Figure 32 shows a flame developed on approximately one quarter of the channel and Figure 33 shows a flame that almost reaches half of the channel. A possible conclusion is that it is the same channel and the flame was developing from the outer edge towards the center of the rotor. However this conclusion cannot be made with just this evidence because the frame speed and the resolution of the camera used low. Flame propagation and channel tracking cannot be made in the video. Flame speed and direction of propagation cannot either be calculated from these pictures.

Despite the information derived from this video does not yield measurable and/or consistent parameters, is important to notice that combustion inside the channel was reached using two sparkplugs rather than one, that these sparkplugs were located on the outer ring of the WDE, and that they were separated approximately 60 degrees from each other. Using sparkplugs separated only 30 degrees did not yield the combustion seen in the video where Figure 32 and Figure 33were extracted from.

Figure 32: Flame developed on the outer quarter of the channel.

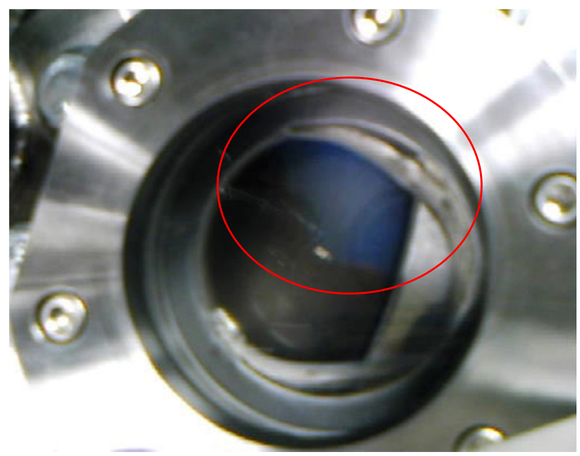

Figure 33: Flame developed on the outer half of the channel.

Follow Up Testing

Figure 34 and Figure 35 were taken the same way as before but testing with the lights off. Lights off make combustion more visible to the camera and different flame positions are now visualized. These two pictures are taken from a video recorded from a test at approximately 500 rpm, which lasts 11 minutes with seven minutes of consistent combustion. The seven minutes started happening after the first three minutes of running the test with un-consistent combustion. Some conclusions from this test are:

- The engine warms up for about three minutes before having consistent combustion
- At this stage of development, the engine can run for seven minutes with consistent combustion, which is the first step to later set up the high speed imaging of combustion.
- This running time with consistent combustion inside the channel accomplishes one of the milestones stated in the contract.

Figure 35 shows the development of two combustion zones one in a similar position as Figure 34 and another one in a later channel after the known combustion zone. At first glance the second flame could be a reflection from the channel currently combusting, however observing the video with detailed attention sometimes there was combustion only at the second position (Figure 36). Why do we have a second combustion going on after the first one? Is there enough oxygen in the channel for such a process? How did it ignite?

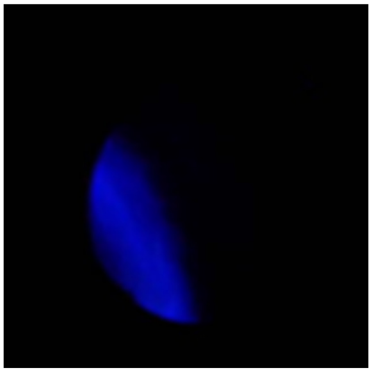

Figure 34: Combustion in first zone.

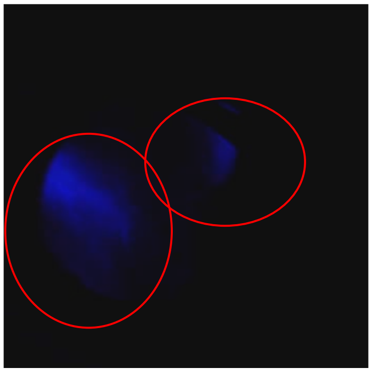

Figure 35: Two combusting channels.

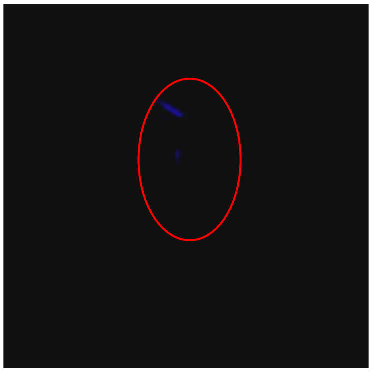

Figure 36: Combustion in second zone

The first conclusion was that the second combustion was ignited by a second spark plug. This sparkplug was connected close to the position where the second combustion is seen. However, there is almost no chance that flame was ignited by the second sparkplug since the flame is angularly right before the spark and in the event flame and sparkplug were aligned the combustion was happening literally instantly, which is un-likely.

The Optical WDE has four sparkplug ports on the outer ring. When locating the window right above the first sparkplug after injection combustion could not be observed. However the engine was hot and it sounded like combustion was happening during testing. This indicates that the ignition delay time of combustion was enough for the channel to completely pass under the window.

Table 5 shows a series of tests ran on the Optical WDE with direct injection of Ethane to do preliminary pattern identification.

RPM	AIR SLPM	FUEL SLPM	Comments		
			No Flames	Flames insdie the engine	Flames in the exhaust
100	400	0.5	X		
100	400	1		X	
100	400	2		X	X
100	400	3			X
100	400	4			X
200	400	0.5	X		
200	400	1	X		
200	400	2	X		
200	400	2.5		X	
200	400	3		X	X
200	400	4			X
300	400	0.5	X		
300	400	1	X		
300	400	2	X		
300	400	2.5	X		
300	400	3	X	X	(intermitted)
300	400	3.5		X	X
300	400	4			X
400	400	0.5	X		
400	400	1	X		
400	400	2	X		
400	400	2.5	X		
400	400	3	X		
400	400	3.5	X		
400	400	4	X		
400	400	5	X		
400	400	5.5		X	X
400	400	6			X(a lot of flames)
500	400	0.5	X		
500	400	1	X		
500	400	2	X		
500	400	2.5	X		
500	400	3	X		
500	400	3.5	X		
500	400	4	X		
500	400	5	X		
500	400	5.5	X		
500	400	6			X

Table 5: Different Condition Testing

Conclusions from this series of tests are that at higher RPM there is no constant combustion inside the channel. Injecting more fuel compensates the effect of speed. However increasing fuel mass flow beyond certain point creates flames at exhaust port rather than in the channel.

<u>High Speed Imaging of Combustion</u>

After the preliminary tests ran with the single window Optical WDE and a webcam, an optical diagnostics test rig was setup at the Combustion Diagnostics Laboratory. This test rig is described in the chapter about experimental facilities. The objective of this test rig is to examine combustion inside the WDE using high speed cameras, infrared cameras and combustion diagnostics laser equipment.

A set up with same conditions as the preliminary tests was made to make high speed imaging of combustion. The first high speed images (Figure 37) were done at 500 frames per second with the engine running at 360 rpm. A total of 0.24 seconds were recorded obtaining 121 images. Figure 37 consists of six of these frames where combustion was captured during a test with apparent consistent combustion. Despite of looking consistent to the eye, high speed imaging shows that there are several channels that do not ignite. When there is ignition the flame jumps from the ignited channel to the surrounding channels igniting them.

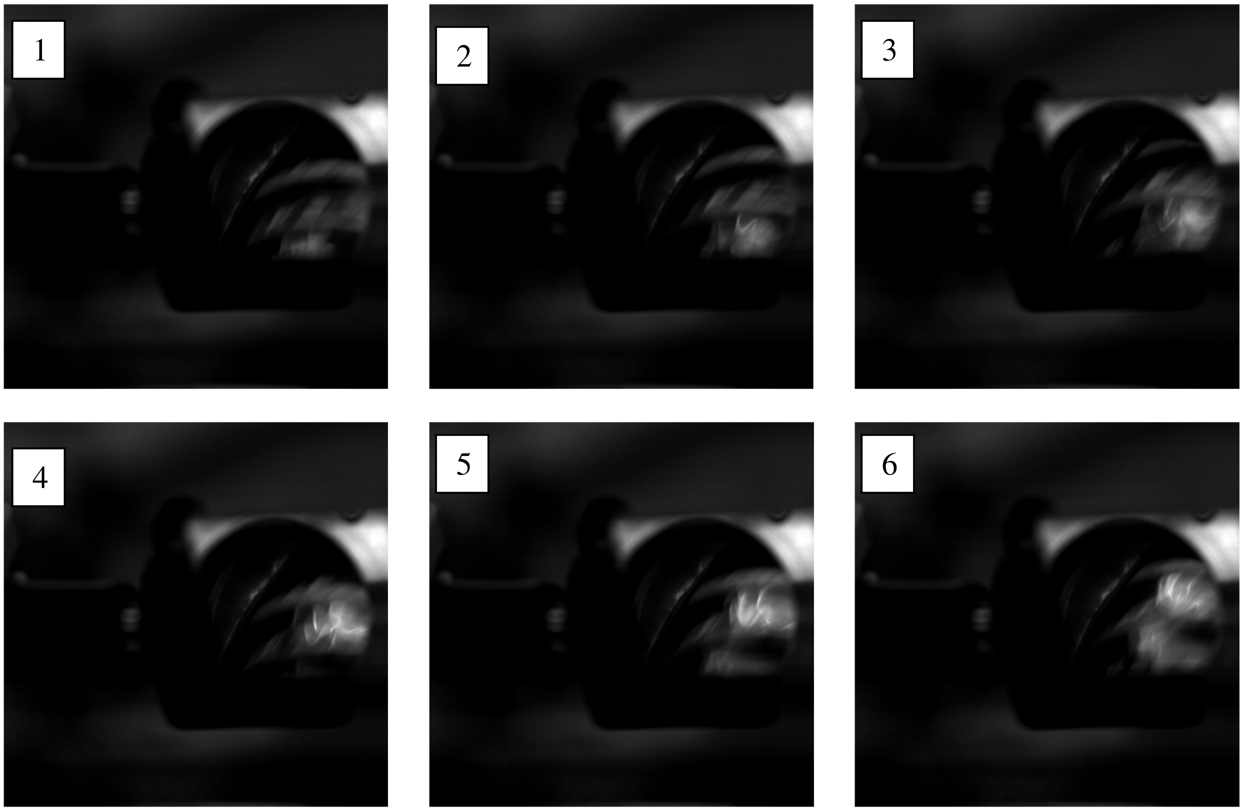

Figure 37: Series of pictures from the first high-speed imaging test

Figure 37**,** shows the evolution of a flame inside the channel which ‘jumps’ to the previous and next channels. A detailed description follows:

1. Frame 1: No flame developed in the channel under the window.
2. Frame 2: The coming channel (in the picture the channel below) has a developing flame apparently moving from the center of the rotor towards the outer ring.
3. Frame 3: The developing flame instead of moving further in the channel jumps towards the channel that was previously under the window.
4. Frame 4: Increased visual radiation from the flame front and the flame distributing to the two adjacent channels. The flame still does not move towards the outer part of the channel.

5. Frame 5: The channel coming towards the window is being ignited with the previous channel flame.
6. Frame 6: Two channels with a ‘shared’ flame.

Despite having high speed imaging of combustion any conclusions made from these images are weak because there is neither certainty that activation energy can be supplied in two stages nor that gases travel backwards through the inlet-rotor gap towards the inlet.

To further examine combustion inside the WDE a second optical top was designed (Figure 31). This top plate contains six windows to allow visualization of different combustion points inside the WDE, and gas-dynamic expansion. This Top-Plate allows for different sparkplug and fuel-injector configuration including fuel injection and ignition from the top of the engine. Top injection and ignition get better access to channels since the open area at the top of the channel is ~3 times bigger than at the side closer outer ring.

Figure 40 (left) shows one of the first tests ran with the multi window Optical WDE. Combustion happening all around the WDE including the exhaust can be observed. This test had fuel rich injection, two sparkplugs igniting the same channel from top and from the side, and injection from the top. The test speed was ~2000 rpm.

Tests were done with different injector sparkplug configuration until find what to the eye was consistent combustion inside the channel (Figure 40). This combustion occurred only at the window after the sparkplugs. High speed imaging (Figure 38) was recorded showing that these conditions developed consistent combustion inside the channel

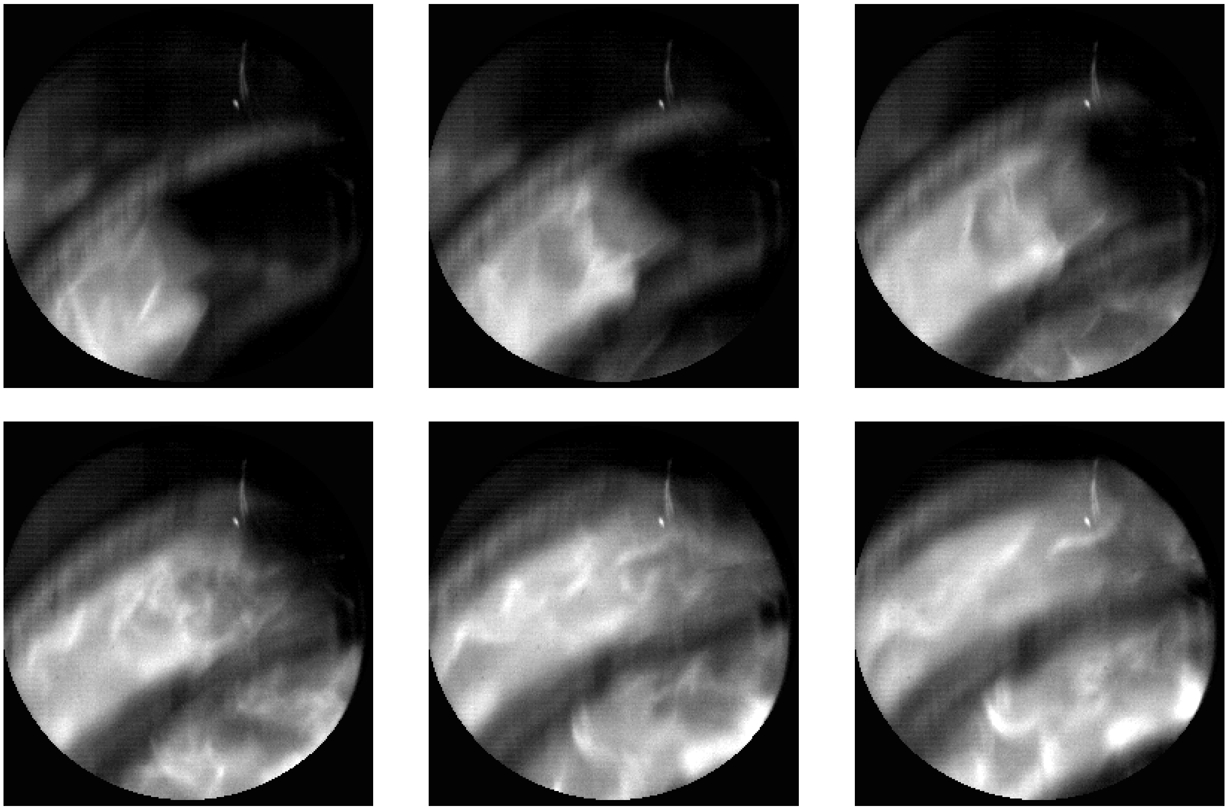

Figure 38: Series of pictures from multi-window WDE high-speed imaging

Figure 38 has six frames from a video recorded at 1000 fps during 2 seconds. Here a flame develops individually in two different channels. During two seconds ~400 channels should pass under the window and when watching the complete video probably 1 or 2 channels raise doubts about being ignited.

Flame Speed Calculations and Experiments.

A study of flame speed is done to understand rotating combustion inside the WDE. No previous experiments or studies on rotating combustion have been found by the author in the literature. The multi-port Optical WDE is used in multiple configurations, described further in this chapter, to understand the effect of rotational speed, direct or premixed fuel injection, spark plug position and spark plug quantity in the flame velocity inside the WDE.

A high-framing-rate complementary metal-oxide-semiconductor (CMOS) color camera (Photron SA-4), for now on called the camera, was used to record videos of the flame inside the WDE at 3600 frames per second (fps). Each case-video, was analyzed using the video editing software, Image J[1].

The Multi-port Optical Wave Disk Engine

The Optical WDE has six optical ports (Figure 39) at the top to allow visual access to the rotating channels where combustion processes can be visualized. It was designed and manufactured, to record high speed images, infrared images, and make laser diagnostics inside the WDE channels during engine operation. The optical windows allow for observations and measurements of the distance traveled by the flame front and intensity of the traveling flames.

[1] Rasband, W.S., ImageJ, U. S. National Institutes of Health, Bethesda, Maryland, USA, http://imagej.nih.gov/ij/, 1997-2012

Fuel injectors can be placed on periphery of the housing, and at the top-plate for different spark plug and fuel-injector configurations.

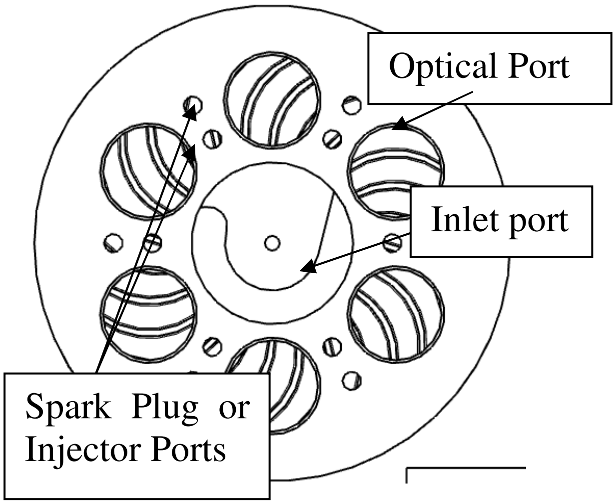

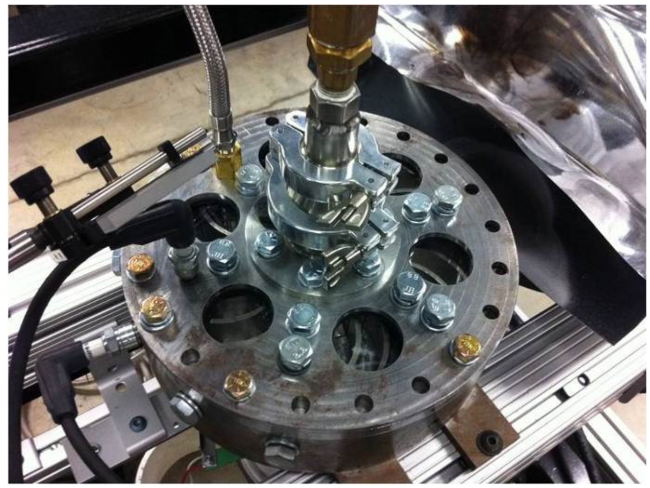

Figure 39: Optical WDE Design and Manufactured

The Optical WDE works bringing air (or air/fuel mixture), through the inlet port, then the flow goes into the channel where is ignited, and later exhausted. In Figure 39(right) the feeding pipeline is connected to the WDE on the z plane; the inlet port takes the airflow moving vertically and shifts the flow to be horizontal, parallel to the rotor. Once the flow enters the channel is kept there and later ignited.

<u>Tests and test Objectives</u>

Preliminary tests show that RPM, Spark Plug (SP) number and position, and fuel injection method have a tangible influence in whether combustion inside the channel happens or not, and how consistent it is. Flame speed is of special interest for WDE design since depending on it the WDE can rotate faster, and efficiency of turbo-machinery is higher at higher speeds. For this reason the tests objective is to find which WDE configuration has the faster flame speed.

Three RPM were selected to run the experiments 400, 1000 and 1500 RPMs. The reason to choose 400 RPM is that is the slowest the control system allows the WDE to be driven. The other two were selected because preliminary tests showed we could control confined flames in the window studied. Figure 40 (left) shows some of the first tests performed with the multi-window Optical WDE. Uncontrolled flame and combustion can be observed all around the WDE, including in the exhaust. RPM and Air-Fuel Ratio (AFR) were changed until consistent combustion was developed and contained inside the channels, i.e. combustion occurred only in the channels immediately following the spark plug (Figure 40, right).

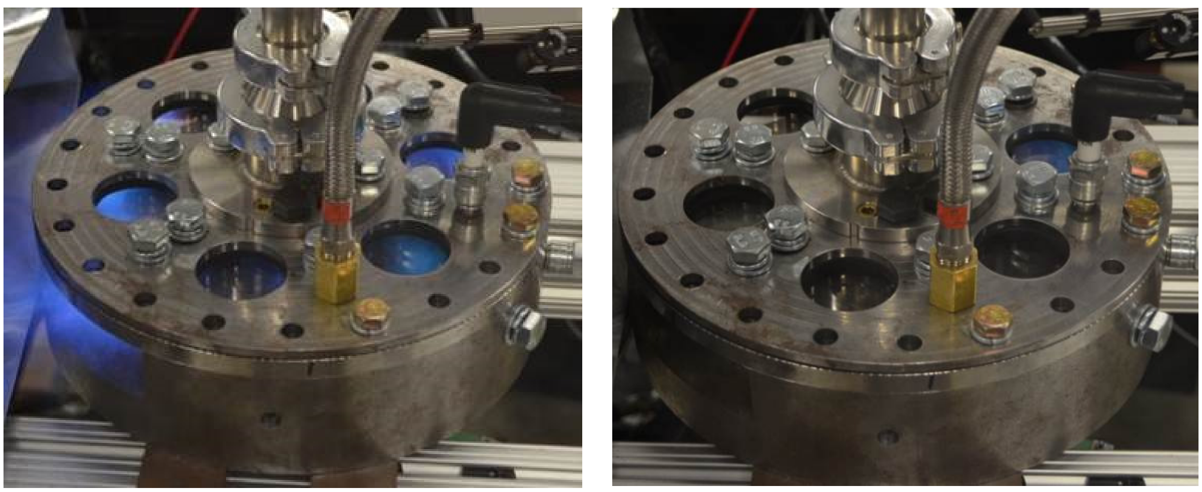

Figure 40: Multi-window Optical WDE showing combustion before ignition optimization (left) and after optimization (right).

For all the tests a 1mm diameter injector was used since in preliminary tests the pressure from the ethane tank (after the regulator) was not enough to have the fuel mass-flow for the rich tests.

<u>Flame Direction</u>

For this study the first test run was to learn the direction of deflagration. The test involves one a mirror at approximately 45 degrees which can flip the image. A ruler was placed on top of the window to learn what direction the flame front travels. Figure 41 shows a set of eight frames from the video done with the ruler. The pictures in Figure 58 are from every other frame, and were subtracted from a specific moment where a rich spot was developed.

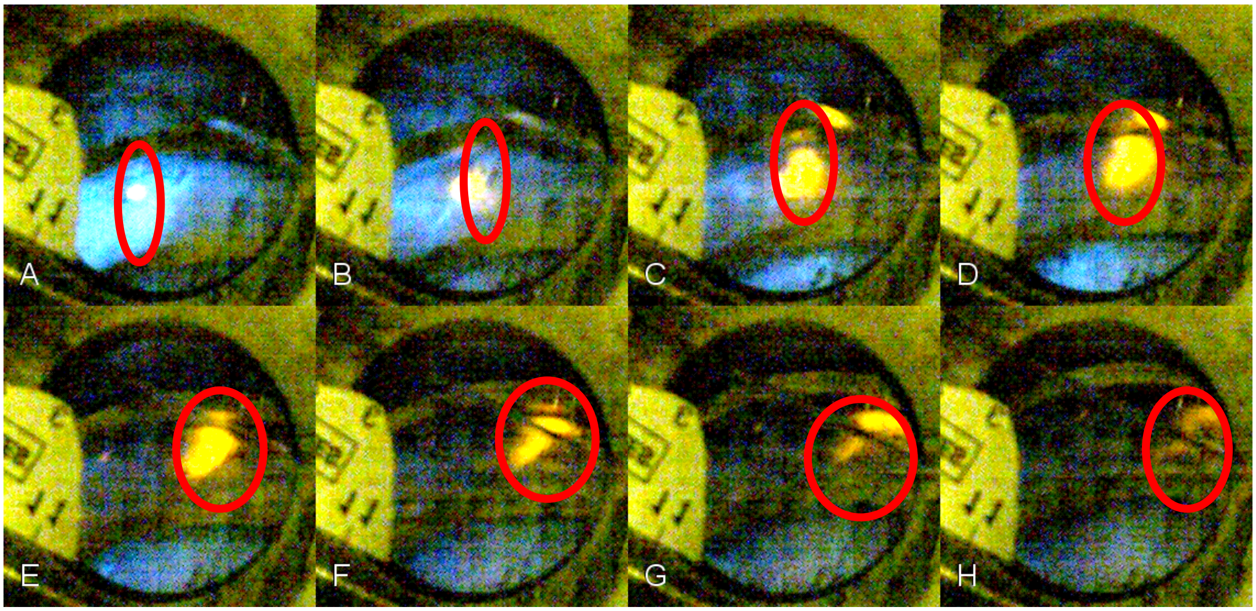

Figure 41: Direction of the Flame

In Figure 41 the rich spot travels towards the descending number on the ruler. In frame A the position of the spot is at about 2 cm, and in frame H the spot reaches the beginning of the ruler which is located towards the inner part of the WDE.

- The direction of the flame in the calibration of direction video is from outside towards inside.
- Knowing how the video displays movement from the mirror consistent observations can be better understood. In general from the analysis of the videos in this study the flame travels from outside towards inside with very few exceptions.

Experimental Cases and Protocol

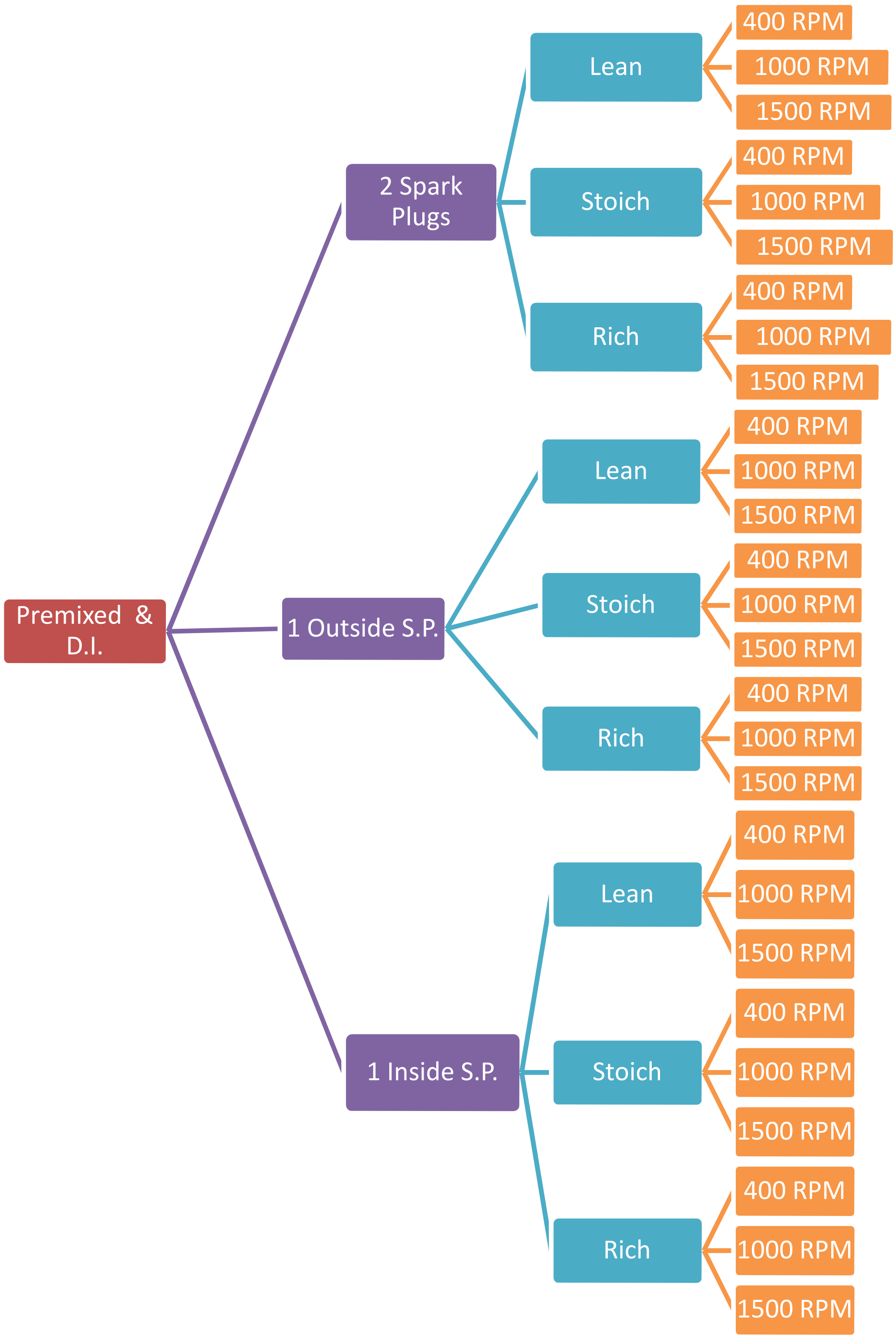

Figure 42: Cases Studied for Direct Injection (D.I.) and Premixed Fuel Flow.

The study takes into account 54 cases (Figure 42). The main two categories are Direct Injection and Premixed Air/Fuel stream; Figure 43 shows a blue square where the air-fuel flow enters the disk, for the premixed flow case, and a green triangle where the injector was located for the Direct Injection (D.I.) case. For each of this two categories three cases were studied: one SP closer to the outer ring (Figure 43, left), one SP closer to the inlet (Figure 43, Center) and two SP (Figure 43, Right). Then for each S.P. category three subcategories are added for lean, stoichiometric, and rich mixture, finally for each of these categories three more categories are measured 400, 1000, and 1500 RPM.

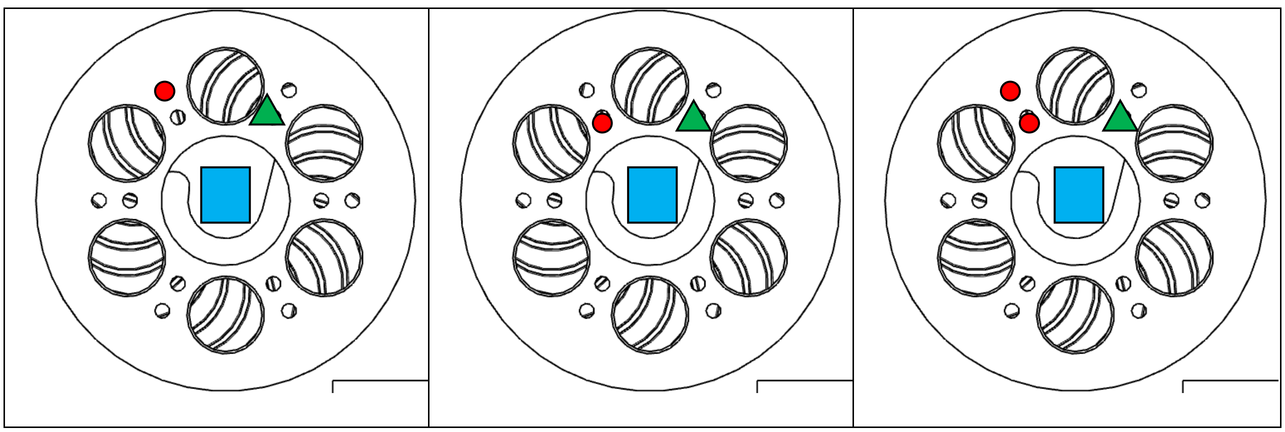

Figure 43:Red Circle Outside Spark Plug (Left), Red Circle Inside Spark Plug (Center), Two Spark Plugs (Right)

For the tests Ethane (C_2H_6) was used. Molecular weight: 30.069g/mol[14]. Upper Explosive Limit (UEL) 12.4% by volume, 12.8% by mass and Lower Explosive Limit (LEL) of 2.91% by volume, 3.02% by mass[16]. The tests were chosen to be inside the Explosion Limits, a mass flow of 400slm of air was standard for all the tests. Figure 44, shows the Air/Fuel ratio, the equivalence ratio, and the Normalized Equivalence Ratio[15], for each case.

	Theoretical	*Experimental*		
	Stoich	**Lean**	**Stoich**	**Rich**
m_{air} *(SLM)*	400	400	400	400
m_{fuel} *(SLM)*	25	14	23	46
(A/F)	16	28.57	17.39	8.70
ϕ *(Eq. Ratio)*	1.00	0.56	0.92	1.84
Φ *(Norm. Eq. Ratio)*	0.50	0.36	0.48	0.65

Figure 44: Air-Fuel Experimental Combinations

Video Name Protocol

Every test has a video whose name explains the test done. An excel file called dissertation files, contains 6 worksheets named with the type of injection, Premixed or D.I., and the Ignition source,: 1Outside Spark Plug (1OSP), 1 Inside Spark Plug (1 ISP) or 2 Spark Plugs (2SP). Each of these sheets has a list of the tests and videos made for that injection-ignition combination and notes taken during the experiments.

The name of the video explains all the data in the experiment. First, equivalence ratio (LEL, Stoichiometric, or UEL), followed by the RPM of the WDE, then by the type of injection and Eq. Ratio again, then the Spark Plug configuration and finally the date. Here is an Example:

LEL-400-DL-1-ISP-6-17-13

LEL	400	DL	1-ISP	6-17-13
Equiv. Ratio	RPM	Direct Injection LEL	1 Inside Spark Plug	Date

Figure 45: Video Name-Protocol Example

Flame Speed Analysis

A flame speed analysis was done from each video using ImageJ. Figure 46 shows how the flame tracking was done. ImageJ let the user pick a straight line of a known object in the video and change the units of the line from pixels to millimeters (in this case). The bottom pictures are a z-plane projection of the average intensity of the videos. This projection was done to have a better defined window edge to calibrate the scale from pixels to mm. The diameter of the optical port is 51mm. Several lines are drawn on the z-plane image to make an average length in pixels of the WDE window because every time a line was drawn a different length in pixels was measured; this consequence of human visual capacity, and picture definition. The biggest difference between lines was of about 4 pixels which makes a maximum error of 2% which by measuring several lines (as shown in Figure 46), can be easily cut to a half having only 1 pixel difference between one line an another. Drawing a line that cuts a circle in a half is done by finding the longest line through the circle; starting at any point and finalizing at the point where the straight line is the longest. As an error factor the videos were made during a 2 month period where the camera was used for several projects and was re-mounted for this project in 2 occasions, since every time the camera is mounted the focal distance has a variation we should account for another 10% in precision decrease.

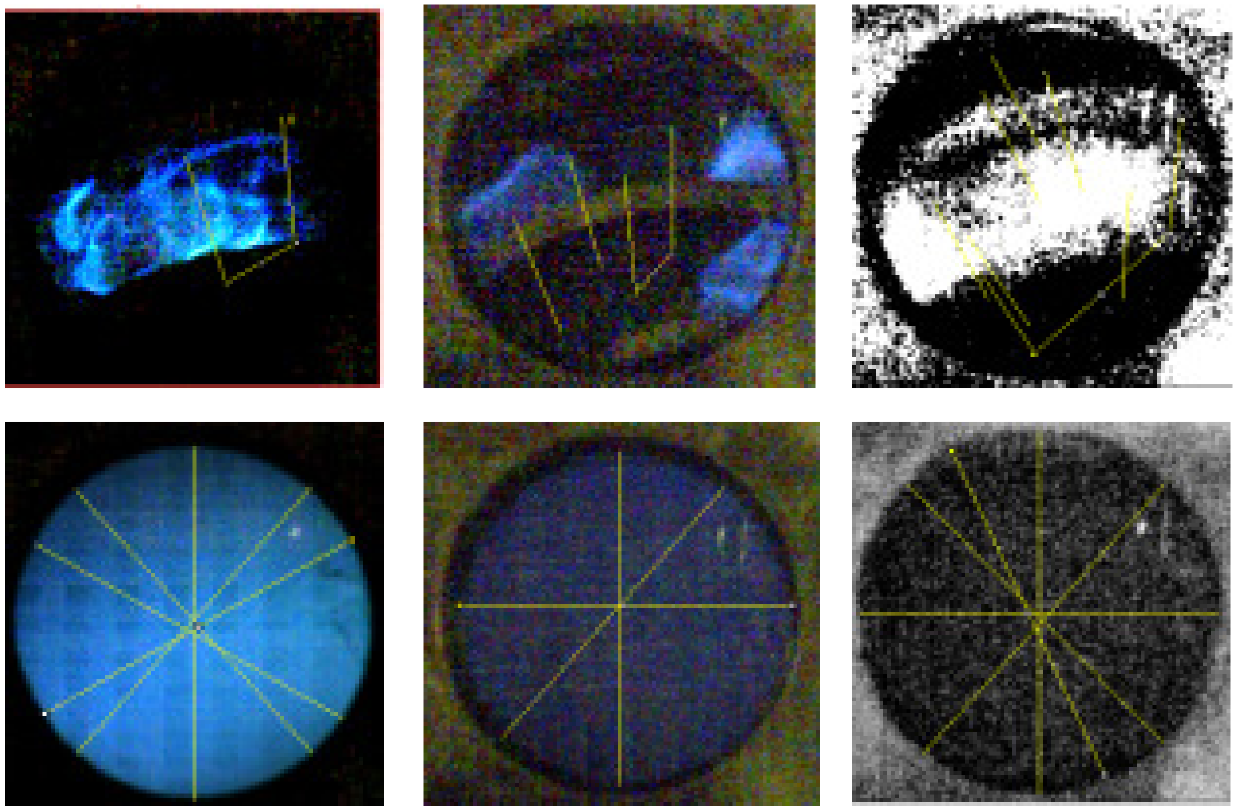

Figure 46: Flame Tracking Images.

Once the pixel to mm ratio is calculated the flame analysis can be done. Every case had many differences in luminosity of the flames, how many channels had flames, and flame speed. For some cases flame luminosity was so low that the video was made binary, black and white (Figure 46, top right), to be able to make a visual assessment of the flame front. Figure 46 (top pictures) show several cases of video enhancing to better measure the flame inside the channel. In this study the subject is flame speed, and from every video the position of five flame fronts were measured and their flame speed calculated. For some videos there were barely five flames that could be tracked, for some there were much more than five and for others none. If at least four flame fronts could be tracked the video was analyzed.

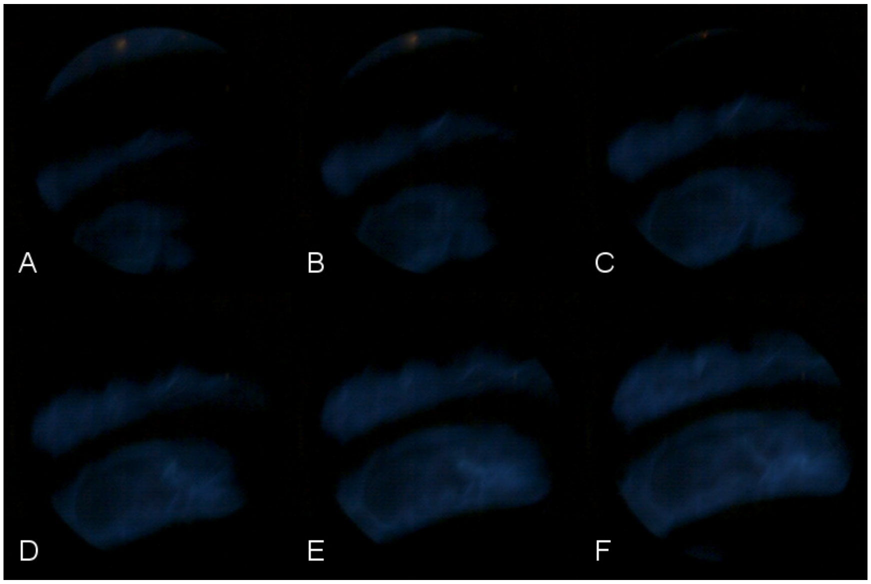

Figure 47: Frames from a Raw Video. (Taken From: STO-1000-PS-1-OSP-5-13-13)

Figure 47 and Figure 48 are the same frames extracted from a video showing the raw image and the enhanced one. The enhancement allows the eye to better see the channel edges and flame front. The enhancement changes the brightness and the contrast of the video. The original video comes in three channels, Red Green and Blue (RGB). ImageJ provides a histogram for each channel where the intensities for every color are displayed. The highest intensities in these videos are in darkest part of the spectrum. By changing the brightness and contrast of each channel, these frequencies can be 'highlighted' to obtain a video like in Figure 48. Once the flame front and channel edges are better defined the flame front tracking can start.

ImageJ allows drawing straight lines over a video frame and keeping them over the next frames. This tool was used to draw a line parallel to the flame front in one frame where the flame front was defined and then do it again five frames later. These two lines show the difference in position of the flame front during five frames time interval. Since the video was recorded at 3600 fps, the time between five frames is 5/3600s, and is constant for all calculations.

The flame front speed estimation is done between frame 1 and frame 5 of each flame front, by marking the line parallel to the flame front at the point where it touches the edge of the channel (Figure 48, Red Circles), and then marking the line at the same edge 5 frames later and measuring a straight line between the two points (Figure 48-F).

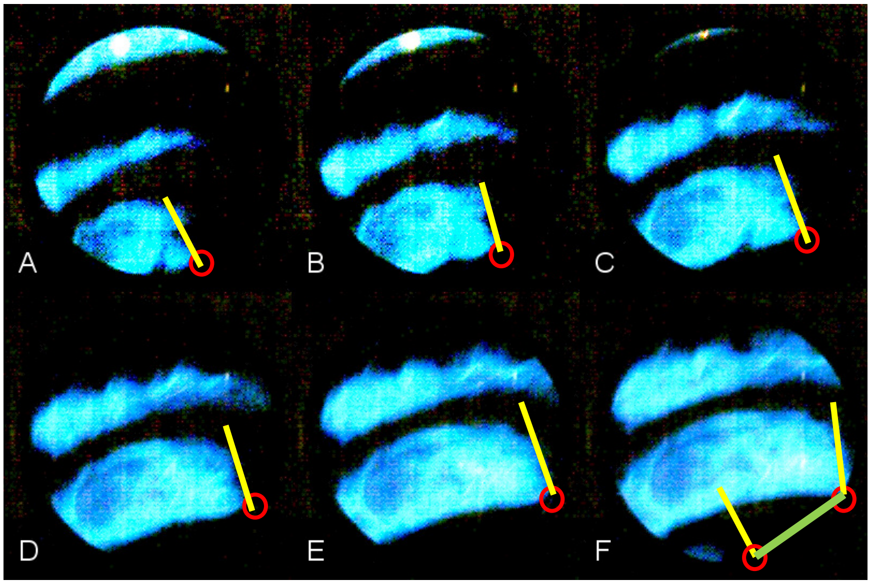

Figure 48: Contrast and Brightness Enhanced from Same Video as Figure 47

The green line, in Figure 48-F, connects two yellow at the point where they touch the edge of the channel. The green-line measures the distance between the flame-front at frame one and frame five. Frame A in Figure 48, is the flame-position in the first frame and Frame F is the flame-position five frames later. The distance covered by the green line is considered a good estimation of flame progression, because we are working with a curved, rotating channel; the edge of the channel works as a good fixed reference point, since a point inside the flame is not traceable, and the direction of the flame changes constantly. The speed then is calculated taking the length of the green line and dividing it by the time it takes to advance five frames in the video (5/3600).

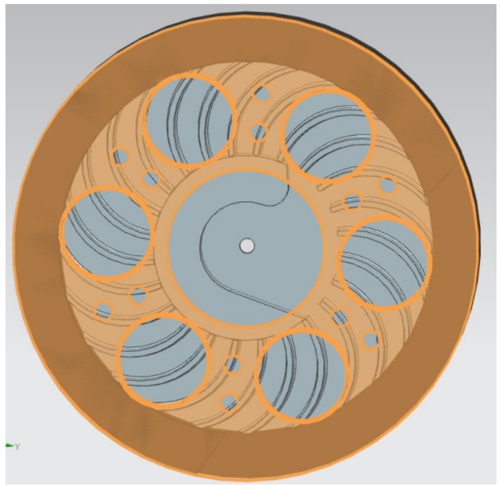

Figure 49: Optical WDE Transparent View

Later in this chapter, when results are analyzed, big differences in flame speed respect to RPM are found. The green line (Figure 48-F) will naturally be longer at higher RPM, a speed correction is calculated respect to the speed of the WDE.

The correction (Figure 50) subtracts the speed of the WDE in rad/s, times the radius to the center of the window (Figure 49, left), which is 75mm, from the calculated speed using Pythagorean Theorem.

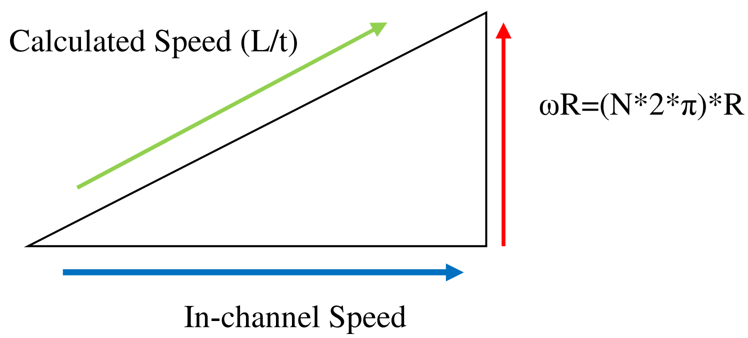

Figure 50: Speed Correction Diagram

Results

Direct Injection 2 Spark Plugs.

Experiment		
File	Fuel/Air Ratio (%)	Observation
LEL-400-DL-2SP-6-18-13	**3.50**	Consistent strong combustion inside the channel.
STO-400-DS-2SP-6-18-13	**5.80**	Flame only at the exhaust.
UEL-400-DU-2SP-6-18-13	**11.50**	No flames either inside the channel or outside the exhaust, no ignition ocurred.
LEL-1000-DL-2SP-6-18-13	**3.50**	Consistent Combustion Inside the Channel.
STO-1000-DS-2SP-6-18-13	**5.80**	Consistent strong combustion inside the channel.
UEL-1000-DU-2SP-6-18-13	**11.50**	Flame at the exhaust Only.
LEL-1500-DL-2SP-6-18-13	**3.50**	Few random explosions inside the channel.
STO-1500-DS-2SP-6-18-13	**5.80**	Consistent Combustion Inside the Channel.
UEL-1500-DU-2SP-6-18-13	**11.50**	No flames either inside the channel or outside the exhaust, no ignition ocurred.

Analysis				
Average Length (mm)	Avg. Speed (m/s)	Length Correction (mm)	Speed Correction (m/s)	Corrected Speed (m/s)
14.80	**10.65**	0.85	3.06	**10.2**
	0.00	0.85	3.06	**#NUM!**
	0.00	**0.85**	3.06	**#NUM!**
16.01	**11.52**	**2.18**	7.85	**8.4**
15.44	**11.12**	**2.18**	7.85	**7.9**
	0.00	**2.18**	7.85	**#NUM!**
21.47	**15.46**	**3.29**	11.84	**9.9**
23.39	**16.84**	**3.29**	11.84	**12.0**
	0.00	**3.29**	11.84	**#NUM!**

Table 6: D.I. 2 SP, Experiment Results and Observations

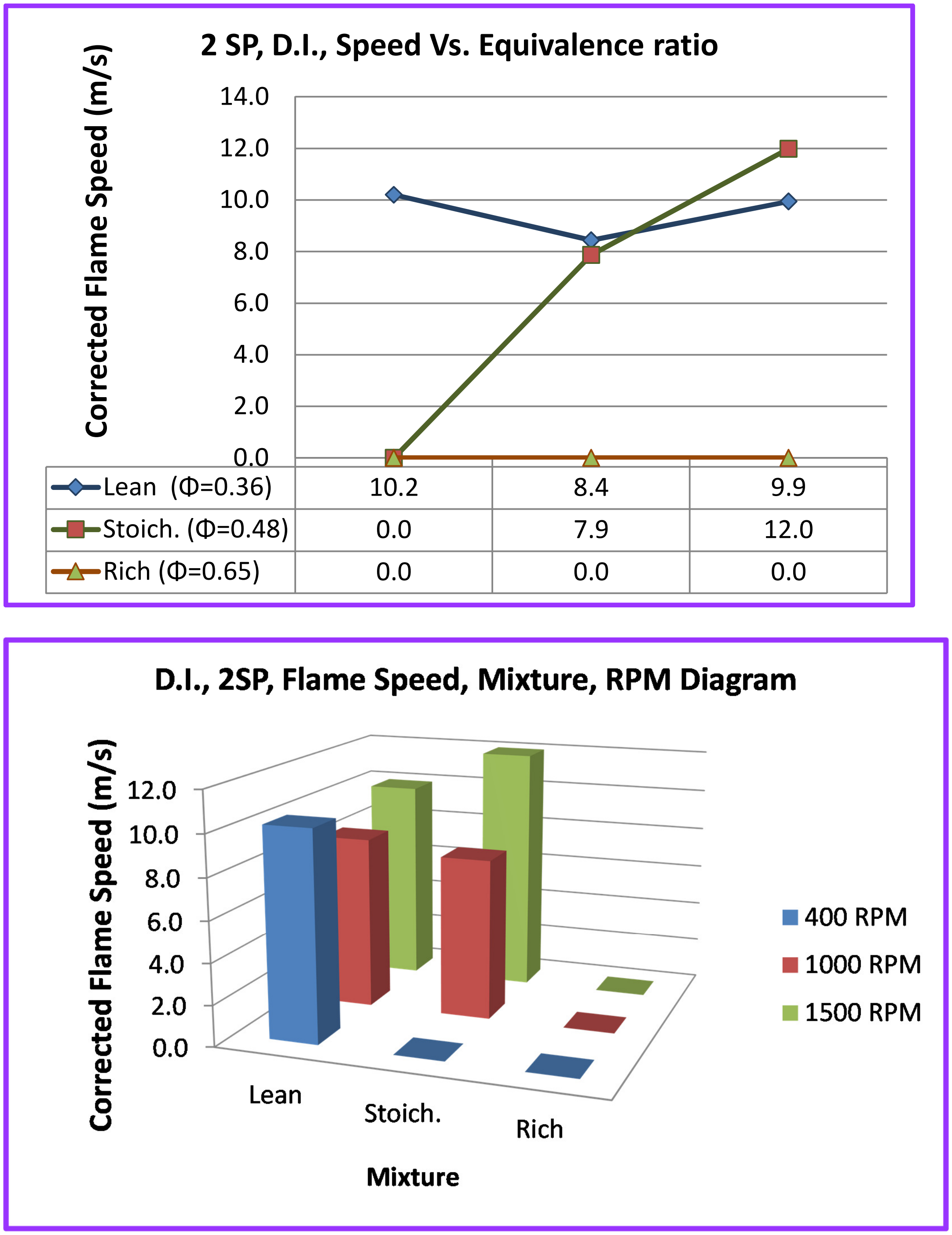

Lean (Φ=0.36)	10.2	8.4	9.9
Stoich. (Φ=0.48)	0.0	7.9	12.0
Rich (Φ=0.65)	0.0	0.0	0.0

Figure 51: D.I. 2 SP, Flame Speed vs. Inputs

Premixed 2 SP

Experiment		
File	Fuel/Air Ratio (%)	Observation
LEL-400-PL-5-10-13	4	Flame contained in channels, no exhaust flame.
STO-400-PS-5-10-13	6	Flame in the channel and Outside the exhaust, sort of evenly
UEL-400-PU-5-10-13	12	Flame only outside the exhaust port
LEL-1000-PL-5-10-13	4	Very scarse flames inside the channel and outside the exhaust.
STO-1000-PS-5-10-13	6	Flame in the channel and Outside the exhaust, sort of evenly
UEL-1000-PU-5-10-13	12	NO flame either inside the channel or Outside the exhaust port
LEL-1500-PL-5-10-13	4	No flames observed in the channel filmed, or outside the exhaust, however few mild explosions were heared and seen in the following windows
STO-1500-PS-5-10-13	6	Sounds like constant combustion inside the channel, however no evident flame is inside, and it seems like the flame developes about 30 to 45 degrees later
UEL-1500-PU-5-10-13	12	No flames either inside the channel or outside the e4xhaust, no ignition ocurred.

Analysis				
Average Length (mm)	Avg. Speed (m/s)	Length Correction (mm)	Speed Correction (m/s)	Corrected Speed (m/s)
17.87	**12.87**	0.85	3.06	**12.50**
26.64	**19.18**	0.85	3.06	**18.94**
#DIV/0!	**0.00**	**0.85**	3.06	**#NUM!**
21.22	**15.28**	**2.18**	7.85	**13.10**
32.80	**23.61**	**2.18**	7.85	**22.27**
	0.00	**2.18**	7.85	**#NUM!**
#DIV/0!	**0.00**	**3.29**	11.84	**#NUM!**
23.64	**17.02**	**3.29**	11.84	**12.23**
	0.00	**3.29**	11.84	**#NUM!**

Table 7: Premixed 2 SP, Experiment Results and Observations

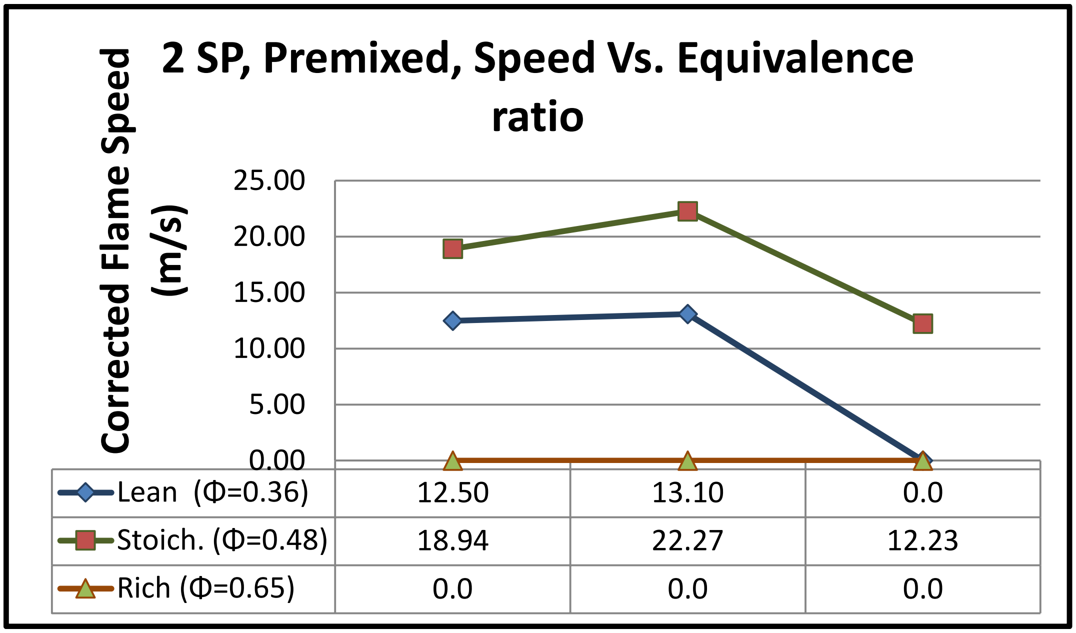

Lean (Φ=0.36)	12.50	13.10	0.0
Stoich. (Φ=0.48)	18.94	22.27	12.23
Rich (Φ=0.65)	0.0	0.0	0.0

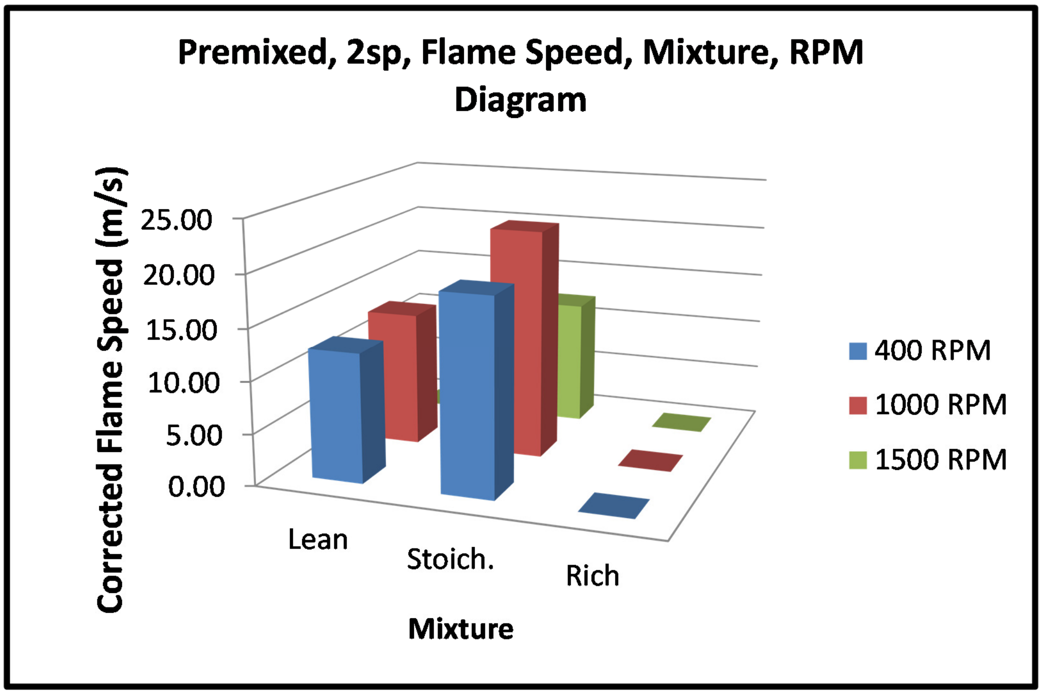

Figure 52: Premixed, 2 SP, Flame Speed vs. Inputs

Direct Injection 1 OSP

Experiment		
File	Fuel/Air Ratio (%)	Observation
LEL-400-DL-1-OSP-6-18-13	4	Consistent combustion inside the channel, loud combustion (semi-consistent) starts at 10slm
STO-400-DS-1-OSP-6-18-13	6	Very few flames inside the channel, and steady flame at the exhaust.
UEL-400-DU-OSP-6-18-13	12	No flames either inside the channel or outside the exhaust, no ignition ocurred.
LEL-1000-DL-1-OSP-6-18-13	4	No flames either inside the channel or outside the exhaust, no ignition ocurred. Ignitions starts at about 18slm.
STO-1000-DS-1-OSP-6-18-13	6	semi-consistent flame inside the channel.
UEL-1000-DU-OSP-6-18-13	12	Steady flame at the exhaust, only.
LEL-1500-DL-1-OSP-6-18-13	4	No flames either inside the channel or outside the exhaust, no ignition ocurred.
STO-1500-DS-1-OSP-6-18-13	6	Consistent combustion inside the channel, loud combustion
UEL-1500-DU-OSP-6-18-13	12	No flames either inside the channel or outside the exhaust, no ignition ocurred.

Analysis				
Average Length (mm)	Avg. Speed (m/s)	Length Correction (mm)	Speed Correction (m/s)	Corrected Speed (m/s)
15.06	**10.84**	0.85	3.06	**10.4**
9.59	**6.90**	0.85	3.06	**6.2**
#DIV/0!	**0.00**	**0.85**	3.06	**#NUM!**
#DIV/0!	**0.00**	**2.18**	7.85	**#NUM!**
21.68	**15.61**	**2.18**	7.85	**13.5**
	0.00	**2.18**	7.85	**#NUM!**
#DIV/0!	**0.00**	**3.29**	11.84	**#NUM!**
28.25	**20.34**	**3.29**	11.84	**16.5**
	0.00	**3.29**	11.84	**#NUM!**

Table 8: D.I., 1OSP, Experiment Results and Observations

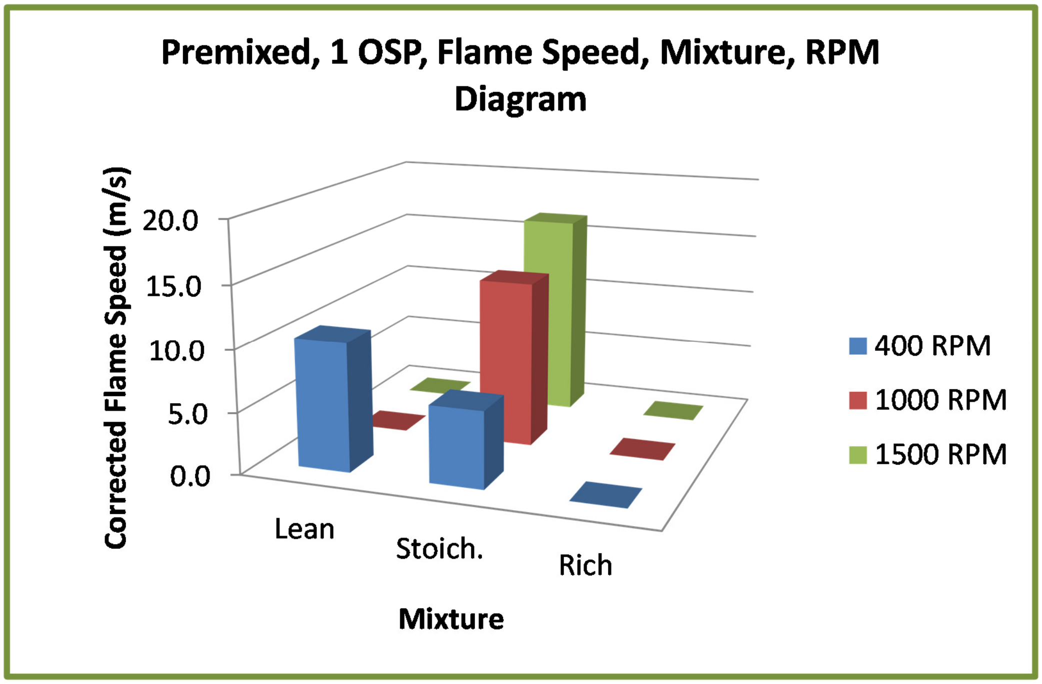

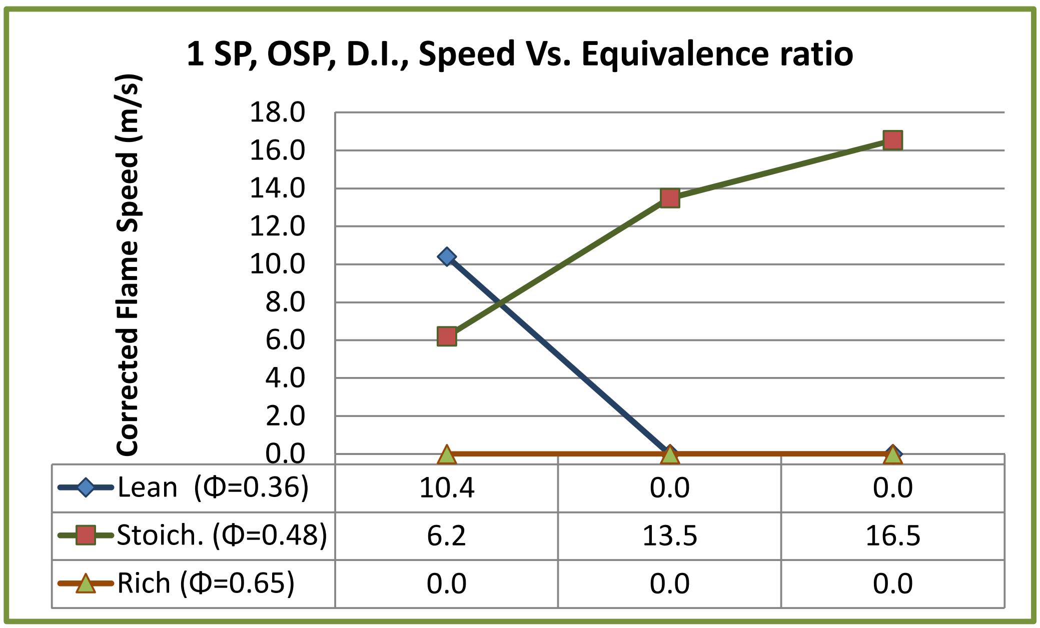

Figure 53: D.I., 1 OSP, Flame Speed vs. Inputs

Premixed 1 OSP

Experiment		
File	**Fuel/Air Ratio (%)**	**Observation**
LEL-400-PL-1-OSP-5-13-13	**3.50**	Flame contained in channels, fairly consistent, no exhaust flame.
STO-400-PS-1-OSP-5-13-13	**5.80**	Flame in the channel, not consistent, and flash-back to the inlet.
UEL-400-PU-1-OSP-5-13-13	12	No ignition at all
LEL-1000-PL-1-OSP-5-13-13	4	Very scarse flames inside the channel.
STO-1000-PS-1-OSP-5-13-13	6	Consistent flame inside the channel. Contained, no flame in the exhaust.
UEL-1000-PU-1-OSP-5-13-13	12	NO flame either inside the channel or Outside the exhaust port
LEL-1500-PL-1-OSP-5-13-13	4	No flames observed in the channel filmed, or outside the exhaust, however few mild explosions were heared.
STO-1500-PS-1-OSP-5-13-13	6	Sounds like constant combustion inside the channel, low intensity flame is inside
UEL-1500-PU-1-OSP-6-13-13	12	No flames either inside the channel or outside the exhaust, no ignition ocurred.

Analysis				
Average Length (mm)	**Avg. Speed (m/s)**	**Length Correction (mm)**	**Speed Correction (m/s)**	**Corrected Speed (m/s)**
11.30	**8.14**	0.85	3.06	**7.5**
11.80	**8.49**	0.85	3.06	**7.9**
#DIV/0!	**0.00**	**0.85**	3.06	**#NUM!**
19.46	**14.01**	**2.18**	7.85	**11.6**
25.75	**18.54**	**2.18**	7.85	**16.8**
	0.00	**2.18**	7.85	**#NUM!**
#DIV/0!	**0.00**	**3.29**	11.84	**#NUM!**
23.37	**16.83**	**3.29**	11.84	**12.0**
	0.00	**3.29**	11.84	**#NUM!**

Table 9: Premixed, 1OSP, Experiment Results and Observations

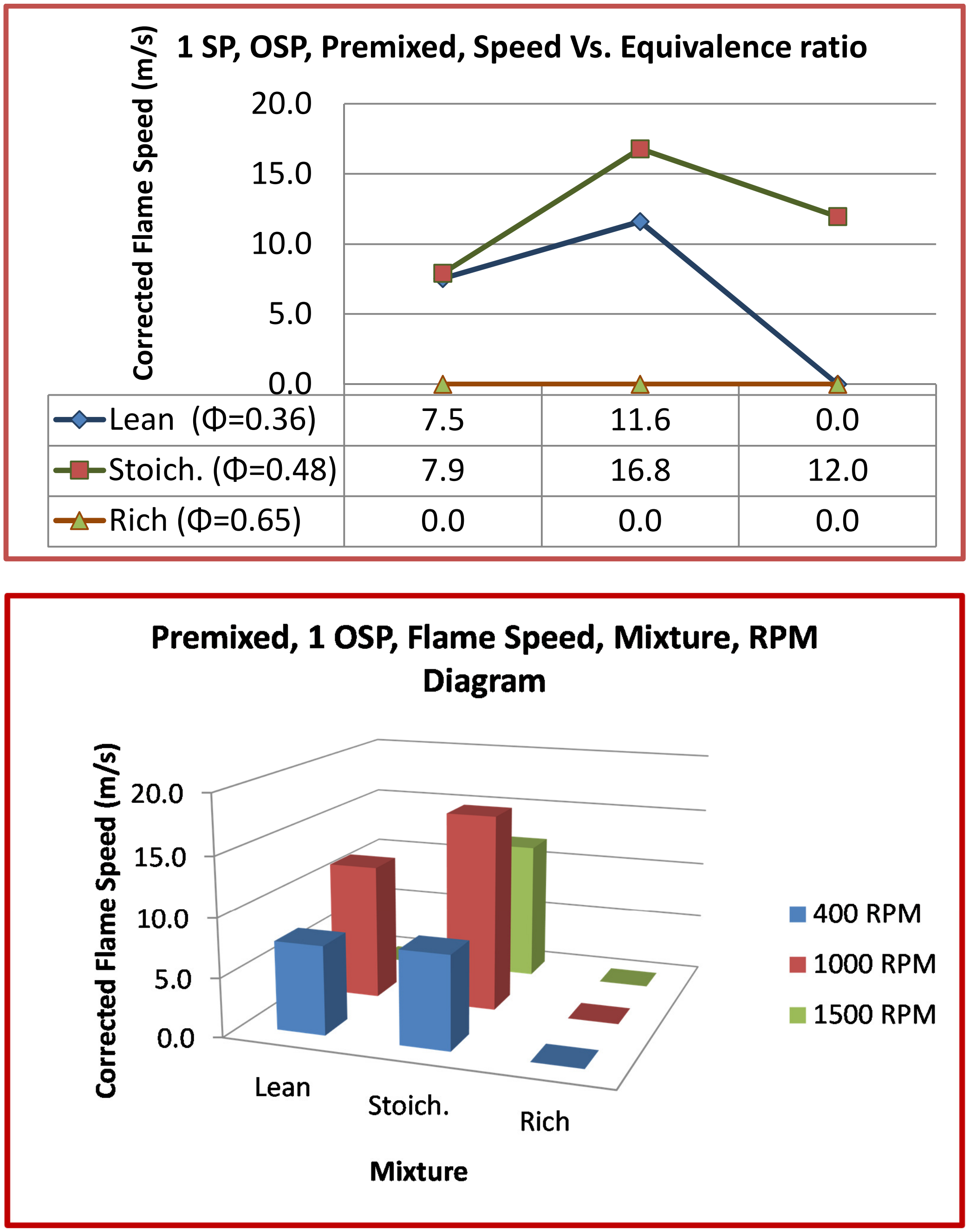

Figure 54: Premixed, 1 OSP, Flame Speed vs. Inputs

Direct Injection ISP

Experiment		
File	Fuel/Air Ratio (%)	Observation
LEL-400-DL-1-ISP-6-17-13	4	Combustions starts with only 7slm, and at 14slm is consistent and strong.
STO-400-DS-1-ISP-6-17-13	6	No flames either inside the channel or outside the exhaust, no ignition ocurred.
UEL-400-DU-ISP-6-17-13	12	No flames either inside the channel or outside the exhaust, no ignition ocurred.
LEL-1000-DL-1-ISP-6-17-13	4	Combustion strats with only 11slm. At 14 slm combustion is consistent. Not as strong as with 400rpm.
STO-1000-DS-1-ISP-6-17-13	6	Consistent combustions inside the channel.
UEL-1000-DU-ISP-6-17-13	12	No flames either inside the channel or outside the exhaust, no ignition ocurred.
LEL-1500-DL-1-ISP-6-17-13	4	Random Combustion Events in the channel, loud. And not consistent.
STO-1500-DS-1-ISP-6-17-13	6	Consistent loud combustions inside the channel.
UEL-1500-DU-ISP-6-17-13	12	No flames either inside the channel or outside the exhaust, no ignition ocurred.

Analysis				
Average Length (mm)	Avg. Speed (m/s)	Length Correction (mm)	Speed Correction (m/s)	Corrected Speed (m/s)
13.27	**9.55**	0.85	3.06	**9.0**
#DIV/0!	**0.00**	0.85	3.06	**#NUM!**
	0.00	**0.85**	3.06	**#NUM!**
15.23	**10.97**	**2.18**	7.85	**7.7**
16.49	**11.87**	**2.18**	7.85	**8.9**
	0.00	**2.18**	7.85	**#NUM!**
20.74	**14.93**	**3.29**	11.84	**9.1**
23.43	**16.87**	**3.29**	11.84	**12.0**
	0	**3.29**	11.84	**#NUM!**

Table 10: D.I., 1ISP, Experiment Results and Observations

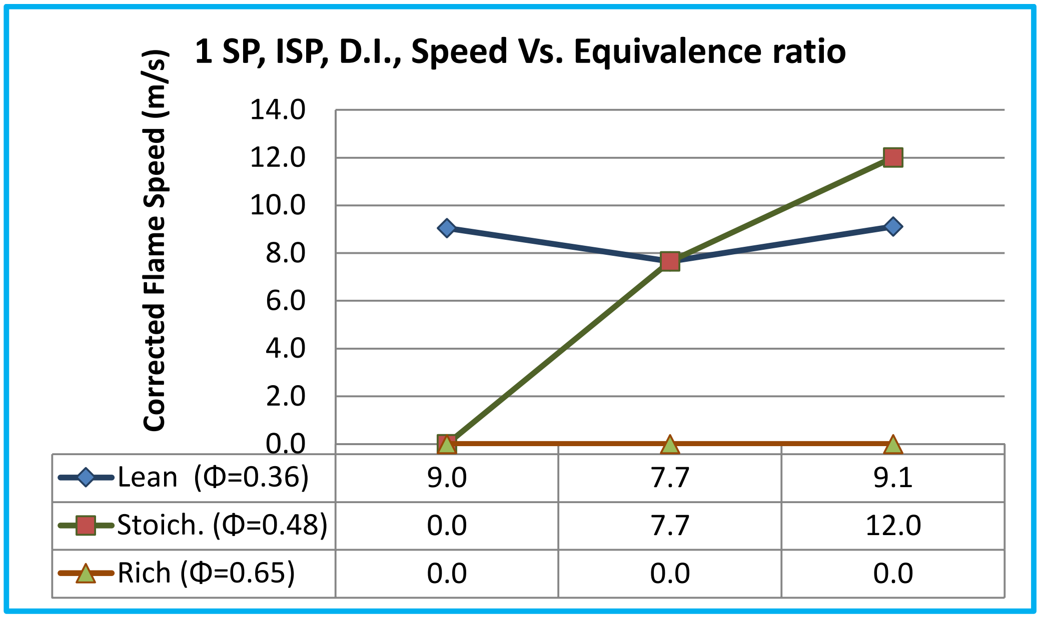

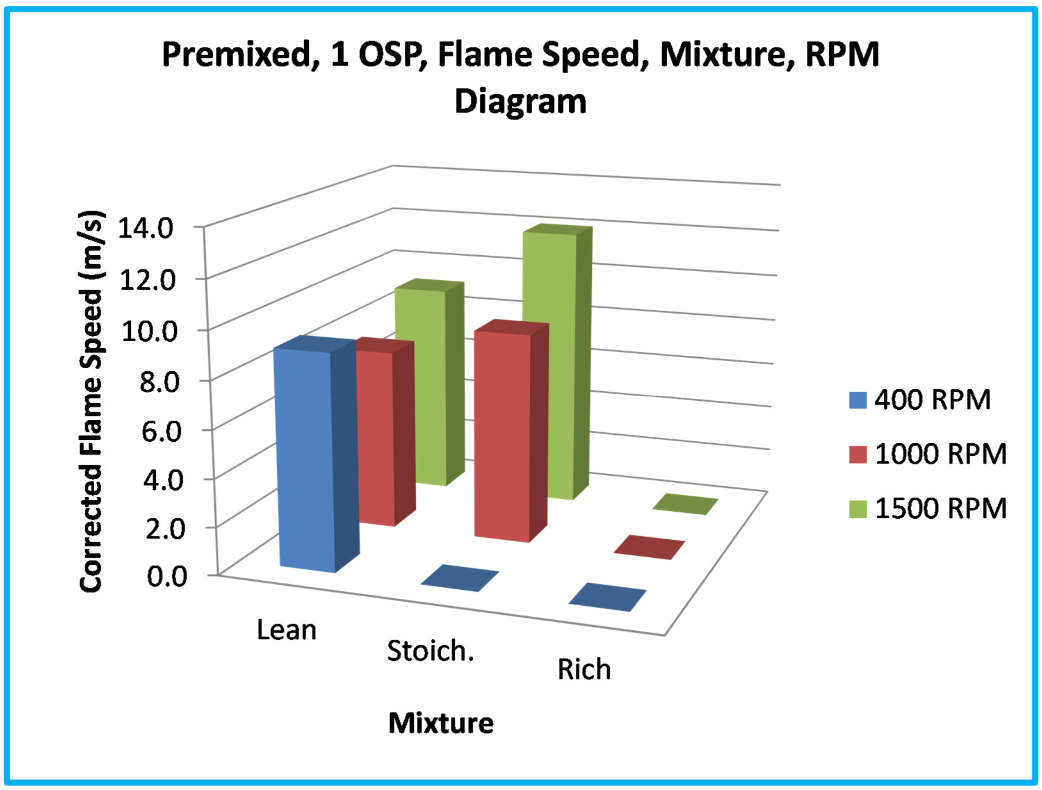

Figure 55: D.I., 1 ISP, Flame Speed vs. Inputs

Premixed 1 ISP

Experiment		
File	**Fuel/Air Ratio (%)**	**Observation**
LEL-400-PL-1-ISP-6-17-13	4	More or less consistent flame in the channel.
STO-400-PS-1-ISP-6-17-13	6	Some flames in the channel, not consistent, and flash-back to the inlet.
UEL-400-PU-ISP-6-17-13	12	No ignition at all
LEL-1000-PL-1-ISP-6-17-13	4	Very scarse flames inside the channel.
STO-1000-PS-1-ISP-6-17-13	6	Flashback to the inlet and flames in the exhaust, almost no flames inside the channel.
UEL-1000-PU-ISP-6-17-13	12	NO flame either inside the channel or Outside the exhaust port
LEL-1500-PL-1-ISP-6-17-13	4	Very few flames observed in the channel filmed, or outside the exhaust, however mild explosions were heared.
STO-1500-PS-1-ISP-6-17-13	6	Sounds like constant combustion inside the channel, low intensity flame is inside, flashback observed.
UEL-1500-PU-ISP-6-17-13	12	No flames either inside the channel or outside the e4xhaust, no ignition ocurred.

Analysis			
Average Length (mm)	**Avg. Speed (m/s)**	**Speed Correction (m/s)**	**Corrected Speed (m/s)**
8.00	**5.76**	3.06	**4.9**
13.79	**9.93**	3.06	**9.4**
	0.00	3.06	**#NUM!**
	0.00	7.85	**#NUM!**
13.92	**10.02**	7.85	**6.2**
	0.00	7.85	**#NUM!**
20.43	**14.71**	11.84	**8.7**
26.36	**18.98**	11.84	**14.8**
	0.00	11.84	**#NUM!**

Table 11: Premixed, 1ISP, Experiment Results and Observations

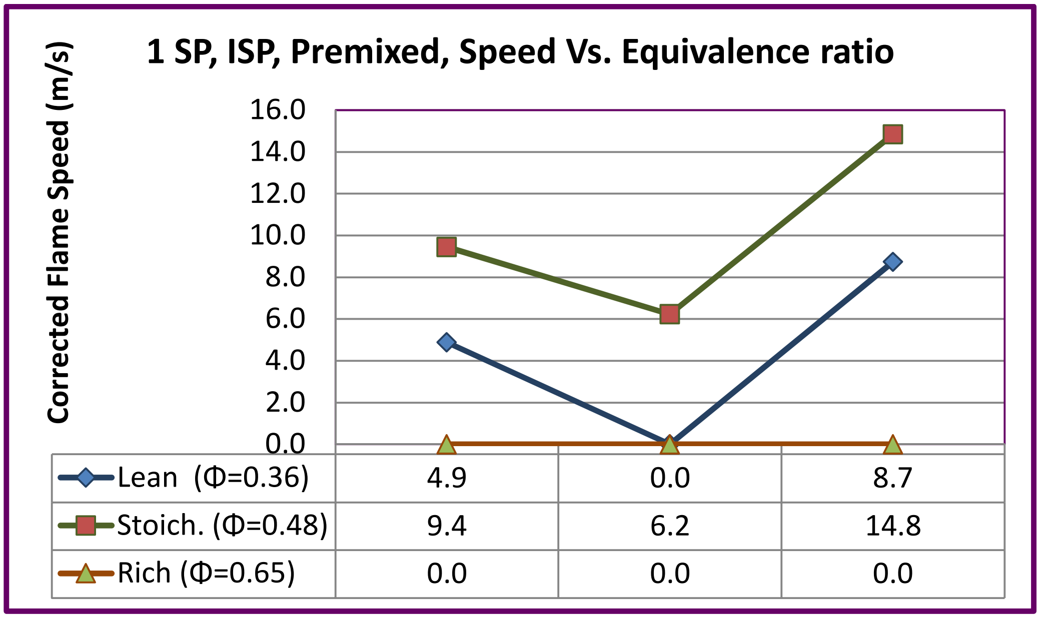

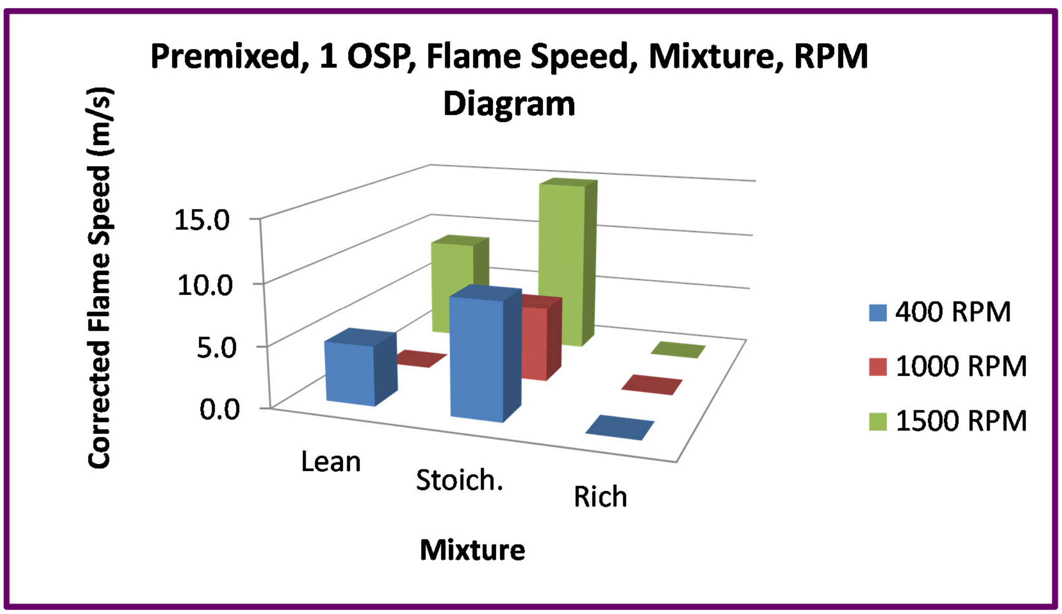

Figure 56: Premixed, 1 ISP, Flame Speed vs. Inputs

<u>Analysis</u>

Results have two several ways of interpretation, from the fluid dynamics point of view, from the combustion point of view and from experimental constraints point of view. In Figure 51 to Figure 56 left graphs represent the Combustion point of view for data interpretation, the right side graphs and Figure 57 represent cases which can be interpreted from a fluid dynamics, and experiment constraints point of view.

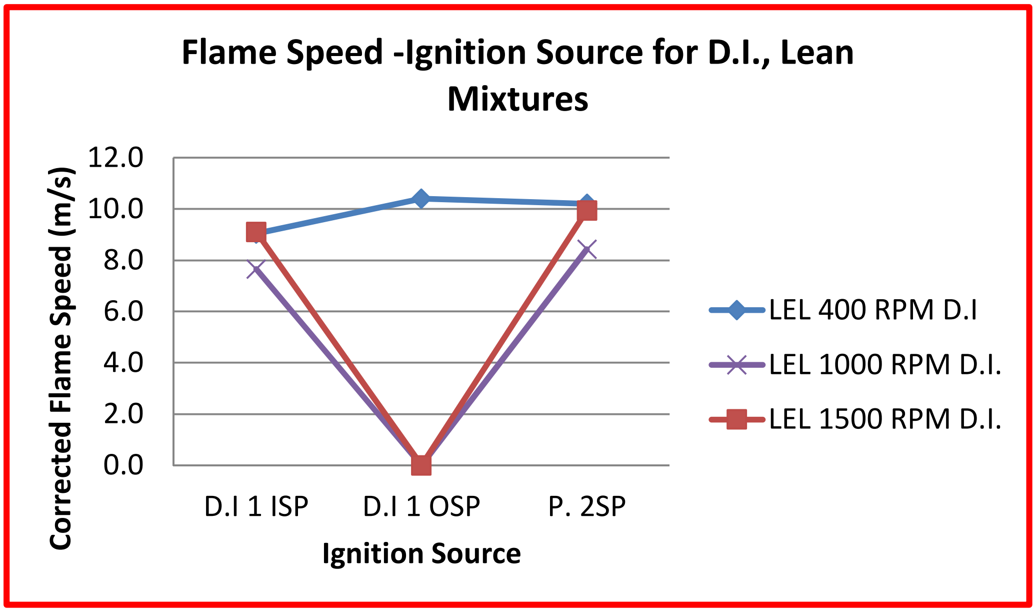

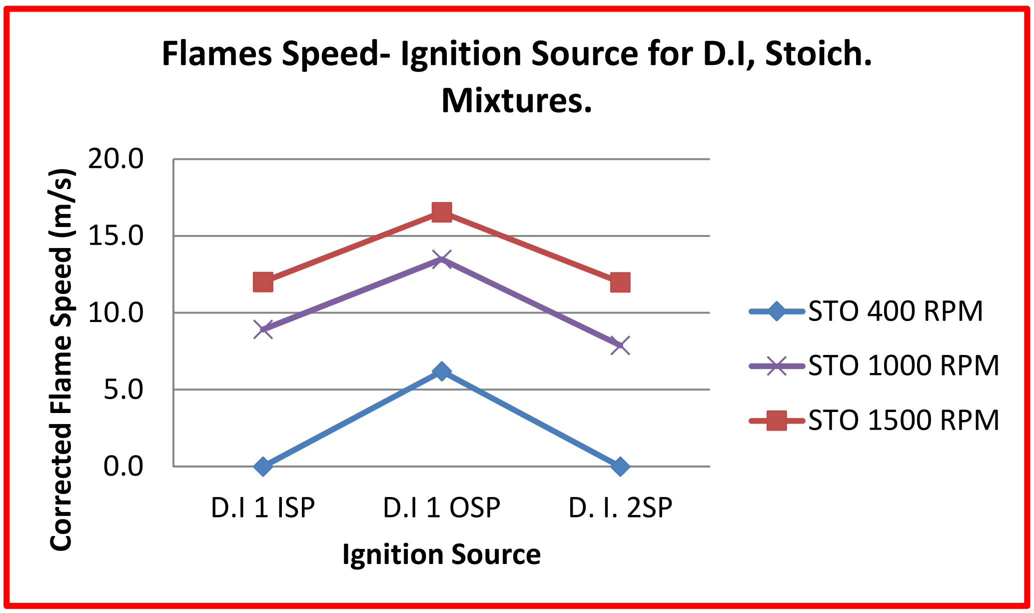

Figure 57: Flame Speed - Ignition Source Graphs

Figure 57 (Cont'd)

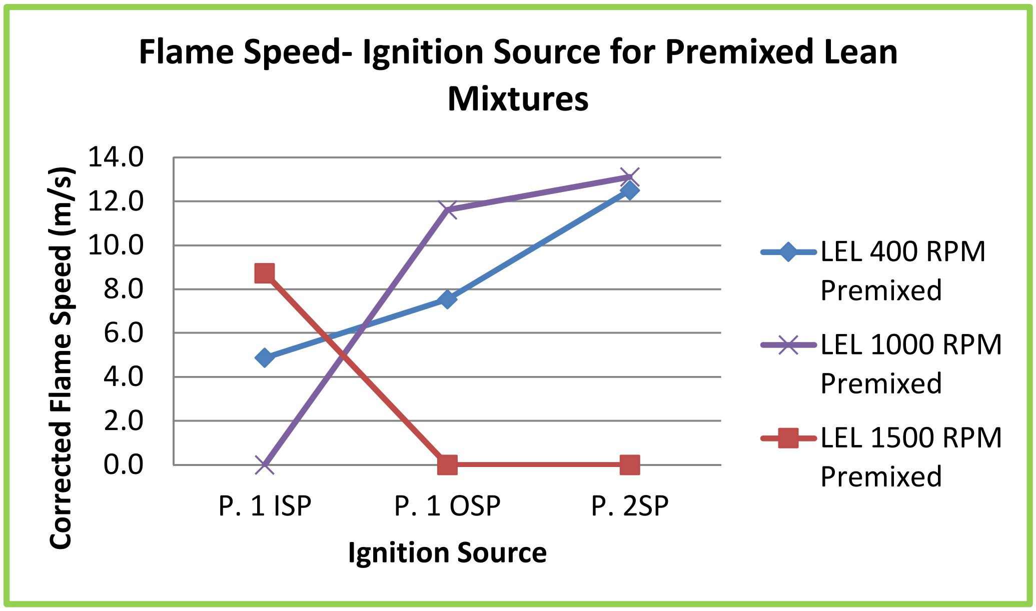

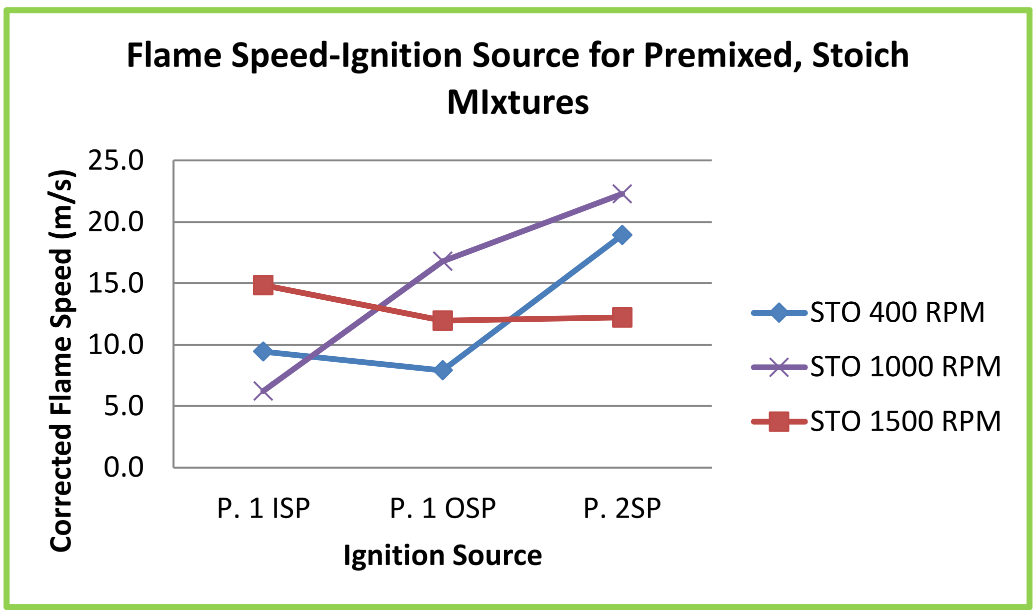

The main observations are:

- No rich mixture was ignited.
- Flame moves from outside to inside of the rotor.
- At 1000RPM and 1500RPM flame speed tends to be higher than at 400RPM.
- Premixed flame speed is faster than Direct Injection flame speed.
- In cases “LEL-1000-PL-1-ISP-6-17-13”, and “LEL-1500-PL-5-10-13” is very difficult to measure the flame, when the video is analyzed, there is a positive in flame existence, but the flame-front is already outside of the window when the images are taken.
- In the 2 SP cases usually 2 flame fronts appear. In cases “STO-1000-DS-2SP-6-18-13”, and “STO-1500-DS-2SP-6-18-13” one of the flame fronts is not possible to follow so the speed calculated could be about half of the real speed.
- Premixed flame tends to increase more its speed with the increase or RPM than Direct Injection flame.
- Rotation changes the capacity of a mixture to Ignite. The Upper and Lower explosion limits move close up towards stoichiometric having a narrower explosion range.
- The spark plug position and amount (Figure 39) have an effect on flame front speed.
    - Two spark plugs increase flame speed, compared to one.
    - The outside Spark Plug relates to higher speeds as opposed to the inside Spark Plug.
    - The synchronicity of the two SP is to ignite the same channel. It shows a flaw on the top plate design: The SP ports are not aligned with the channel. The spark happens rather close to the walls of the channel, small delays on the spark signal can make the spark happen in a place that will not reach the bulk of the mixture.

Making the combustion chain reaction, inside the channel, slower, weak or non-existent.

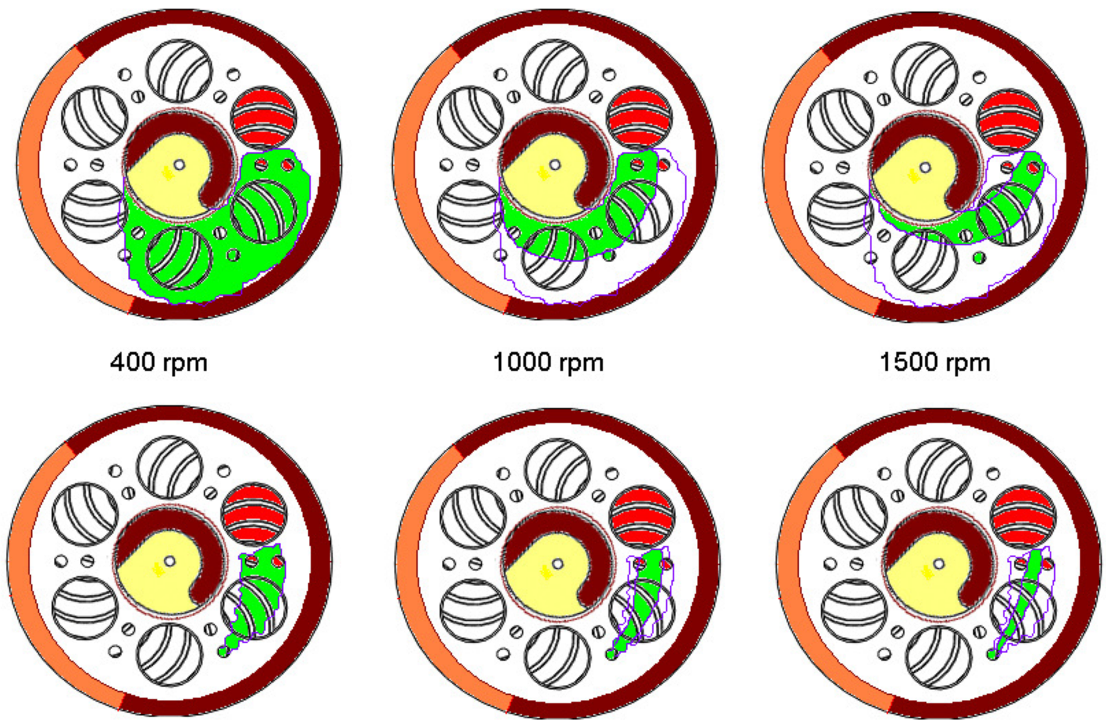

Figure 58: Hypotheses of Air-Fuel Flow Distribution for RPM and Fuel Injection Type.

- Figure 58 shows how results suggest the air-fuel flow is moving through the WDE for each RPM and Injection Type case.
    - In direct injection cases, higher speed gives less time for diffusion, hence is harder to ignite the mixture (Figure 58, bottom figures).
    - Centrifugal force moves the higher density fluid towards the outer part of the channel.

Conclusions and Future Work

This work shows that rotating combustion is possible and behaves similarly to stationary combustion. However the main parameters have interesting changes.

- The explosion limits narrow up closer to the stoichiometric equivalence ratio.
- Diffusion and Flame speed are enhanced by the turbulence generated from the rotational speed of the rotor.
- More spark plugs enhance flame speed for premixed cases but just slightly for direct injection cases.
- A flame speed of 20m/s which is approximately the highest measured in this study would allow a one cycle WDE speed up to ~16000 RPM with combustion happening during 90% of a revolution. Since WDE efficiency has a strong correlation to the speed of the rotor this study shows it is feasible to have an engine rotating at higher speeds than today's capabilities without combustion problems.
- A new design of optical top plate in which spark plugs are aligned with the channel is suggested in order to diminish variability of the observations made.

REFERENCES

REFERENCES

1. *Statistical Review of World Energy 2011 | BP*. 2012; Available from: http://www.bp.com/sectionbodycopy.do?categoryId=7500&contentId=7068481.

2. He, Y., S. Wang, and K.K. Lai, *Global economic activity and crude oil prices: A cointegration analysis.* Energy Economics, 2010. **32**(4): p. 868-876.

3. *U.S. Energy Facts - Energy Explained, Your Guide To Understanding Energy*. 2012; Available from: http://www.eia.gov/energyexplained/index.cfm?page=us_energy_home.

4. Dubord, S.J., *EPA Declares Carbon Dioxide a Danger to Public Health*, in *The New American*. 2009.

5. *Weekly U.S. All Grades All Formulations Retail Gasoline Prices (Dollars per Gallon).* 2012; Available from: http://www.eia.gov/dnav/pet/hist/LeafHandler.ashx?n=PET&s=EMM_EPM0_PTE_NUS_DPG&f=W.

6. *EIA - Economic Effects of High Oil Prices*. 2012; Available from: http://205.254.135.24/oiaf/aeo/otheranalysis/aeo_2006analysispapers/efhop.html.

7. Cullen, J.M. and J.M. Allwood, *Theoretical efficiency limits for energy conversion devices.* Energy, 2010. **35**(5): p. 2059-2069.

8. Akbari, P., R. Nalim, and N. Muller, *A Review of Wave Rotor Technology and Its Applications.* ASME Conference Proceedings, 2004. **2004**(47179): p. 81-103.

9. Piechna, J., et al., *Radial-flow wave rotor concepts, unconventional designs and applications.* IMECE2004-59022, 2004.

10. Akbari, P. and N. Mueller, *Wave rotor research program at michigan state university.* AIAA Paper, 2005. **3844**: p. 10-13.

11. Weber, H.E., *Shock wave engine design*. 1995: Wiley New York.

12. Kurec, K., J. Piechna, and N. Müller, *NUMERICAL INVESTIGATION OF THE RADIAL DISK INTERNAL COMBUSTION ENGINE.*

13. Zauner, E. and F. Spinnier, *Operational behavior of a Pressure Wave Machine with Constant Volume Combustion*. 1994, ABB Technical Report.

14. Turns, S.R., *An introduction to combustion*. Vol. 499. 1996: McGraw-Hill New York.

15. Law, C.K., *Combustion physics*. 2006: Cambridge University Press.

16. Liao, C., et al., *Flammability limits of combustible gases and vapors measured by a tubular flame method.* Fire Safety Journal, 1996. **27**(1): p. 49-68.